NORTHWESTERN UNIVERSITY

Structure and Function of Coordination Sites in Metal Trafficking Proteins

A DISSERTATION
SUBMITTED TO THE GRADUATE SCHOOL
IN PARTIAL FULFILLMENT OF THE REQUIREMENTS

For the degree
DOCTOR OF PHILOSOPHY
Field of Chemistry

By
LYDIA ANNE FINNEY
EVANSTON, ILLINOIS

EVANSTON, ILLINOIS
December, 2008

© Copyright by Lydia Anne Finney 2008

All Rights Reserved

ABSTRACT

Structure and Function of Coordination Sites in Metal Trafficking Proteins

Lydia Anne Finney

Many metal ions are of critical importance in many cellular functions. The very properties of these metal ions that make them useful also make them toxic to the cell. In the course of evolution, many metal ion homeostasis systems have developed to provide balance between the necessity and toxicity of these nutrients. All of the metal trafficking proteins that have been structurally characterized to date form a unique subset of the known metalloproteins, and have coordination chemistry tailored by nature to their specific role. Here we present insights into the coordination chemistry of Atx1, a yeast copper chaperone protein, PcoC, a bacterial copper detoxification protein, and ZntA, a bacterial zinc export pump.

Despite the fact that these proteins bind different metal ions, and are found in different organisms, they share common characteristics that set them apart from other metalloproteins.

They bind their metal ions with coordination chemistry unlike that for other known proteins that bind the same metal. Additionally, they tend to exhibit metal-ion-dependent interactions. As bioinorganic chemists uncover more of these trafficking and transport pathways, other interesting biological coordination environments will likely be revealed.

Thomas V. O'Halloran, Ph.D.
Dissertation Advisor

ACKNOWLEDGEMENTS

I first acknowledge my advisor, Thomas V. O'Halloran, since without his concommittant efforts, none of my work would have been possible. Of his many outstanding qualities, I have most come to admire his remarkable patience. He has truly inspired me to nurture this virtue as a scientist.

I also recognize the great contribution of all my many coworkers and collaborators. Specifically, Christopher Singer, David Huffman, Caryn Outten, Wayne Outten, Andrew Torres, and Tracey Rae provided me with much of my initial technical training. Working alongside Janet Wolford and Nina Brown, I have learned much more biology and medicine than I ever anticipated. Eric Kawamoto played a key role in my efforts through his consistent encouragement. My collaborators, Simone Ciofi-Baffoni and his coworkers at CERM, Dan Tobin and the Penner-Hahn Lab, and Amy Wernimont and the Rosenzweig Lab all deserve much credit for this work as well. Additionally, my efforts were greatly aided by the scientific discussions with and technical support of many members of the Godwin Lab.

I am also very grateful to the Fannie and John Hertz Foundation, who have provided me with five years of generous support.

My family has been my bastion of support. They have provided me with the balance necessary to pursue these scientific questions with persistence and diligence. I thank my parents, James F. and Mary T. Finney, and my brothers, William F. and James T. Finney. Finally, I thank my husband, Jean Dee Breshears, my ultimate co-conspirator both in science and in all other aspects of life.

TABLE OF CONTENTS

COPYRIGHT....2
ABSTRACT....3
ACKNOWLEDGEMENTS....5
TABLE OF CONTENTS....6
LIST OF TABLES....8
LIST OF FIGURES....9

CHAPTER 1 Introduction and Scope of Thesis....12

Early Insights into the Coordination Chemistry of Metal Ion Homeostasis Proteins....14
Copper Homeostasis in Yeast....15
Copper Homeostasis in *E.coli*....19
Zinc Homeostasis in Bacteria....22
Emerging Metal Trafficking Systems....24
Scope of Thesis....27

CHAPTER 2 Novel Metal Ion Coordination and Metal-Dependent Protein-Protein Interactions in PcoC....28

Abstract....28
Introduction....29
Experimental Procedures....35
Results....37
Discussion....43

CHAPTER 3 Chapter 4. ZntA(46-118): The Structure of Zinc-Specific Atx1 homolog suggests biologically novel Zn(II) coordination....46

Abstract....46
Introduction....47
Experimental Procedures....49
Results....56
Discussion....69

CHAPTER 4 The N-terminal Domain of ZntA, ZntA(46-118), Forms a Metal-Bridged Dimer at Low Zn(II) Levels....80
Abstract....80

Introduction 82
Experimental Procedures 84
Results 87
Discussion 96

CHAPTER 5 ZntA(1-118): An Additional N-terminal Tail with an Unusual Cysteine-rich Domain has a Significant Impact on Metal Ion Coordination 102

Abstract 102
Introduction 104
Experimental Procedures 107
Results 112
Discussion 119

REFERENCES 125

APPENDIX A Preparation of ZntA Mutants to Explore the Role of D58 in Metal Ion Selectivity 143

CURRICULUM VITAE 150

LIST OF TABLES

Chapter 1

Table 1-1. Total metal ion content of *E. coli* 13

Chapter 4

Table 4-1. Zn(II)-ZntA(46-118) EXAFS fit results 90

Table 4-2. Cd(II)-ZntA(46-118) EXAFS fit results 93

Table 4-3. Comparison of Co-ZntA(46-118) UV-Vis to other peptide models 99

LIST OF FIGURES

CHAPTER 1

Figure 1-1. Cu Trafficking in *S. cerevisiase.* 18

Figure 1-2. Copper Traffficking in the Periplasm. 20

Figure 1-3. Zinc Homeostasis in *E. coli.* 23

CHAPTER 2

Figure 2-1. Fourier Transform of k^3-weighted EXAFS data for Cu(II) PcoC and Cu(I) PcoC.....32

Figure 2-2. High Resolution Crystal Structures of PcoC and Selenomethionine-PcoC.....33

Figure 2-3. Analytical Gel Filtration of apo- and Cu(II) PcoC.....38

Figure 2-4. Extinction Profile for the apo- and copper form of PcoC.....40

Figure 2-5. PcoC Sedimentation Equilibrium Data Analysis.....41

Figure 2-6. Monomer-Dimer Distribution Plots for the apo and copper form of PcoC 42

CHAPTER 3

Figure 3-1. Superposition of 2D ^{15}N-^{1}H HSQC Spectra of Zn(II) and apo-^{15}N ZntA(46-118).....57

Figure 3-2. Number of meaningful NOEs per Residue of apo- and Zn(II)-ZntA(46-118).....59

Figure 3-3. RMSD per Residue form the Mean Structure of apo- and Zn(II)-ZntA(46-118) 60

Figure 3-4. Backbone Atoms for Solution Structures of apo- and Zn(II)-ZntA(46-118).....62

Figure 3-5. Experimental ^{15}N Relaxation Parameters for apo- and Zn(II)-ZntA(46-118) 66

Figure 3-6. Comparison between the Backbone of apo-ZntA(46-118) and Zn(II)-ZntA(46-118)70

Figure 3-7. Comparison of the Backbone of Zn-ZntA(46-118) with Cu(I)-Ccc2a from *S. cerevisiae* and Cu(I)-CopAb from *B. subtilis* 76

Figure 3-8. Comparison of the Backbone of Zn-ZntA(46-118) with Hg(II)-MerP from *S. flexineri* 78

CHAPTER 4

Figure 4-1. The k^3-weighted Zn(II) K-edge EXAFS data on Zn(II)-ZntA(46-118).....88

Figure 4-2. Fourier Transform of the EXAFS data on Zn(II)-ZntA(46-118).....89

Figure 4-3. Gel Filtration Chromatograms of ZntA(46-118).....91

Figure 4-4. ^{113}Cd-NMR of ^{113}Cd-ZntA(46-118).....94

Figure 4-5. UV-Vis of Co(II)-ZntA(46-118).....95

CHAPTER 5

Figure 5-1. Sequence of ZntA(1-118) and Homology with other Atx1-like Proteins and Domains. 106

Figure 5-2. Copy Number of ZntA as a Function of added Zn(II) 113

Figure 5-3. SDS-PAGE Gel of Zn(II)-ZntA(1-118).....114

Figure 5-3. MALDI-TOF Mass Spectrum of Zn(II)-ZntA(1-118).....115

Figure 5-5. HSQC Plots of apo- and Zn(II)-ZntA(46-118) 119

Figure 5-6. UV-Vis of apo-, Co(II)-, and Zn(II)-ZntA(1-118).....120

Figure 5-7. Hypothetical Functional Role for the Unstructured N-Terminal Moiety.....124

APPENDIX A

Figure A-1. Sequence Alignment of Zinc and Cadmium-transporting ATP-ases.....144

Figure A-2. Amino Acids used in Mutating Aspartate 58 146

Figure A-3. Overexpression gels of D58R, D58T, and D58N mutants of ZntA(46-118) and ZntA(1-118) 148

CHAPTER 1

Introduction and Scope of Thesis

Life sustains itself through a variety of chemical processes. These processes often make use of cellular catalysts, such as enzymes, so they can occur in the environment of the cell and on a rapid timescale. Many of these enzymes utilize a metal ion in their active site to achieve their particular chemistry. These metals are sometimes referred to as 'trace elements,' but in many cases this is a misnomer. Studies of transition metal quotas of *Escherichia coli*, for instance, reveal that individual bacteria concentrate zinc and iron by several orders of magnitude relative to the concentration in a typical growth medium until they achieve a quota of about $2x\ 10^5$ atoms per cell, equivalent to a total concentration of about 0.1 millimolar(1). Metals such as copper and manganese are maintained in the 10-100 μM range. Other metals are also concentrated by the cell to a narrow, fixed $[metal]_{total}$. (Table 1-1)

While these metal ions are necessary components of the active sites of these enzymes, taken alone they are also efficient catalysts themselves. Outside of the controlling environment of an enzyme, metal ions are capable of catalyzing many other adventitious, deleterious reactions. How, then, are these metal ions taken in by the cell and incorporated into the enzymes that use them without these adverse reactions? Many proteins are involved in trafficking these

Metal Quotas in E. coli *(7)*

K, Mg	**Ca, Zn, Fe**	**Cu, Mn, Mo, Se**	**V, Co, Ni**
10^8 atoms/cell	10^5 atoms/cell	10^4 atoms/cell	*Low abundance*
>10 millimolar	~0.1 millimolar	~10 micromolar	*Low abundance*

Table 1-1. The total metal ion content of *E. coli.* Many metals are concentrated by the cell to a narrow, fixed, total concentration. Clearly, many transition metals are abundant in the cell, but so are metalloproteins, which correspond to about a third of all structurally characterized proteins.

metal ions from the pumps that import them to their target enzymes. Through these pathways, the metal ion concentration inside of cells is tightly controlled, and in some cases has been shown to be less than one ion per cell. One of the keys to understanding the mechanism of this control lies in coordination chemistry.

As one might imagine, these trafficking proteins poise their inorganic chemistry in a manner that allows rapid bond making and breaking at the metal center upon cue. One of the emerging themes is unexpected: metal exchange is accomplished with active site chemistry unlike that seen in any of the hundreds of known metalloenzymes' coordination environments.

Early Insights into the Coordination Chemistry of Metal Ion Homeostasis Proteins

From a historical point of view the first studied, best understood intracellular metal transport proteins are ferritin and transferrin. The coordination chemistry of these proteins is unusual: ferritin has a semi-stable mineral hydrous ferric oxide core inside an oligiomeric protein shell, while transferrin is a smaller serum protein that coordinates iron through two tyrosine oxygens, two bicarbonate oxygens, one histidine nitrogen and one aspartate carboxylate oxygen(2). This coordination of an otherwise labile anion, bicarbonate leads to unusually inert coordination environment for the Fe(III) and remains unprecedented in among metalloproteins. The iron atoms in both ferritin and transferin are stable and kinetically inert until a triggering reaction is initiated: in the case of ferritin, the trigger is reduction of the Fe(III) to the more labile ferrous iron. In the case of transferrrin it is the protonation of the bicarbonate and loss of CO_2 that drives a conformational change that ultimately releases the Fe(III) into the low pH

environment of the endocytic vesicle. With out the triggering event, the iron bound by these proteins is not directly biologically accessible to chemical or biological chelators. The downstream mechanisms by which the iron bound by transferrin or ferritin reaches enzyme active sites in the cell are not yet understood.

Copper Homeostasis in Yeast

Among the best understood intracellular metal trafficking systems is that of Cu(I) in yeast (3) and the atypical coordination environment observed here for copper provides a mechanistic basis for the dual requirements of tight binding and facile transfer of the copper to the target protein (4). The first copper chaperone, Atx1, was identified by Culotta and coworkers in elegant genetic screens for new oxidative stress functions in *Saccharomyces cerevisiae* (5,6). With the discoveries of the Cu(I) chemistry of yeast Atx1 and its partnerships, a copper chaperone function was established(7,8).

Separately, another yeast protein, the copper chaperone for superoxide dismutase (CCS), was shown to be required for superoxide dismutase activity (6). Through these studies, in parallel with structural studies of other homologous proteins, the–GMXCXXC- motif has emerged as a key element in a highly conserved metal handling domain(9-13). Many proteins containing this motif are now known to bind Cu(I) with two cysteines in a low coordination number environment that allows for very tight binding but that can nonetheless allow entrance of a third binding residue or ligand from outside the protein, or domain, itself. Either environment

is unlike those seen in any other structurally characterized mononuclear Cu(I) proteins, which typically exhibit a coordination number of four. An adjacent lysine sterically hinders the approach of a third ligand, but conformational changes, which may be associated with protein docking, could then allow the partner protein, a domain of Ccc2, to access the anionic Cu(I)(S-Cys)$_2$ site (9,14). Ultimately, this domain transfers the copper into a trans-Golgi compartment where it can be incorporated into multicopper oxidases like ceruloplasm and Fet3, as well as other copper enzymes such as lysyl oxidase (Figure 1-1). Such interactions may also occur if Atx1 obtains Cu(I) from Ctr1 in vivo. Atx1 can obtain its copper cargo in vitro from a domain of the high affinity copper uptake protein Ctr1 (15); however, Ctr1 independent pathways can be involved in vivo (7). These systems have recently been reviewed, and current studies are revealing further details of these copper trafficking pathways, both in yeast as well as for an unusual thylakoid Atx1 in photosynthetic bacteria (4,11,16-20). Spectroscopic studies have since suggested that this coordination is commonplace in other copper transporting and trafficking proteins, including the *Enterococcus hirea* transporter and chaperone, CopB and CopZ, and is thought to be present in an emerging list of homologous bacterial proteins (21,22). The structures and mechanism of these proteins have recently been reviewed elsewhere (23,24) .

Cu(I) is also coordinated by cysteinates, although in a slightly different fashion, in the Cox17 protein, which is involved in assembly of the copper cofactor in the mitochondria protein cytochrome oxidase (CO) (25,26) . In some forms of the isolated protein, copper is trigonally coordinated, either in a single hexanuclear cluster or two trinuclear Cu(I) clusters, in a manner more similar to the metallothioneins and Cu(I) transcription factors than the other copper

chaperones (27). Evaluation of this coordination site, and the specific role of the Cox17 protein, is ongoing but recent studies suggest that Cox17 is not necessarily involved in conducting copper to the mitochondria, rather it plays a key role in assembly of the active CO in the intermembrane space of the mitochondria.

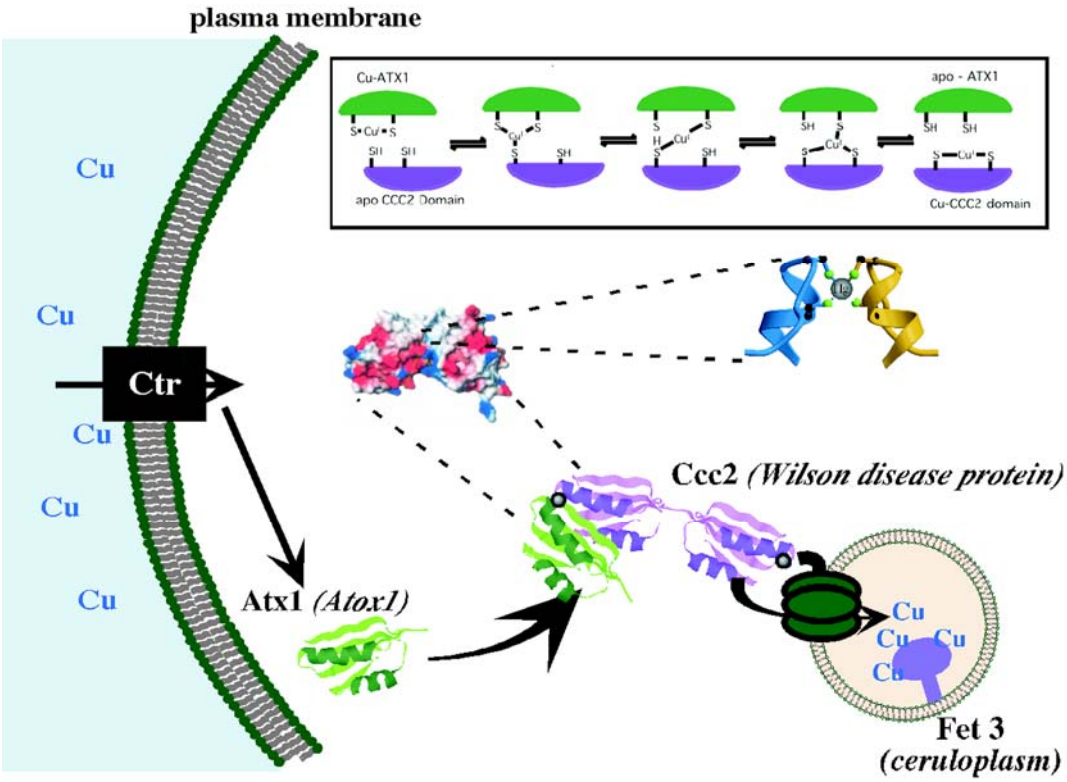

Figure 1-1. Copper trafficking in *S. cerevisiae*. In the cytoplasm of yeast, Cu(I) can be conducted by the Atx1 copper chaperone, which delivers Cu to its target protein Ccc2. Ccc2 then brings Cu into a trans-Golgi compartment, where it is utilized by the multi-copper oxidase, Fet3. The names of the human homologs are shown in parentheses. A hypothetical mechanism for Cu(I) transfer involving the electrostatic docking of the partners is inset. The formation of a metal-bridged intermediate is supported by the crystal structure of Atox1, which is shown.

Copper Homeostasis in *E.coli*

A plethora of new proteins involved in copper and zinc homeostasis have been found in *E. coli* and some adopt new types of Cu(I)-thioether coordination chemistry in proteins involving methionine (Met)-rich motifs, as well as special use of the periplasm. A series of genes (Figure 1-2) are induced in a step-wise fashion as the copper concentration in the growth medium is increased (28). The first are CueO, a multicopper oxidase whose expression is controlled by CueR (29), and CopA, a transporter related to the Menkes Disease protein which pumps copper from the cytoplasm into the periplasm (30-33). CueO and related proteins, like PcoA, are proposed to convert Cu(I) to less toxic Cu(II) (34); however, its exact role is not yet established (35). If copper concentrations continue to rise, the CusCBFA genes are induced by a two-component system (CusRS), which typically monitors stress in the cell envelope and which is particularly effective in anaerobic copper stress conditions (30).

If increasing copper concentrations overwhelm these chromosomally encoded pathways, cells that harbor either the *pco* (*E. coli*) or *cop* (*P. syringae*) copper resistance plasmids can invoke one last line of defense. The *pco* operon includes the bacterial multicopperoxidase PcoA, and its putative partner, PcoC, both of which are exported to the periplasm (36). Recently published spectroscopic and crystallographic data for PcoC, and NMR studies of the closely

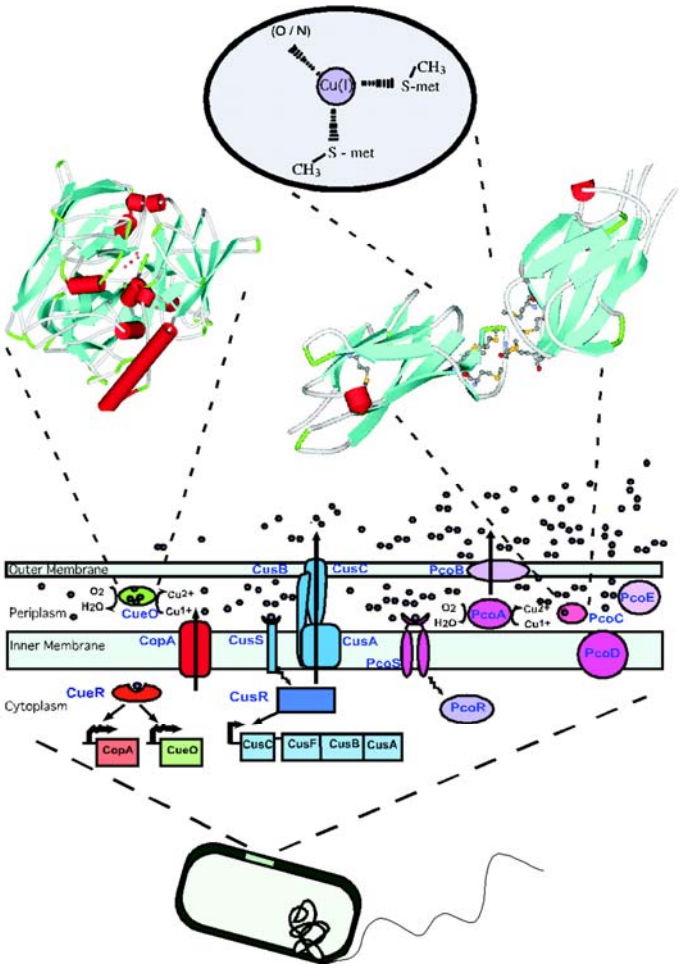

Figure 1-2. Copper Trafficking in the Periplasm. The periplasm, a compartment of the cell envelope of Gram-negative bacteria, is proving to be an important site of Cu trafficking and utilization. Cellular Cu efflux is controlled in *E. coli* by the *cue, cus, and pco* operons, each of which is induced at different levels of Cu stress by different metalloregulatory proteins. Recent structural insights for CueO and PcoC are highlighted. The cartoons of Cu ions (purple balls) represent various levels of total Cu content in the periplasm.

related *P. syringae* protein, CopC, reveal a biologically unprecedented thioether ligation (34,35,37-39). The studies of PcoC reveal a cuperodoxin fold that binds Cu(I) through two Met sulfur atoms and one nitrogen or oxygen ligand, in a hydrophobic, Met-rich loop which, intriguingly, is exposed to solvent on the protein surface. Yet Cu(II) in the same protein binds water as well as two histidine imidazole ligands and two other nitrogen or oxygen ligands. In the case of CopC, where the coordination of Cu(II) and overall fold are similar, these are Asp side chains (38).This chemistry of the Cu(I) center in PcoC is reminiscent of the low coordination number Atx1 chemistry that is sterically protected but allows a partner protein to access the site via conformational changes and coordination of an incoming sidechain (10). The crystal structure of the apo form of PcoC suggests a flexible environment that can, like Atx1, stabilize two, three or four coordinate geometry for the bound metal (37). These low coordination number environments are well poised for metal transfer chemistry. It is interesting that all of the copper trafficking proteins shown in Figure 1 are involved in copper egress from the cytoplasm or the periplasm, out of the cell, and so far no copper uptake genes have been identified in *E.coli* to date.

Zinc Homeostasis in Bacteria

Zinc trafficking proteins are also proving to be sources of unprecedented biological coordination sites. Recently, the solution structure of an Atx1-like N-terminal domain of the bacterial zinc efflux P-type ATPase ZntA was reported(40). This protein contains a –GMDCXXC- motif, similar to the metal binding motif in the copper trafficking proteins(24). However, this protein was shown to bind zinc with at least two cysteine sulfur atoms and at least one aspartate oxygen atom, with a potential fourth oxygen or nitrogen ligand from solvent or buffer. This zinc environment had previously not been seen in any of the structurally characterized Zn(II) proteins(41). Exactly how metal ion selectivity in P-type ATPases such as ZntA is achieved despite having –GMXCXXC- motifs that are otherwise similar to the Cu(I)-specific transporters has been a controversial topic(42-46). The binding of aspartate to the zinc ion as well as the two expected cysteines gives a complex with an overall charge of –1, which would prevent ionization of any water bound in the fourth site. This is one way that the transporter can suppress catalytic chemistry typical of hydrolytic zinc enzymes while leaving a labile coordination site open to the next protein that will acquire the Zn(II) ion.

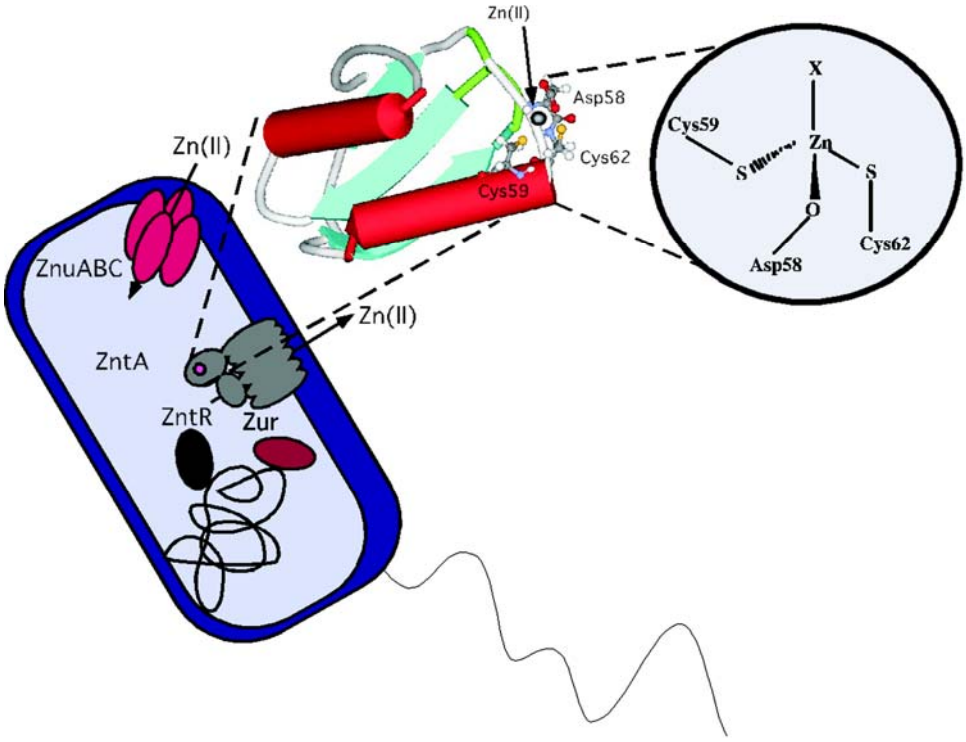

Figure 1-3. Zinc Homeostasis in *E.coli.* The trafficking of Zn(II) in the cell is controlled by the metal-sensitive regulatory proteins Zur and ZntR, which regulate the transcription of the pumps ZnuABC and ZntA, respectively. The recently determined structure of a metal-binding domain of ZntA is inset.

Zinc trafficking in yeast is also beginning to be unraveled. The ZIP (Zrt-,Irt-like Proteins) family of proteins is involved in zinc import into the cytoplasm. They are predicted to have eight transmembrane domains and domains IV-VIII in these proteins are highly conserved. These transmembrane domains contain conserved histidines, which may be important in zinc binding. . Likewise, the CDF family of transporters has been implicated in the transport of zinc out of the cytoplasm of yeast cells. They are predicted to have six transmembrane domains and a potential cytoplasmic metal binding motif, -H(D/E)XHWXLTX$_8$H- , but neither the coordination chemistry or mechanism of any of these His-rich domains is known. These have recently been reviewed, as have the metallothionein transcription factors which are of central importance in yeast zinc homeostasis (47-49).

Emerging Metal Trafficking Systems.

Many other areas of metal ion trafficking are being elucidated, and we are beginning to understand how the intracellular speciation of other metal ions compares with copper and zinc. A notable example is heme iron transport and delivery to cytochrome c. Recently, this process has been shown, in bacteria, to occur by means of a putative heme chaperone protein, CcmE, a periplasmic protein (50). Similarly to other metallochaperones, the heme is thought bound by CcmE in a transient manner (51). Indeed, the recent NMR structure of CcmE showed that there

is no classic heme binding site in the protein, and that, somewhat perplexingly, CcmE would not bind heme *in vitro* (52). This implies that the physiological function of CcmE can only be carried out through protein-protein interactions; this behavior of CcmE is consistent with the paradigm presented by the copper and zinc transporting proteins.

Another area of metal ion trafficking where a remarkable amount of progress is being made is in the study of a nickel homeostasis operon of *E. coli, nikABCDE*. Transcription of this gene cluster is regulated by the Ni-responsive repressor protein NikR. These studies find that *in vivo*, NikR is present in the cell at concentrations of at least 200 nM and that it binds nickel at picomolar levels, which seems to indicate that as is the case for copper and zinc, there is no free nickel in *E. coli*, although other interpretations have been suggested (53). Likewise, this protein also binds nickel with unique coordination chemistry (54). Other areas of nickel trafficking are also quickly expanding this picture (55-57).

These new advances place the ongoing discussion about free iron in the cytoplasm in a new light. It has been proposed that chemically free, or perhaps more precisely, 'biologically available' pools of iron can be detected in *E. coli*, by Electron Paramagnetic Resonance spectroscopy (EPR) in whole cell extracts (58). If there were pools of free iron ions in the cytoplasm, it would represent an anomaly to these trends. Indeed, complex transport and regulatory mechanisms for iron are also an area of current study. Most human diseases of iron transport are caused by iron overload and are most often a result of mutations in iron export genes (59). Additionally, a suppressor screen has identified a gene in yeast, *ccc1*, the overexpression of which is able to prevent mitochondrial accumulation of iron in the absence of

the yeast frataxin homolog (yfh1) gene, causing it instead to accumulate in the vacuole (60,61). Other studies, such as those identifying manganese trafficking in yeast by Smf2p (62), and divalent cation transport by NRAMP/DTF proteins (59) illustrate how eukaryotic cells stringently control distribution of metal ions between specialized compartments; however little is known about the coordination chemistry of these proteins to date. Taken together, these studies indicate that additional intracellular iron, zinc and manganese trafficking pathways are yet to be found. The discovery and study of such proteins and pathways is highly anticipated.

Scope of Thesis

The metal ion trafficking systems described here represent a few of the mechanisms utilized by cells to control the activity of metal ions. At the start of this work, very few of these proteins were well characterized, and the effect of the metal ions on the function of the proteins was not well understood. In the course of our attempts to elucidate the structural aspects of these proteins, we discovered commonalities that set the coordination chemistry of metal trafficking proteins apart.

Chapter Two describes the characterization of PcoC, which like Atx1, has unusual coordination chemistry and also is found to exhibit metal-dependent homo-oligomerization. Chapter Three examines the structure of the Atx1-like domain of ZntA, Znta(46-118), and Chapter Four finds evidence of unusual coordination and metal-dependent interactions in this truncation. Chapter Five investigates the role of the first 45, N-terminal, cysteine-rich residues of ZntA, which have been found to increase the susceptibility of the protein to proteolysis, and to be remarkably flexible.

Future studies of the mechanistic aspects of interactions between metal trafficking proteins will likely show that the metal ions are guided along particular pathways through the influence of protein-protein interactions on the kinetics of metal transfer. The metal-dependent protein-protein interactions seen here are suggestive of the importance of these pathways.

CHAPTER 2

Novel Metal Ion Coordination and Metal-Dependant Protein-Protein Interactions in PcoC

Abstract

The biophysical properties of the periplasmic copper protein PcoC have been investigated to reconcile crystallographic and EXAFS data on the structure of this protein. PcoC is a small soluble protein that is thought to transfer copper to PcoA, a multicopper oxidase, in the periplasm of *E. coli*. Crystallographic data had revealed two potential configurations of a dimer. EXAFS data indicated two different coordination modes, for Cu(I) and Cu(II), respectively, by this protein. To determine whether the tendency of this protein to homodimerize might factor into the different coordination sites seen, experiments that examined the dimerization state of this protein under different states of metallation were undertaken. The results demonstrated that this protein shares many commonalities with other metal-trafficking proteins, such as the prototypical system of Atx1 and Ccc2a. Among the features observed were the soft, flexible coordination site for Cu(I), and metal-induced homodimerization. While the specific role of PcoC in the detoxification of *E. coli* at high levels of copper remains unclear, the fact that Cu(I) greatly enhances homodimerization of this protein suggests that a role of copper delivery would be well suited to its biophysical properties.

Introduction

Copper is an essential element for cellular growth and is incorporated into a variety of proteins and enzymes. Copper salts are also potent antimicrobial and antifungal agents that are widely used to control plant pathogens (1). Wild-type *Escherichia coli* have several chromosomally encoded copper tolerance loci (2-6); however, organisms containing plasmid based resistance genes are able to survive in significantly higher levels of environmental copper and are thus termed copper resistant (7). The pco containing plasmid was found in a plasmid in *Escherichia coli* culture isolated from a piggery where $CuSO_4$ was used as an antibiotic and growth promoting additive (8,9). The plasmid containing the cop operon was found in *Pseudomonas syringae* growing on tomato plants treated with a copper-containing bactericide (10,11). A similar operon has been isolated from the walnut pathogen *Xanthomonas campestris* (12,13).

Copper resistance in the *E. coli pco* system is conferred by a plasmid containing at least seven genes that facilitate copper efflux (14,15). While several of these genes encode integral membrane proteins, none are members of known families of transporters. Two proteins are predicted to be soluble in the periplasm: PcoC, a small 103 a.a. protein, and PcoA, a 565 a.a. protein. PcoA bears some sequence similarity to the multicopper oxidases (16), including the yeast ferroxidase Fet3 (17,18), the human ferroxidase ceruloplasmin (19), ascorbate oxidase and laccase in plants, the manganese oxidase CumA in *Pseudomonas putida* (20), and the

chromosomal multicopper oxidase CueO of *E.coli* (21,22).

Homologues of PcoA and PcoC from *Pseudomonas syringae* have been purified with bound copper (23); however, no biochemical assays or spectroscopic data is available. These proteins were proposed to protect the cells by sequestering copper, as has been proposed for the ability of yeast metallothionein to protect that organism from elevated copper concentrations. A hallmark of the bacterial copper resistance proteins PcoA and PcoC is the presence of methionine-rich sequence motifs, which are postulated to be involved in copper binding (12,14,24,25). In eukaryotes methionine motifs are present in the Ctr family of membrane transporters (26,27). In prokaryotes, these motifs are found in plasmid- and chomosomally-encoded copper proteins including the *pco* (plasmid-borne copper resistance), *cop* (copper resistance) and *cue* (Cu export) operons.

PcoC bears no primary sequence homology to other structurally or functionally characterized copper-containing proteins. It is homologous to proteins from other copper resistance operons (13,23), however copper coordination chemistry has yet to be examined in any of these cases. Two of the three histidines of PcoC and all of the methionines are conserved among its homologues. PcoC may serve as a factor to present copper to PcoA or to escort copper out of the cell. A functional precedence for a metallochaperone function can be found in Atx1, a soluble 8 kD copper trafficking protein in yeast. Atx1 shuttles copper to a homologous domain of the enzyme Ccc2 (28), a P-type ATPase that translocates copper across a vesicular membrane for eventual incorporation into Fet3 (18). Rae et al. have shown that the cytosol of eukaryotic cells has an overcapacity for copper chelation and typically maintains less than one free copper ion

per cell (29). If a similar situation exists in prokaryotes, then a general function of the resistance pathway, including PcoA and PcoC, may be to maintain the cellular copper quota under conditions of copper excess through an export mechanism.

A demonstrated, essential role in vivo for both PcoA and PcoC is that inactivation of PcoC or PcoA causes cells to become more sensitive to excess environmental copper than wild type cells. A multicopper oxidase function has also been assigned to PcoA, based on the copper-inducible oxidase activity of periplasmic extracts. In our model PcoC acquires Cu(I) in the periplasm, then docks with PcoA, to effect oxidation to the less toxic Cu(II) form.

PcoC and CopC both contain a MTXMXGMXXH/MXPM sequence motif. Purified PcoC (30) and CopC (23) both bind one copper ion per monomer. The oxidation state of this copper ion in vivo is not known, but in vitro PcoC can bind either Cu(I) or Cu(II) (30). Characterization of Cu(II) PcoC by electron nuclear double resonance (ENDOR),1 electron spin echo modulation (ESEEM) (30), and extended X-ray absorption fine structure (EXAFS) spectroscopies (31) indicates that this protein binds Cu(II) via two or more His and a water in a tetragonally distorted site. EXAFS studies of the Cu(I) form of the protein reveal a quite different environment: a three coordinate Cu(I) bound to two Met and a His (32)(Figure 2-1). While the tetragonal Cu(II) site is observed in many other metalloproteins, is no such precedent is known for the proposed Cu(I) thioether site. In order to develop a structural basis for testing the proposed functions of these proteins and to gain insight into the role of the methionine motifs, the high resolution X-ray structure of PcoC (33).

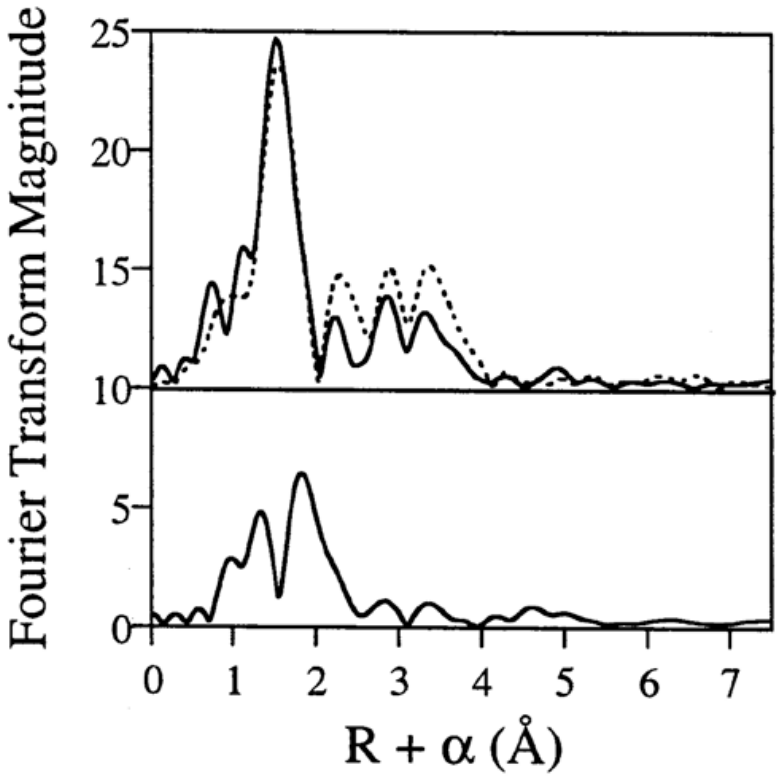

Figure 2-1. Fourier transform of k^3-weighted EXAFS (k = 2-13 Å^{-1}) data for Cu(II)-PcoC (top, solid line) and Cu(I)-PcoC (bottom) (32). Data for Cu(II)tetraimidazole (dotted line, top) are shown for comparison.

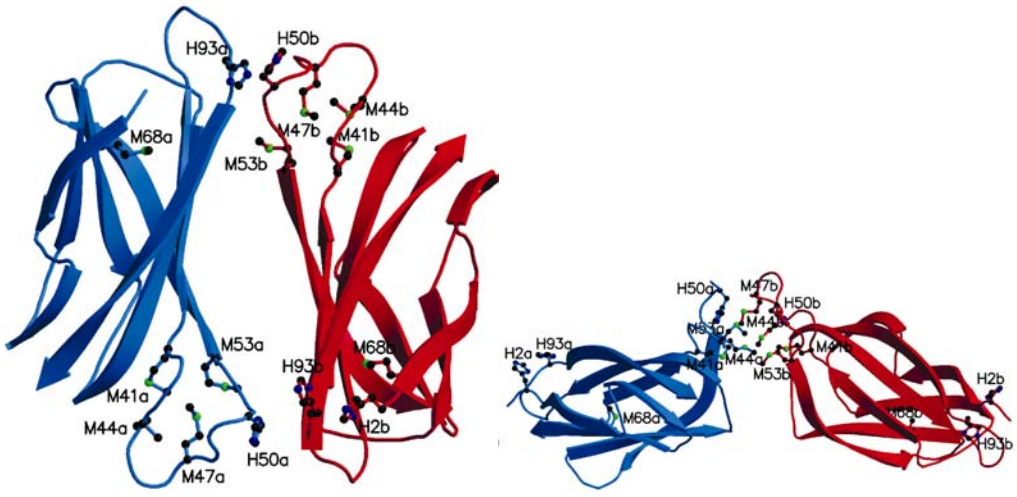

Figure 2-2. High Resolution Crystal Structures of PcoC and Selenomethionine-PcoC (33). A) Ribbon diagram of the SEMET structure of PcoC with one molecule in blue and the second molecule in red. Methionine and histidine residues are shown as ball-and-stick representations and labeled. B) Ribbon diagram of the NATIVE structure of PcoC with one molecule in blue and the second molecule in red. Methionine and histidine residues are shown as ball-and-stick representations and labeled.

has been determined, concluding that the Met motifs can be involved with metal coordination, however these hydrophobic regions are unexpectedly found on the surface. (Figure 2-2) The crystal structures and EXAFS data on PcoC indicate that the coordination in this protein may mirror that of the copper chaperones Atx1 and PcoC. The crystal structures determined presented two possible dimerizaton configurations. The EXAFS data suggested novel, mononuclear Cu(I) coordination. To answer the question of whether the dimer was metal-bridged in solution, and to determine if the presence of metal affected the homo-oligomerization state of the protein, the biophysical properties of PcoC were investigated by analytical gel filtration and analytical ultracentrifugation.

Experimental Procedures

Analytical gel filtration of Cu(I)- and apo- PcoC. Analytical gel filtration was performed on a Superdex 75 HR 10/30 column at 4°ΔC using a BIO-RAD Biologic HR chromatography system. After equilibration in 10 mM HEPES, 250 mM NaCl, pH 7.5, 75 μL of 200 μM apo- or Cu(I) were injected onto the column. The samples were then eluted in 10 mM HEPES, 250 mM NaCl, pH 7.5 at a flow rate of 0.5 mL/minute. The retention volume (V_e) of each peak was recorded. These retention volumes were then compared to a calibration curve of vitamin B12, aprotinin, and Rnase A where $(V_e-V_o)/(V_t-V_o)$ was plotted against the log of the molecular weight to give a straight line, V_o being the void volume of the column and V_t the bed volume of the column. Extinction coefficients at 280 nm of 8460 M-1cm-1 for apo-PcoC and 11,926 M-1cm-1 for Cu(I)-PcoC were used to normalize the two chromatograms.

Analytical Ultracentrifugation of Cu(I) and apo-PcoC. In collaboration with Kate Spiegel and Dr. Borres Demeler, all sedimentation equilibrium experiments were performed with a Beckman Optima XL-A at the Keck Biophysical Facility at Northwestern University. Data analysis was performed with UltraScan version 6.0 (developed by B. Demeler) (34). Hydrodynamic corrections for buffer conditions were made according to data published by Laue et al (35), and as implemented in UltraScan. The partial specific volume of PcoC was estimated according to the method by Cohn and Edsall, and as implemented in UltraScan (*PcoC* partial specific volume: 0.73726 ccm/g) (36). 95% confidence statistics were determined using Monte

Carlo analyses, which were calculated on a 40-processor Linux Beowulf cluster configured with Slackware Linux version 7.0. All samples were analyzed in a buffer containing 10 mM sodium phosphate buffer, pH 7.5, with 250 mM NaCl. Sedimentation equilibrium experiments were performed at 4°C and speeds ranging between 20,000 - 50,000 rpm with 8,000 - 6000 rpm increments. Equilibrium times were estimated using the finite element approach-to-equilibrium simulation module in UltraScan and determined to be as followed: [20 krpm: 41 hrs, 28 krpm: 94 hrs, 36 krpm: 147 hrs, 44 krpm: 154 hrs, 50 krpm: 176 hrs]. The samples were centrifuged in six-channel epon-filled centerpieces in the AN-50-TI rotor. For each sample, six loading concentrations were measured. The optical density of the samples were 0.3, 0.5 and 0.7 OD at 230 nm and 280 nm for the apo-PcoC sample and 0.2, 0.3, and 0.4 OD at 280nm and 0.3, 0.5, and 0.7 OD at 230 nm for the Cu(I)-PcoC sample. Scans were collected in radial step mode with 0.001 cm step size setting and 15 replicates. When globally fitting data from different wavelengths to concentration-dependent models like reversibly self-associating monomer-dimer models, the extinction differences at multiple wavelengths need to be taken into account. To this end, wavelength scans between 200 and 340 nm were taken in triplicate at 1 nm stepsize setting with 10 replicates. Six different loading concentrations were measured and data between 0 and 0.9 OD were collected. Extinction profiles were generated by globally fitting all scans to sums of 5 Gaussian terms, resulting in a extinction profile for the protein. The profile is normalized using the extinction coefficients at 280 nm of 8460 $M^{-1}cm^{-1}$ for the apo-sample and 11926 $M^{-1}cm^{-1}$ for the Cu(I) sample determined from Beers Law plots on solutions calibrated by total protein hydrolysis. Values at 230 nm can then be read off of the fitted profile.

Results

Analytical gel filtration of Cu(I) and apo-PcoC. Analytical gel filtration of apo-PcoC shows two peaks, one calibrating approximately 16 kDa and a second calibrating to approximately 41 kDa (Figure 2-3). These two peaks are also seen in Cu(I)-PcoC, however the area under the curve of the higher molecular weight peak increases by 68% and the area of the lower molecular weight peak decreases by 23% in the Cu(I) case. Metal binding thus enhances the self-association of PcoC to form a higher order oligomeric state which is most likely a dimer. The apparent MW is somewhat higher than anticipated for spherically symmetric monomer; however, recent crystallographic data suggest that the apo protein is quite oblate and this may account for the higher mobility. Given the oblate nature of the apo-protein, the copper loaded form is also likely to have a large aspect ratio as well. In this case the metal induced oligomer is most likely a dimer.

Analytical Ultracentrifugation of Cu(I) and apo-PcoC. While analytical gel filtration results indicate some self-association of apo-PcoC is readily observed in solution, (30) these studies did not resolve the oligomerization state of aggregates. In fact, the apparent MWs did not clearly correspond to monomers or dimers. The structural data presented here reveal a significant deviation of the monomer from spherical symmetry suggesting that the protein may exhibit atypical hydrodynamic properties. To delineate the oligomerization state of the protein in solution and to frame the energtics of oligomerization, analytical ultracentrifugation of apo- and Cu(I)-PcoC

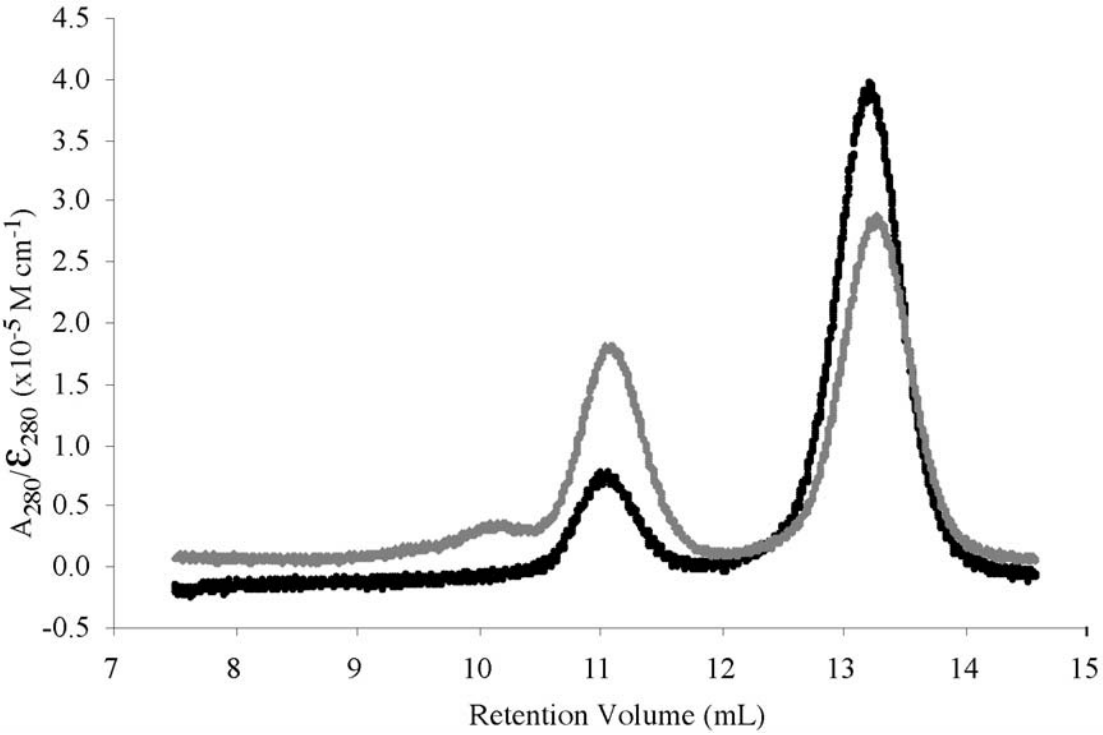

Figure 2-3. Analytical Gel Filtration of apo- and Cu(I)-PcoC . The chromatogram of apo-PcoC is shown in black and that of Cu(I)-PcoC is shown in gray. The presence of two peaks in the chromatogram may indicate the transient formation of a higher molecular weight aggregate in the solution state.

was performed. A large concentration range can be accomplished by varying the loading concentration and the wavelength of the measurement, which exploits the various absorption properties of the protein. Extinction profiles generated from the global fits, resulted in the extinction profiles shown in Figure 2-4. These correspond as expected to the spectra determined separately corroborating the global fits. By globally fitting data observed under multiple conditions, such as multiple rotor speeds and multiple loading concentrations, it is possible to enhance the confidence in each fitted parameter value (37). In such a fit, parameters such as monomer molecular weight and association constants are considered global parameters and forced to be the same for all included data sets. For the global equilibrium analysis, 21 equilibrium scans from the copper form and 17 from the apo form ranging in speeds between 20,000 rpm and 50,000 rpm and loading concentrations between 0.2 to 0.7 OD at both 230 nm and 280 nm were fitted to single ideal and monomer-dimer (Figure 2-5) and monomer-dimer tetramer reversibly self-associating models. For both forms of PcoC the fitting statistics improved significantly when monomer-dimer models were fitted compared to single ideal species models, but no improvement was determined in changing the model to a monomer-dimer-tetramer model (data not shown). The improvement of the fit in going from single ideal species model to monomer-dimer model was most pronounced for the Cu(I) form of PcoC, which forms a tighter dimer . Thus, the system could be well described by a monomer-dimer equilibrium model. This can be further seen in random residuals for the latter fit. A distribution of monomer and dimer species over the analyzed concentration range is shown in Figure 2-6.

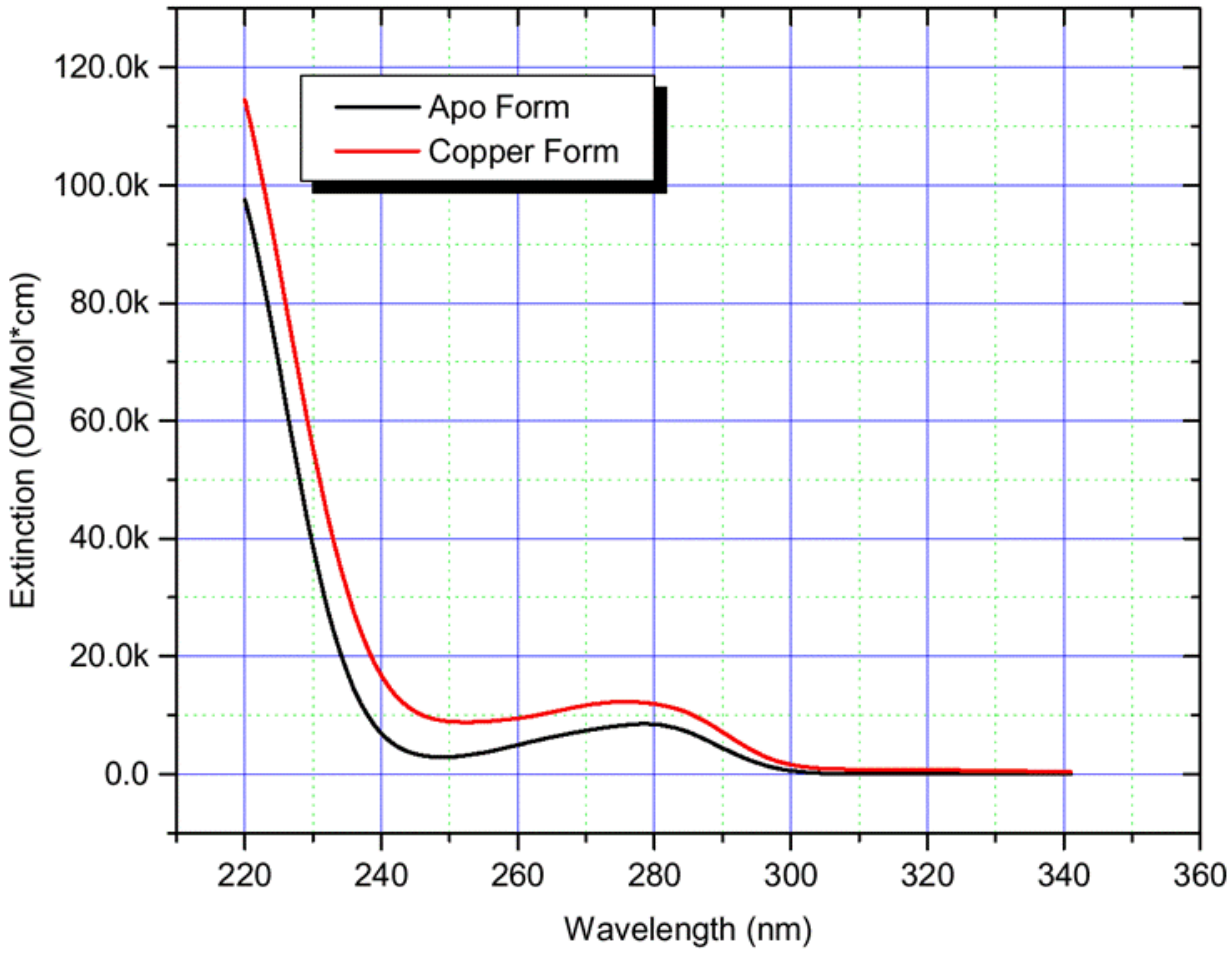

Figure 2-4. Extinction profile for the apo (black) and copper (red) form of PcoC. The profile was calculated from a global fit to multiple wavelength scans of the apo form as implemented in UltraScan. The profile has been normalized at 280 nm according to the method of Gill and von Hippel (38).

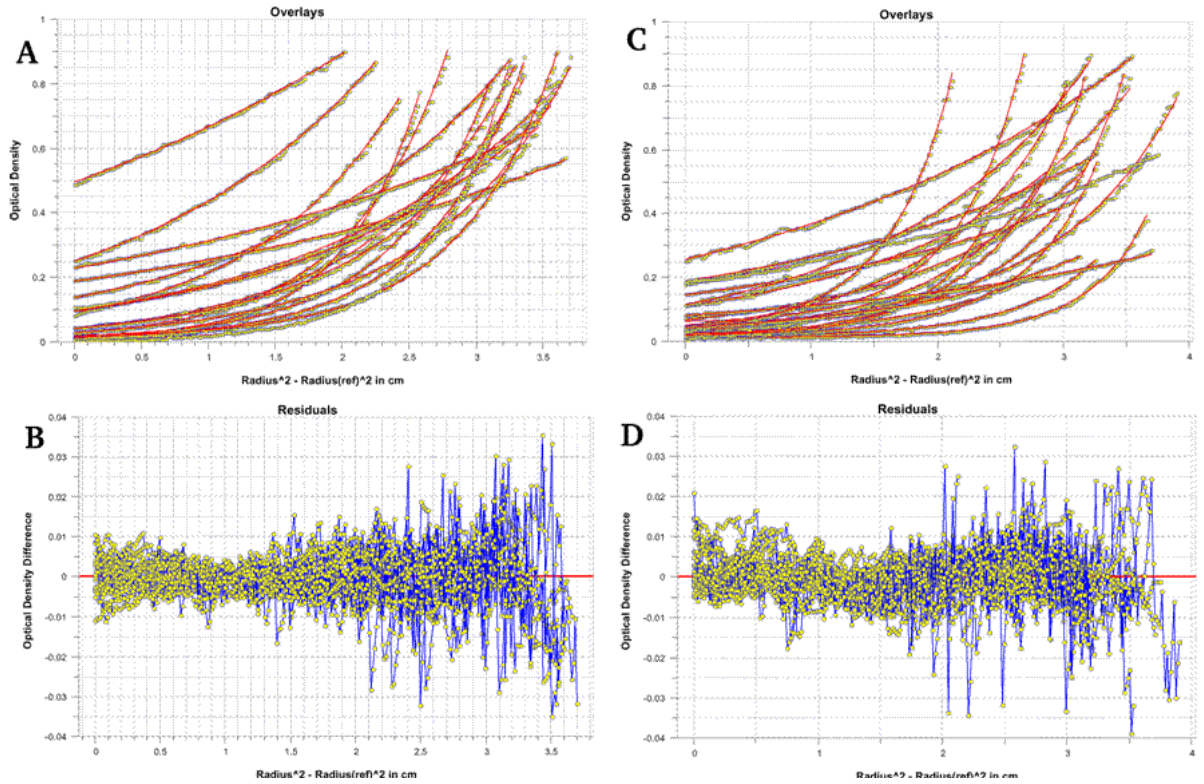

Figure 2-5. PcoC sedimentation equilibrium data analysis. Global monomer-dimer fit for the apo form (overlays in panel A, residuals in panel B) and the copper form (overlays in panel C and residuals in panel D). The residuals are randomly scattered about the mean, and increase in magnitude at higher optical densities because of loss of signal.

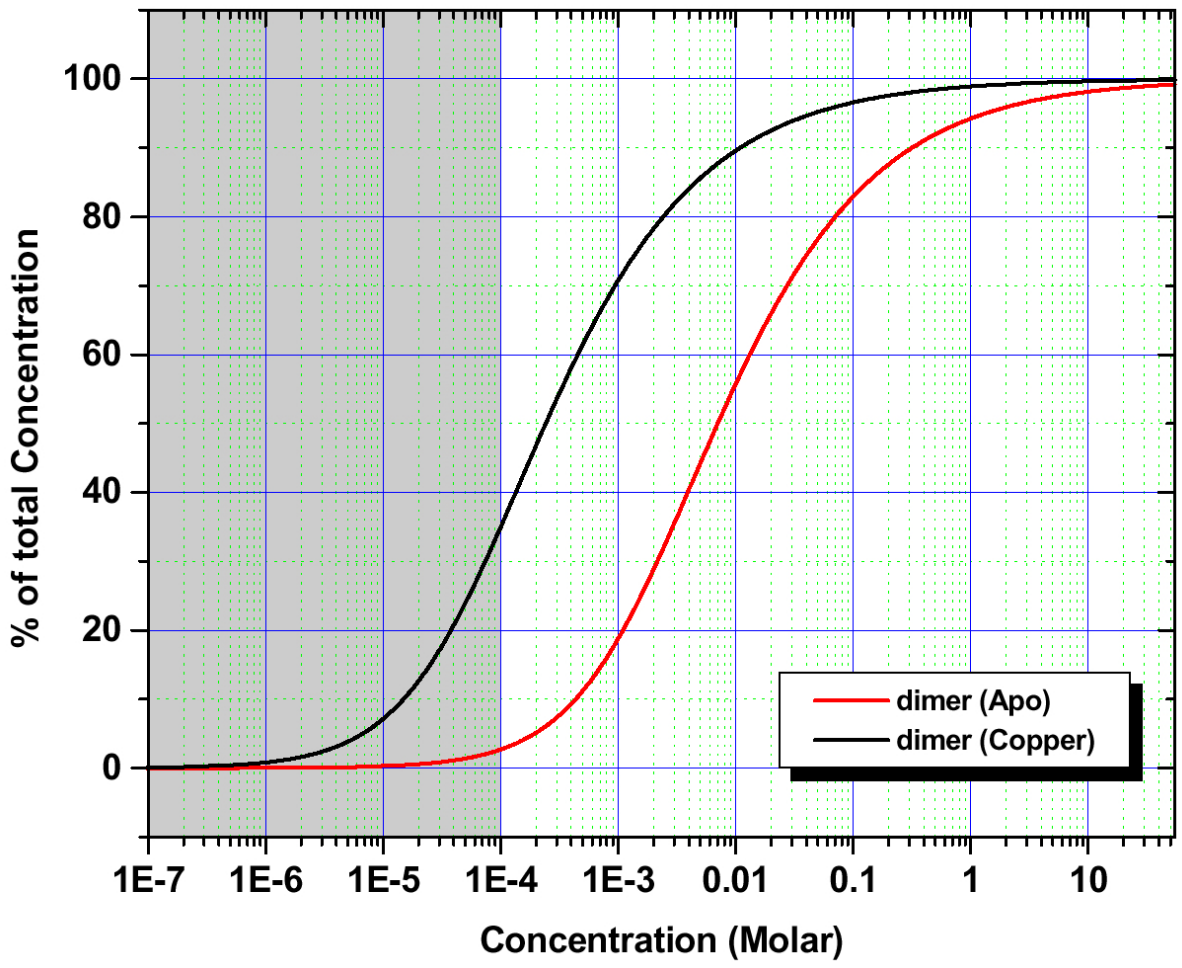

Figure 2-6. Monomer-dimer distribution plots for the apo (red) and the copper form (black) of PcoC. The relative dimer concentration is shown in black and the relative monomer concentration is shown red. The area inside the blue box indicates the concentration range in which the measurements were made. Due to the weak association of the apo form, very little dimer was observed at the concentration at which the measurements were taken.

Discussion

An analogy with the Atx1 copper chaperone (39)which delivers its metal ion cargo to the homologous domains of a copper processing enzyme, Ccc2, PcoC has been proposed to function as a copper chaperone that docks with the multiple repeats of Met-rich repeats of PcoA. The Cu(I) delivered by PcoC to PcoA would not become one of the catalytic coppers of the multicopper oxidase, but would rather be a source of reducing equivalents for the PcoA enzyme. A precedent for a transition metal acting as a substrate that provides reducing equivalents to an oxidase can be bound in the ferroxidase activities of ceruloplasmin and Fet3, multicopper oxidases which can catalyze the oxidation of Fe(II)(19). In the case of PcoA, oxidation would convert Cu(I) to the less toxic Cu(II) form(21) that could be subsequently conducted to other proteins in the copper resistance pathway for export across the outer cell wall. Other functions cannot be ruled out. For instance the copper-loaded form of PcoC may simply serve to catalyze electron transfer to the O_2-dependent multicopper oxidase PcoA or PcoC mayserve as a shuttle to deliver Cu(I) to an outer membrane component like PcoB. In the latter scenario, PcoA might contribute to the resistance by acting as a terminal oxidase that energizes membrane bound copper transport proteins.

Consistent with this model, PcoC possesses many of the characteristics that are increasingly seen to be shared in common among metal trafficking proteins. The soft, methionine-rich coordination chemistry us unlike that known for any other mononuclear Cu(I)

protein. Additionally, the work present in this chapter demonstrates a tendency for this protein to homodimerize in a metal-dependent manner.

The analytical gel filtration results indicate that on a qualitative level, Cu(I)-PcoC tends to form more homodimer than apo-PcoC under the same conditions. Since the interactions of a chromatography process can perturb the thermodynamic equilibria of such systems, while this data is qualitatively conclusive, it does not provide a good measure of the thermodynamics.

The fact that the PcoC dimer did run at a slightly higher apparent molecular weight than anticipated provides further confirmation that the NATIVE crystal structure may be more representative of the solution state of this dimer than the SEMET structure. Consistent with this result, the oblateness of this model is considerably greater than the SEMET structure. Since the calibration of analytical gel filtration chromatography is performed on globular proteins, the oblateness of a given protein is seen as a deviation from its expected retention volume.

However, in this case, the deviation from the expected retention volume of the dimer could also be interpreted to mean that in fact it is not a dimeric species but perhaps a trimeric species. To better resolve this issue, as well as to gain additional information about the strength of these interactions and to quantify how much they are increased by Cu(I), their interaction was investigated by analytical ultracentrifugation.

Equilibrium experiments performed on the copper and apo forms of PcoC are consistent with a reversibly self-associating monomer-dimer system, however the association constant is quite weak and the variance at 95% confidence level is high. Consistent with gel filtration data (30) a significantly stronger dimerization is observed for the Cu(I)-form. The monomer

molecular weights determined were in excellent agreement with the theoretical molecular weight derived from the protein sequence and with the molecular weight of 11,045 Da as determined by MALDI-TOF mass spectrometry of the pure apo-protein.

Taken together, these results demonstrate that PcoC can form stable, albeit weakly associated dimeric species in solution, leading us to conclude that the protein-protein contacts in the solid state may not be the result of adventitious packing interactions. The fact that two different types of dimers can be crystallized is consistent with a weakly associating system and a low barrier for the interconversion of the two dimeric forms. At this point, however, we cannot say whether the H-H or the H-T dimer, if either, is the dominant species in solution. The fact that Cu(I) binding favors significantly favors dimer formation ($\Delta(\Delta G°\Delta)$ = -8.0 kJ/mole) and the fact that XAS results indicate that Cu(I) binds to at least one Met and one His suggests that the H-T may be the preferred configuration for the Cu(I) protein; however at this time there is no proof of this model.

The unusual, solvent-exposed coordination chemistry, metal-induced homo-dimerization, and weak protein-protein interactions shown by this protein are consistent with its role as a metal trafficking protein. As an increasing number of these systems are identified and characterized, these characteristics are proving to be commonalities shared by metal trafficking proteins as unique to their function. It is remarkable that although our prototypical case, that of Atx1 and Ccc2a, is a pair of cytoplasmic, eukaryotic proteins, and here we have instead a quite different situation with a bacterial, periplasmic protein, yet still they accomplish similar roles using similar chemistry.

CHAPTER 3

ZntA(46-118): The Structure of Zinc-Specific Atx1 homolog suggests biologically novel Zn(II) coordination

Abstract

Many transition metals, including zinc, are both physiologically necessary and toxic when accumulated at high level. To provide the necessary levels under such strict control, the metal ions inside the cell are controlled by a variety of import, trafficking, and export proteins. E. coli, for example has several zinc transporting proteins, including the export pump ZntA, which is a P-type ATPase, and uses energy to actively pump zinc out of the cell. It is predicted to consist of two cytoplasmic and eight transmembrane domains. The structure of one of these cytoplasmic domains, ZntA(46-118), which is homologous to the yeast copper chaperone Atx1, was determined by NMR. Its bears remarkable homology to Atx1, even within its conserved –(M,L)XCXXC- metal binding motif, which raises the question of how this domain is able to selectively bind zinc whereas its counterpart binds copper. Additionally, the NMR structure revealed a biologically novel –cys-cys-asp- coordination of the zinc ion in the case where the protein is fully loaded with one zinc per monomer.

Introduction

Zinc is a transition metal element that is vital to cellular function and is actively concentrated by most cells. The extent of accumulation can be represented as the total number of zinc atoms per cell, a value known as the zinc quota. In *E. coli*, the zinc quota is maintained within a very narrow range corresponding to ca. 0.1-0.2 mM total Zn(II), even when the extracellular zinc concentration is increased from nanomolar to micromolar levels (1). When the Zn(II) concentration in a nutrient-rich medium is elevated beyond millimolar values, this metal is quite toxic, presumably because the cell accumulates Zn(II) beyond the acceptable zinc quota. Bacteria such as *E. coli* respond to excessive Zn(II) stress via inducible expression of several genes, however only a few proteins involved in bacterial zinc homeostasis machinery are known at this time. These include three zinc-responsive metalloregulatory proteins (1-7) which exert metal responsive transcriptional control of several *E. coli* operons. Calibration of two of these intracellular zinc sensors indicates that in spite of the high concentration of total zinc in a bacterium, the concentration of free Zn(II) is vanishingly small (1). In light of this, we have begun to examine the inorganic chemistry and structure of the cellular machinery that controls the availability of zinc within the cell. This machinery includes a group of membrane-spanning transporter proteins involved in the uptake or export of Zn(II) ions. Interestingly enough, we

have found in this system once again that metal trafficking appears to be accomplished using biologically novel, solvent exposed coordination chemistry.

E. coli has several zinc transporting proteins, including the P1-type ATPase ZntA, which is a Pb(II)/Cd(II)/Zn(II) export protein. Like other P1-type ATPases, ZntA is predicted to consist of two cytoplasmic and eight transmembrane domains (8). The N-terminal, cytoplasmic, 46-118 domain of ZntA exhibits a conserved –XXCXXC- metal binding motif and has been predicted to have a β–α–β–β–α–β fold (9). This domain has been shown to increase the overall catalytic rate of metal transfer by increasing the rate of metal ion binding to the transporter, even if it is not essential under some growth conditions (10).

These structural characteristics are shared by two distinct subgroups of the P1-type ATPase family that can be distinguished based on physiological data: those that transport metal ions such as Cu(I) and Ag(I), and those that predominantly handle divalent metals such as Zn(II), Cd(II) and Pb(II) (11). Detailed sequence alignment studies have suggested that the presence of negatively charged residues in the vicinity of the metal binding site may modulate the affinity of the protein for divalent over monovalent metal ions. In particular, the aspartate, located in the metal binding motif of ZntA, -GMDCXXC-, may be implicated in this role (9).

While many structures of Zn(II) containing metabolic enzymes are known, much less is known about the three dimensional structure, energetics, coordination chemistry or mechanisms of zinc transport proteins. The coordination chemistry in these two classes is expected to be quite different. In the case of the metabolic metalloenzymes, a Zn(II) cofactor is typically bound

tightly and the off-rate for loss of zinc can often be longer than the life time of the cell. The sensor and transport proteins on the other hand must be able to achieve rapid on and off rates.

To understand how the structure of the N-terminus of ZntA achieves its metal ion specificity and to gain an understanding of the surface of this domain, a region of the cytosolic N-terminal domain of ZntA that exhibited strong homology to the copper chaperone Atx1 was cloned and expressed. The solution structure was determined both in the apo- form as well as with zinc bound by NMR.

Experimental Procedures

ZntA(46-118) Cloning and Purification. ZntA(46-118) was cloned as previously described(12). The resulting plasmid, pET11c/ZntA(46-118), was transformed into BL21(DE3) (Novagen) for overexpression. The cells were grown in 9 L of LB / (100 μg/ml) carbenicillin at 37°C with shaking until OD_{600} = 0.6. At this point, protein expression was induced with the addition of 400 μM IPTG, and 2.5 hours later the cells were harvested by centrifugation and stored at -80 °C. After three freeze-thaw cycles, the cells were resuspended in 250 mL 50 mM Mes-Na, pH 6.0, 2 mM EDTA, 5 mM DTT. The cells were incubated on ice for 1.5 hours and then centrifuged to remove the cell debris. The freeze-thaw supernatant was loaded onto a DEAE anion exchange column (Pharmacia) equilibrated with 20 mM Mes, pH 6.0, 50 mM NaCl, 5 mM DTT. ZntA(46-118) did not bind to this column and was collected in the flow-through. The protein was

concentrated and loaded onto a High Load Superdex 75 gel filtration column (Pharmacia) equilibrated with 20 mM Mes, pH 6.0, 200 mM NaCl, 5 mM DTT. Fractions containing ZntA(46-118) were pooled, concentrated to ~ 1 mL, and stored in 20 mM Mes, pH 6.0, 200 mM NaCl, 5 mM DTT + 5% glycerol at -80 °C. MALDI-TOF analysis of this protein showed a molecular mass of 7925.7 Da, which indicates that the first methionine, corresponding to the start codon, is removed (calculated weight without 1^{st} Met = 7930.8 g). Typical yield is 51 mg per liter of cell culture.

Preparation of ^{15}N-labeled ZntA(46-118). ^{15}N labeled samples were prepared by inoculating a transformed colony of BL21(DE3)/pET11c/ZntA(46-118) into 5mL of LB / (500 μg/ml) carbenicillin and incubating with shaking at 37°C overnight. The culture was then pelleted, and the pellet was resuspended into 1L of minimal media for labeling (11.3 g Na_2HPO_4 $7H_2O$, 3 g KH_2PO_4, 0.5 g NaCl, 2 g $^{15}NH_4Cl$ per 1L) supplemented with 15 mL of 20% glucose, 2 mL of 1M $MgSO_4$, 2 mL of 0.2% thiamine, and 1 mL of 100 mg/mL carbenicillin. This culture was then incubated at 37°C until the absorbance at 600 nm is 0.6 a.u. At this point protein expression was induced with the addition of 500 μM IPTG, the culture was further supplemented with 1 g $^{15}NH_4Cl$ and 4 g glucose, and 8 hours later the cells were harvested by centrifugation and stored at -80 °C. The protein was then extracted and purified as described above. The purified protein was stored at -80°C in 20 mM Mes, pH 6.0, 200 mM NaCl, 5 mM DTT. Typical yield of ^{15}N-labeled protein was 23 mg per liter of cell culture.

NMR Sample Preparation. As a precaution against disulfide formation in proteins that contain a CXXC motif, these samples were prepared in a Vac atmospheres nitrogen chamber at 12 degrees Celsius. Protein concentrations were determined by the Bradford assay. This assay is run relative to a bovine IgG standard, which induced less dye color development than ZntA(46-118). Therefore, the concentration of a sample of ZntA(46-118) was independently calibrated by amino acid hydrolysis and it was determined that the Bradford assay overestimates the concentration of ZntA(46-118) by a factor of 2.15. Zinc concentration was determined by ICP-AES. The zinc/protein ratio was 0.9 with a protein concentration of 1.5 mM. The NMR samples of apo and metal loaded ZntA(46-118) were in 100 mM sodium phosphate buffer, pH 7, 90% H_2O/10% D_2O. The final protein concentration ranges between 1.5 and 2 mM. No exogenous thiols were added to the sample buffer in the case of Zn(II) form, while 2mM DTT was necessary to have a stable sample of the apo form. Approximately 0.6 ml of sample was loaded into high quality NMR tubes (Wilmad 535-PP 5 mm) that were capped with latex serum caps in the Vac Atmospheres chamber.

NMR measurements.

NMR measurements and data analysis were performed by our collaborators at CERM, University of Florence. The NMR spectra were acquired at 298 K on Avance 800, 700 and 600 Bruker spectrometers operating at a proton nominal frequency of 800.13 MHz, 700.13 MHz and

600.13 MHz, respectively. A QXI probe was used on the Avance 800 spectrometer and a TXI 5-mm probe was used on the 700 and 600 spectrometers. All probes were equipped with Pulsed Field Gradients along the z-axis. 2D TOCSY (13,14) spectra were recorded on the 700 or 600 MHz spectrometers with a spin-lock time of 100 ms, a recycle time of 1 s and a spectral window of 15 ppm. 2D NOESY maps (15,16) were acquired on the 800 or 700 MHz spectrometers with a mixing time of 100 ms, a recycle time of 1 ms and a spectral window of 15 ppm.

The 2D ^{15}N-^{1}H HSQC [44] maps and 3D NOESY-^{15}N HSQC experiments (100 ms mixing time) (17-19) were obtained at 700 MHz with an INEPT delay of 5.3 ms, a recycle time of 1s and spectral windows of 15 ppm and 33 ppm for the ^{1}H and ^{15}N dimensions, respectively (^{15}N labeled samples). HNHA experiments (20) were performed at 600 MHz to determine $^{3}J_{HNH\alpha}$ coupling constants.

Quadrature detection in the indirect dimensions was performed in the TPPI mode (16), and water suppression was achieved through WATERGATE sequence (21) in all NMR experiments. The 2D data consisted of 2K data points in the acquisition dimension and of 1K data points in the indirect dimension. All 3D and 2D spectra were processed using the standard Bruker software (XWINNMR) and analyzed on PC Linux computers through the XEASY program.

Constraints used in structure calculations. The NOESY peaks used for structure calculations were integrated in the 2D and 3D NOESY maps, and the volumes converted into upper distance limits with the program CALIBA (22). The calibration curves were adjusted

iteratively as the structure calculations proceeded. Stereospecific assignments of diastereotopic protons were obtained using the program GLOMSA(22). $^{3}J_{HNH\alpha}$ coupling constants were transformed in the backbone dihedral angles ϕ by means of the appropriate Karplus curve (20), with the ϕ angle ranges between –155° and –85° for $^{3}J_{HNH\alpha}$ larger than 8 Hz and between –70° and –30° for $^{3}J_{HNH\alpha}$ values lower than 4.5 Hz (23). Backbone dihedral angles ψ for residues (i-1) have been determined from the ratio of the intensity of the NOE cross peaks between the $H_{\alpha}H_{N}$(i-1,i) and $H_{N}H_{\alpha}$(i,i), found on the ^{15}N plane of residue (i) in the ^{15}N NOESY-HSQC (24,25). Ratio values for residue (i-1) larger than 1 are found for ψ values ranging between 60° and 180°, which are characteristic of β strands, while values smaller than 1 are obtained for ψ values between –60° and -20°, which are present in right handed α-helices (25). These angles were used as constraints in the DYANA calculations and Restrained Energy Minimization refinement.

Structure calculations

The structure calculations were performed using the program DYANA (26). The zinc ion was included in the calculations of the zinc-loaded form by adding a new residue in the amino acid sequence. This residue is formed from a chain of dummy atoms which have the van der Waals radii set to zero so they can freely penetrate into the protein and one atom with a radius of 1.4 Å, which mimics the zinc ion. The sulfur atoms of Cys 59 and Cys 62 and one oxygen atom of the side chain of Asp 58 were linked to the metal ion through upper distance limits of 2.5 Å.

This approach does not impose any fixed orientation of the ligands with respect to the zinc ion. 300 random conformers were annealed in 10000 steps using NOE and dihedral angle constraints. The 30 conformers with the lowest target function constitute the final family. Restrained Energy Minimization was then applied through SANDER module of AMBER 5.0 program package(27). The force field parameters for the zinc(II) ion were adapted from those already reported for similar zinc sites in zinc proteins and complexes (28-31). The NOE and dihedral angle constraints were applied with force constants of 50 kcal mol^{-1} $Å^{-2}$ and 32 kcal mol^{-1} rad^{-2}, respectively.

The program CORMA (32), which is based on relaxation matrix calculations, was used to check the agreement between the experimental and the back calculated NOESY cross-peaks, obtained from calculated structure. The quality of the structures were evaluated through Ramachandran plots using the programs PROCHECK (33) and PROCHECK-NMR (33). Structure calculations and analyses were performed on a Linux cluster processor computers.

Relaxation Measurements and Analysis

Relaxation experiments were collected on a Bruker Avance 600 spectrometer, operating at proton nominal frequencies of 600.13 MHz. 15N longitudinal and transverse relaxation rates, R1 and R2, were measured with pulse sequences already reported (34), but appropriately modified to eliminate cross correlation between dipolar and chemical-shift anisotropy relaxation mechanisms (35-37) and with pulsed field gradients to suppress the water signal. Relaxation rates were obtained using delays in the pulse sequence of 10, 40, 70, 150, 250, 380, 540, 740,

1000, 1350, 2000, and 3000 ms, for R1, and of 7.8, 15.5, 31.0, 62.1, 77.6, 108.6, 139.7, 170.7, 186.2, 217.3, 263.8 and 357.0 ms, for R2. Refocusing delays of 450 ms and for the Zn(II)-bound form also of 1150 ms were used in the R2 measurements. 1024 × 256 data points were collected for each map, using 8 scans for each experiment. The recycle delay was set to 2.5 s for both rates measurements. Spectral window of 40 ppm in the F1 (15N frequency) dimension and of 16 ppm in the F2 (1H frequency) dimension were used. Quadrature detection in F1 was obtained by using the TPPI method(16). Integration of cross peaks for all spectra was performed by using the standard routine of the XWINNMR program. Relaxation rates R1 and R2 were determined by fitting the cross-peak intensities (I) measured as a function of the delay within the pulse sequence, to a single exponential decay (38,39).

Errors on the rates were estimated through a Monte Carlo approach (40-42). An estimate of the overall tumbling correlation time and the local correlation times for the NH vector of each residue were derived from the measured R2/R1 ratios (R2 values with a refocusing delay of 450 ms are used in this estimate). In this analysis the relaxation rates of NHs experiencing exchange processes, which can contribute to the R2 value, were discarded. Residues are considered as experiencing conformational exchange processes if the following condition applies (43):

$$\left(\langle 1/R_2\rangle - 1/R_{2n}\right)/\langle 1/R_2\rangle - \left(\langle 1/R_1\rangle - 1/R_{1n}\right)/\langle 1/R_1\rangle > 1.5\times \mathrm{SD} \qquad [1]$$

Where $R_{2n,}$ R_{1n} are the R_2, R_1 values of residue n, $\langle 1/R_2\rangle, \langle 1/R_1\rangle$ are the average rates and SD is the standard deviation of the quantity in Eq. 1.

Results

Sequence-specific assignment of apo- and Zn(II)-ZntA(46-118)

The ^{15}N- HSQC maps of apo- and Zn(II)-ZntA(46-118) are shown in Figure 3-1A. A few signals exhibit sizable shift variations between the apo and the metal bound forms. Comparison of the weighted average chemical shift differences $\Delta_{avg}(HN)$ (i.e., $\{[(\Delta H)^2 + (\Delta N/5)^2]/2\}^{1/2}$, where ΔH and ΔN are chemical shift differences for ^{1}H and ^{15}N, respectively) (Figure 3-1B) (44) reveals that the largest shift differences are in stretches 57-65 and 81-85. The HN resonances of Asp 58, Cys 59, Ala 61 and Cys 62 experience the largest chemical shift differences and, in some cases, a sizeable broadening of these peaks is observed when the metal is absent. The chemical shift differences here observed are larger than those observed between the apo- and copper bound forms of other metal chaperones (45), but are similar to those observed in MerP, a protein involved in the transport of bi-positive mercury ions and displaying the same fold (46). All the other residues of the two forms have small or negligible chemical shift differences.

Assignments of the resonances of apo- and Zn(II)-ZntA(46-118) started from the analysis of the ^{15}N HSQC maps which allowed the identification of the ^{15}N and ^{1}HN resonances. Analysis of the 3D NOESY-HSQC and of 2D NOESY and TOCSY allowed sequence-specific assignment. Signals of 72 out of 73 residues were assigned both in the apo and Zn(II) forms of

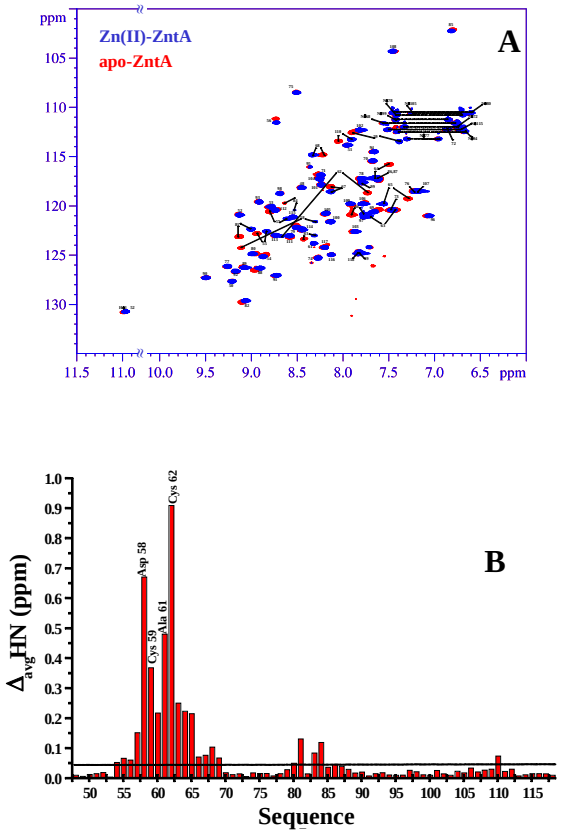

Figure 3-1. (a) Superposition of 2D ^{15}N–^{1}H HSQC spectra (600 MHz, 298 K) of Zn(II)-^{15}NZntA(46–118) (blue) and of the apo-^{15}NZntA(46– 118) (red). For both samples the protein concentration was about 1.5 mM, in 100 mM phosphate buffer. (b) The weighted average chemical shift differences D_{avg}(HN) (see the text) are shown. The line represents the error in the D_{avg}(HN) determination. Chemical shift differences are not reported for residues 46–47, as their ^{1}H–^{15}N cross-peaks are not observed for both forms.

ZntA(46-118). The first residue has not been identified in both forms. Both in the apo and in the Zn(II)-loaded proteins about 95% of the proton resonances could be located in the maps and 71 out of 73 ^{15}N backbone amide resonances have been assigned. The amide resonances are missing for the residues 46 and 47.

Secondary structures of apo- and Zn(II)-ZntA(46-118) from NMR data

The pattern of assigned NOEs indicated the presence of a few secondary structure elements. From their analysis it is apparent that the secondary structure is not significantly affected by the presence or absence of the zinc ion. Short and medium range backbone NOEs indicated the presence of two helices, characterized by a high number of sequential and medium range connectivities, of the type $d_{NN}(i,i+1)$, $d_{NN}(i,i+2)$, $d_{\alpha N}(i,i+3)$, $d_{\alpha N}(i,i+4)$, $d_{\alpha\beta}(i,i+3)$. These two helices involve residues 61-72 and 97-108. From the analysis of all backbone NOEs, four antiparallel β-strands, involving residues 48-54, 76-82, 86-93, 111-114 can be individuated. The pattern of NOEs shows that the typical folding pattern of the copper chaperones, "open-faced β-sandwich" fold (β1-α1-β2-β3-α2-β4), is present also in this protein (47-49).

Solution Structure Calculations and Analysis of apo-ZntA(46-118)

A total of 3284 NOESY cross-peaks was assigned, integrated and transformed in upper distance limits with the program CALIBA (22). They corresponded to 2208 upper distance limits, of which 1772 were found to be meaningful. The number of NOEs per residue is reported in Figure 3-2A. The average number of meaningful NOEs per residue is 24. 40 dihedral ϕ angle

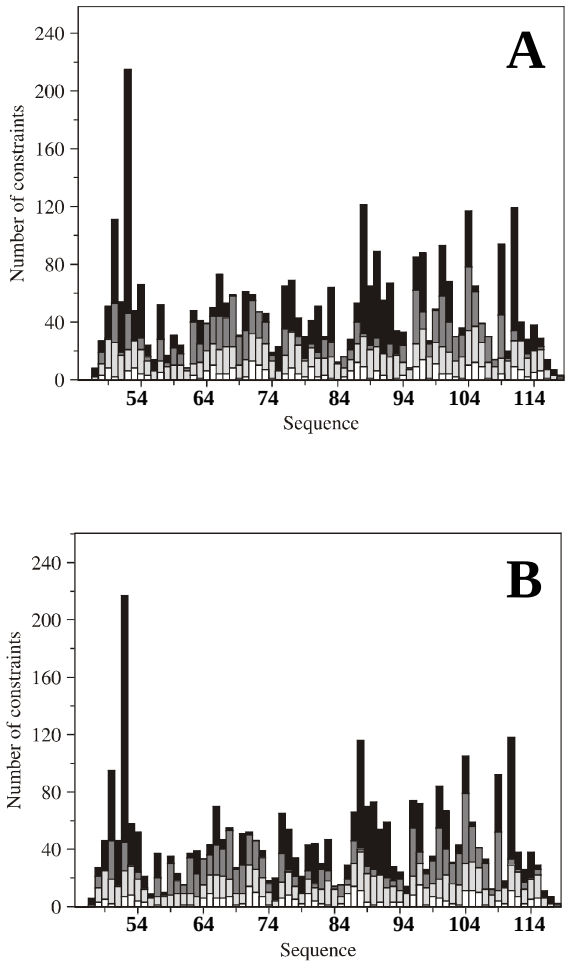

Figure 3-2. Number of meaningful NOEs per residue for apo-ZntA(46–118) (a) and Zn(II)-ZntA(46–118) (b) White, light gray, dark gray and black bars indicate intra-residue, sequential and medium-range and long-range connectivities, respectively.

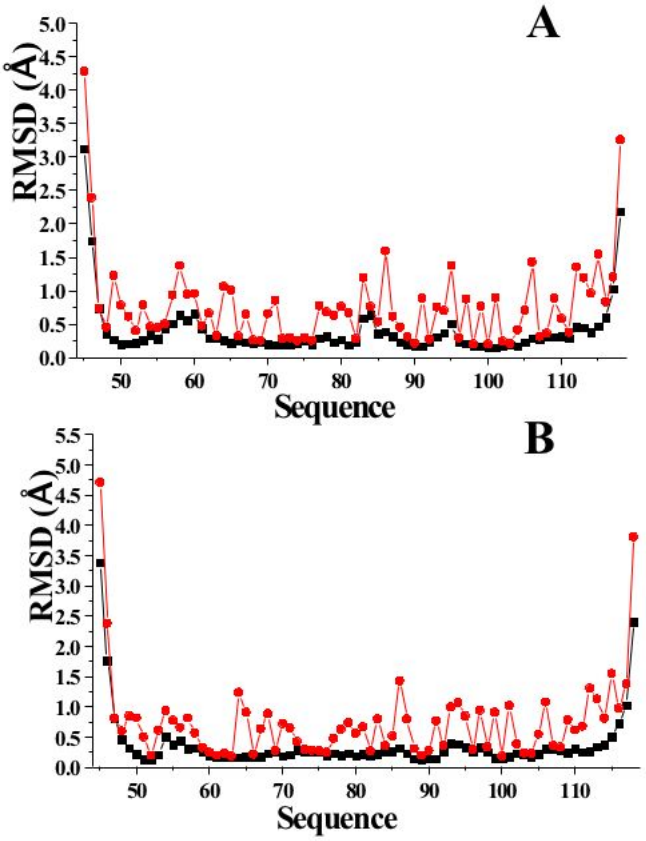

Figure 3-3. RMSD per residue from the mean structure of (a) apo-ZntA(46–118) and of (b) Zn(II)-ZntA(46–118) for the backbone (squares) and all heavy atoms (circles) of the REM structure of 30 conformers.

constraints and 47 ψ angle constraints were measured and used in the structural calculations. A total of 35 proton pairs were stereospecifically assigned through the program GLOMSA (22).

The 30 conformers constituting the final DYANA family had an average total target function of 0.55 ± 0.08 $Å^2$ and an average RMSD values to the mean structure (for residues 48-116) of 0.37 ± 0.06 Å for the backbone and of 0.83 ± 0.06 Å for the heavy atom. The family of conformers was then subjected to further refinement through Restrained Energy Minimization (REM) (27). The REM family has contributions to the average target function of 0.35 ± 0.08 $Å^2$ and of 0.04 ± 0.01 rad^2 from NOEs and the dihedral angle constraints, respectively. The average RMSD values (for residues 48-116) for the family with respect to the mean structure are 0.35 ± 0.06 Å for the backbone and 0.85 ± 0.07 Å for the heavy atoms. The RMSD values per residue of the final REM family to the mean structure are shown in Figure 3-3A.

The final family of conformers, shown in Figure 3-4A, was analyzed with PROCHECK-NMR (50). According to this program, the secondary structure elements in the energy minimized mean structure involve residues 48-55 (β1), 60-72 (α1), 75-82 (β2), 87-93 (β3), 96-108 (α2), and 110-114 (β4). Analysis of the NOE patterns has led substantially to the same conclusions (see before). In the energy minimized average structure, 76.5% of the residues are in the most favored regions of the Ramachandran plot, 17.6% of the residues are in the allowed regions and 5.9% of residues are in the generously allowed region. No residues are in the disallowed regions.

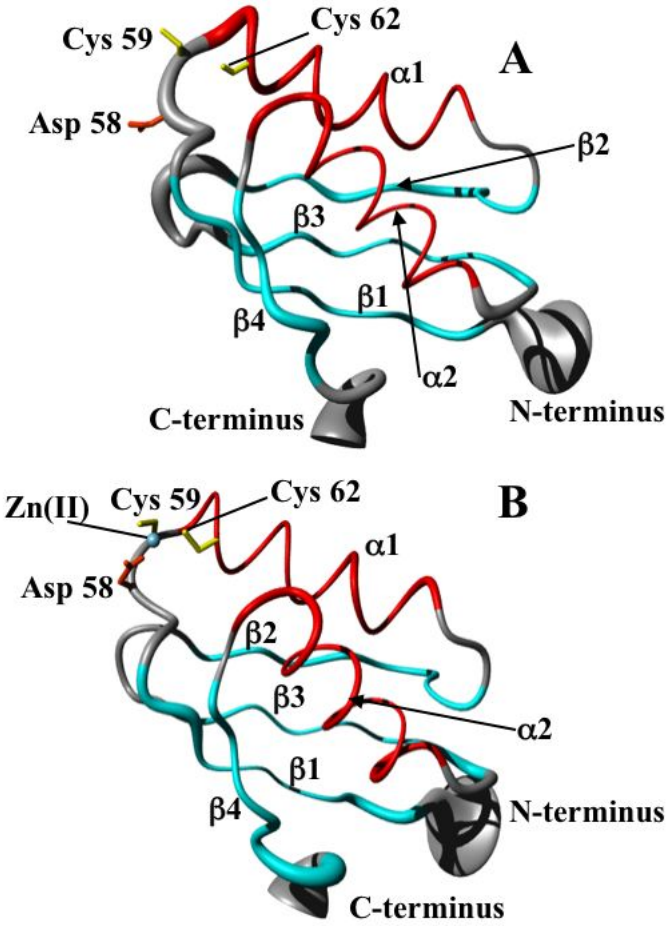

Figure 3-4. Backbone atoms for the solution structures (a) apo-ZntA(46–118) and (b) Zn(II)-ZntA(46–118) as a tube with variable radius, proportional to the backbone RMSD value of each residue. The side-chains of Asp58, Cys59, Cys62 and the Zn(II) ion are also shown. The secondary structure elements are indicated. The figure was generated with the program MOLMOL.

Solution Structure Calculations and Analysis of Zn(II)-ZntA(46-118)

A total of 2977 NOESY cross-peaks were assigned, integrated and transformed in upper distance limits with the program CALIBA (22). They corresponded to 2089 unique upper distance limits, of which 1656 were found to be meaningful. The number of NOEs per residue is reported in Figure 3-2B. The average number of meaningful NOEs per residue is 23 for Zn(II)-ZntA(46-118). 39 dihedral ϕ angle constraints and 47 ψ angle constraints were measured and used in the structural calculations. A total of 34 proton pairs were stereospecifically assigned through the program GLOMSA (22).

The structural calculations were initially performed applying upper distance limits only between the zinc ion and the two cysteines. The resulting family has a target function of 0.22 ± 0.03 $Å^2$ and average RMSD values to the mean structure (for residues 48-116) of 0.30 ± 0.07 Å for the backbone and 0.78 ± 0.10 Å for the heavy atoms. The low target function value supports the good quality of the structure; however, the zinc(II) ion typically exhibits a coordination number of 4 or higher. From a comparative analysis of sequences of putative zinc and cadmium transporting ATPases it emerges that a Asp residue is conserved in the metal binding consensus motif x'DCx'''x''''C (x'=M, L), which may facilitate the binding of a divalent cation(9). This residue is in fact present in the Zn(II)-ZntA(46-118) sequence. The backbone HN resonances of this residue, Asp 58, and those of Cys 59 and 62 as well, experience also larger chemical shift differences when comparing the apo and zinc loaded proteins. Finally, in the family of the conformers calculated with the zinc ion coordinated only to the two cysteines, one oxygen (Oδ1) of the carboxylate of Asp 58 is located at only 4.0 ± 1.0 Å from the zinc ion. No other amino

acids with potential ligating groups are within a suitable distance to coordinate the zinc ion. All these data support that Asp 58 is a potential ligand of the zinc ion. Therefore, we performed again the DYANA calculations with the Oδ1 of carboxylate of Asp 58 with an upper distance limit of 2.5 Å to the zinc(II) ion. The 30 conformers constituting the final DYANA family had an average target function of 0.21 ± 0.04 $Å^2$, i.e. identical to that obtained without this constraint. This indicates that the experimental constraints, which produce a structure at very high resolution, are completely consistent with a bond between the zinc ion and one or both of the oxygen atoms of Asp 58. The zinc site is quite solvent exposed, as it can be found from solvent accessibility calculations. This might suggest that the zinc coordination sphere may be completed by a water molecule or by an exogenous ligand.

The average RMSD values to the mean structure (for residues 48-116) are 0.31 ± 0.08 Å for the backbone and 0.77 ± 0.10 Å for the heavy atoms. The family of conformers was then subjected to further refinement through energy minimization(27). The REM family has contributions to the average target function of 0.37 ± 0.04 $Å^2$ and of 0.04 ± 0.02 rad^2 from NOEs and the dihedral angle constraints, respectively. The average RMSD values (for residues 48-116) for the family with respect to the mean structure are 0.31 ± 0.08 Å for the backbone and 0.79 ± 0.11 Å for the heavy atoms. The RMSD values per residue of the final REM family to the mean structure are shown in Figure 3-3B. It can be noted, as for the apo form, that the protein is very well defined throughout its the sequence with the exception of the N- and, in particular, the C-terminus parts.

The final family of conformers, shown in Figure 3-4B, was analyzed with PROCHECK-NMR (50). According to this program, the secondary structure elements in the energy minimized mean structure involve residues 48-55 (β1), 59-72 (α1), 75-82 (β2), 87-93 (β3), 96-108 (α2), and 110-116 (β4). The only relevant secondary structure difference with respect to the apo form is found for Cys 59 which has been processed by PROCHECK as an extension of helix α2 in the zinc bound state. In the energy minimized average structure, 69.1% of the residues are in the most favored regions of the Ramachandran plot, 23.5% of the residues are in the allowed regions, 7.4% of residues are in the generously allowed region and no residues are in the disallowed regions.

Mobility of Zn(II)- and apo-form of ZntA(46-118)

The experimental R_1 and R_2 values, measured at 600 MHz, of the amide ^{15}N nuclei of Zn(II)- and apo-ZntA(46-118) are plotted as a function of the protein sequence in Figure 3-5. For the Zn(II)-bound form R_2 values were measured with two refocusing delays to get information on the presence of possible exchange processes. In the Zn(II)- and apo-forms reliable R_1 and R_2 values have been obtained for 69 and 68 residues, respectively, out of the 71 assigned backbone NH resonances. In both forms the ^{1}H-^{15}N signals of the Arg 49 and Glu 118 amides are overlapped and their relaxation rates cannot be estimated and in the apo-form relaxation rate of ^{15}N backbone atom of Ala 60 could not be measured due to a poor signal to noise ratio of the

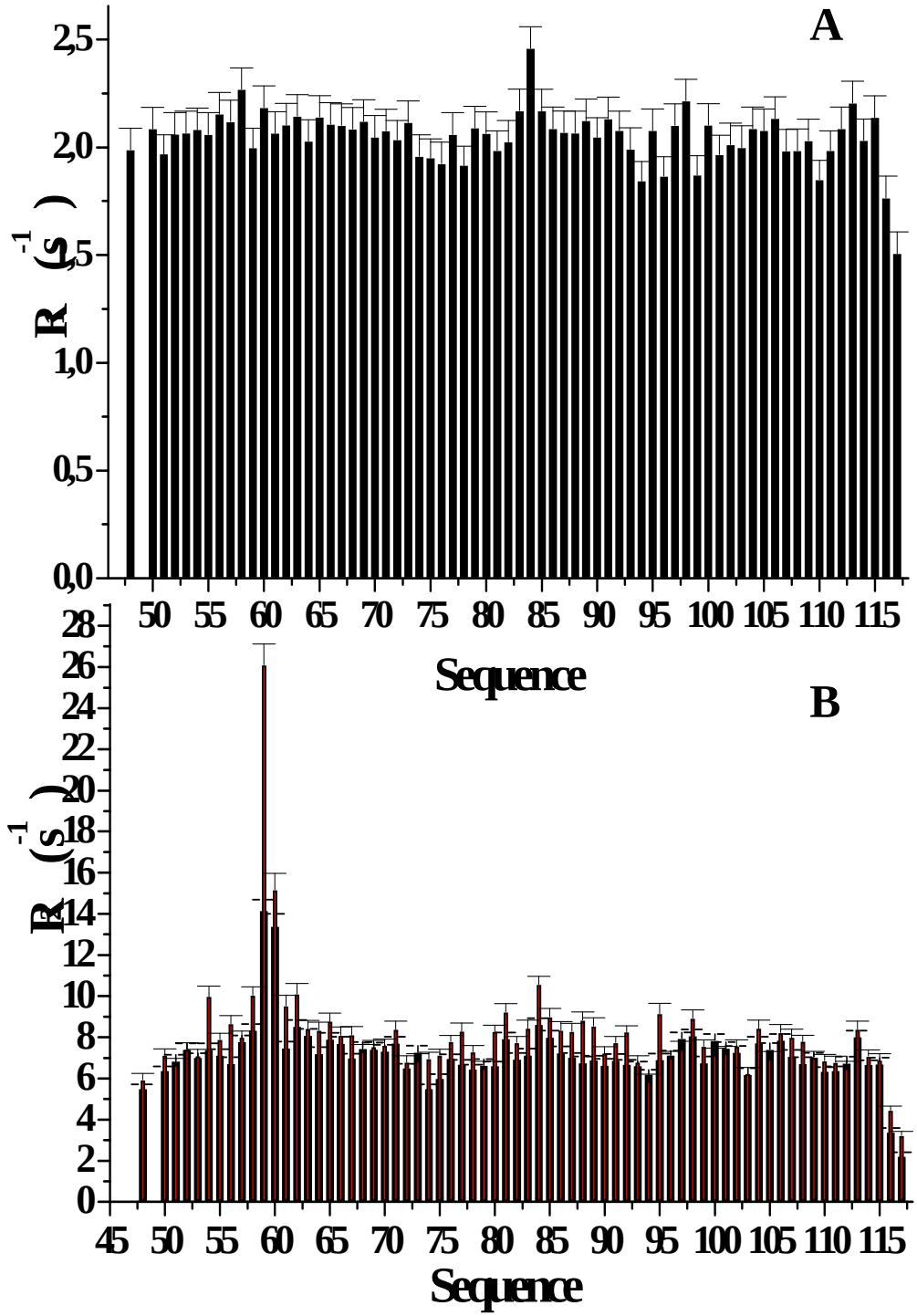

Figure 3-5. Experimental 15N relaxation parameters (a) R1 and (b) R2 for each residue in (black) Zn(II)- and (red) apo-ZntA(46–118) collected at 600 MHz.

peaks as a consequence of its line broadening. Average values of relaxation parameters R_1 and R_2 are 2.06 ± 0.10 s^{-1} and 7.13 ± 0.66 s^{-1} for the Zn(II)-form and 2.16 ± 0.09 s^{-1} and 6.69 ± 0.50 s^{-1} for the apo-form, respectively, considering only NHs R_1 and R_2 values within one standard deviation from the mean value. Two regions in both forms of the protein experience R_2 values deviating more than one SD from the mean value . The first region involves residues located in the zinc binding loop. In the Zn(II)-form, the zinc ligand Cys 59 and Ala 60 experience R_2 values higher than the average, suggesting that conformational exchange processes occurring in the ms-μs timescale contribute to the R_2 relaxation rate. Moreover, in the apo-form also Asp 58, Cys 62, i.e. the other Cys ligand, and Ala 61 show an increase in their R_2 values. In the Zn-bound form, measurements have been also preformed with long delays in the pulse train. They provided, only for residues 59 and 60 much higher R_2 rates, thus confirming the presence of conformational exchange processes. These result suggest that exchange motions in the ms-μs timescale are occurring in the metal binding loop. In the Zn(II)-form they involve only one of the zinc ligands and might contribute for an easy metal release of the metallochaperone; the same behavior was also observed for the N-terminal cysteine ligand in Cu(I)-Ccc2a (45). In the apo form these conformational exchange motions expand to the other two metal binding ligands, possibly making the empty metal binding site flexible enough to interact with the partner protein.

The other region of the protein with R_2 values deviating more than one SD from the mean value involves the C-terminal part of the protein, residues 116-117, which on the contrary shows reduced R_2 values respect to the mean value. This behavior suggests a flexibility in the ps-ns

timescale of this C-terminal protein segment, consistent with its low number of NOEs and high RMSD values. Indeed, it has been observed that unstructured protein regions show lower R_2 values than those typical of well-folded protein (51).

From the R_2/R_1 ratio an estimate of the τ_m was calculated for the protein. The values of τ_m is 4.9 ± 0.3 ns and 4.5 ± 0.3 ns for Zn(II)- and apo-ZntA(46-118), respectively. This value is consistent with the expectation from Stokes-Einstein isotropic model (52) for a molecule of about 8 kDa and is indicative of absence of aggregation. This value is very similar to those estimated, using the same approach, for other metal chaperones with analogous folding (45).

Discussion

Overall Structure of ZntA(46-118). The structures of apo and Zn(II)-ZntA(46-118), shown in Figure 3-4A and 3-4B, are well defined over all their sequences, with the exception of the C- and N-terminal regions which are disordered due to the lack of NOEs constraints. The average backbone RMSD value between the two minimized mean structures is 0.85 Å indicating that the overall folding of the zinc-bound and the zinc-free forms are essentially identical (Figure 3-6A). All the secondary structure elements are well superimposed. Loop 5, which contains the conserved residue Tyr 109, does not show any conformational change upon metal binding (Figure 3-6B). In the metal binding loop the side-chains of the two cysteine ligands and, in particular, of the potential ligand Asp 58 (RMSD HA 1.93 Å) are disordered in the apo state and span different conformations due to the small number of NOEs. When the metal is bound to the protein, the side chain of Asp 58 becomes more defined (RMSD heavy atoms 1.18 Å, in the absence of any bond between the Asp residue and the zinc ion; RMSD heavy atoms 0.84 Å, when a bond Asp/zinc ion is imposed in the strucrural calculations). Furthermore the conformation of all the three ligands does not change, on average, if the bonds with the metal ion are imposed or not in the structural calculations.

A novel Zinc Coordination environment. The most striking difference between the apo and Zn(II) structures is observed in the region containing the zinc binding ligands and in loop 3. In particular, residues 56-61, belonging to loop 1 and the first turn of helix α1, show a decrease in disorder, with backbone RMSD values of the family relative to the mean structure decreasing

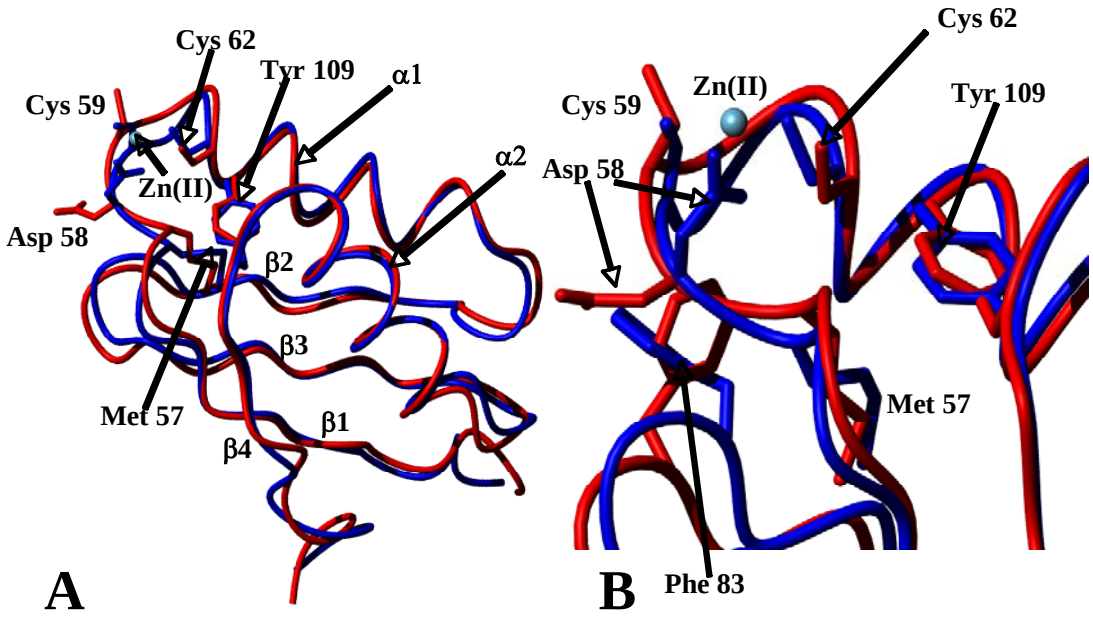

Figure 3-6. (a) Comparison between the backbone of apo- ZntA(46–118) (red) and Zn(II)- ZntA(46–118) (blue) and (b) of the metal binding region. The secondary structure elements are indicated. The ligands involved in the zinc binding, the Zn(II) ion and other relevant residues are shown.

from 0.69 Å in zinc-free form, to 0.29 Å, in the zinc-bound form (Figure 3-3). Loop 1 shows the largest difference in the local RMSD, with the most significant conformational changes involving Cys 59 and Asp 58 which move close to the zinc ion in the zinc-bound form, while Cys 62, located in helix α1, does not change orientation (Figure 3-6B).

In addition to two Cys and an Asp residues, a water or an exogenous molecule may complete the four coordinate geometry, since the zinc is rather solvent exposed. Calculations of the solvent accessibility show that exposure of Asp 58 and Cys 59 is high and remarkably increases when zinc is removed (from 33% and 26% in zinc bound form to 42% and 37% in apo form, respectively for the two residues), while Cys 62 is more buried (with 14% accessible surface for both zinc and apo forms). This solvent accessibility of a majority of the metal binding side chains is an emerging feature in the active site of these transport and chaperone domains (9,48,53). In contrast, most metal binding ligands in metalloenzyme active sites or the so-called structural zinc sites are more buried (54). The accessibility is likely to allow for rapid access of partner proteins to the metal site and thus facilitate metal transfer. Regardless of the precise nature of the additional exogenous ligand to zinc in this sample, this structure provides the first example to our knowledge of a zinc ion bound in a protein to two Cys and one Asp. Precedents for Asp or Cys ligands to zinc can be found in many types of hydrolytic zinc enzymes and zinc finger proteins(54), but the tridentate chelation of Zn(II) by two protein-based thiolates and one carboxylate is unprecedented for a zinc metalloprotein (55) [http://metallo.scripps.edu]. Two important caveats should be underscored for this novel Zn(Asp)$(Cys)_2$ site. First, given the limitations of NOE distance constraints in NMR methods, neither the precise Zn(II) coordination

number nor the geometry are resolved with the data in hand. Secondly, this is one domain of the cytosolic portion of ZntA. The P-type ATPase transporters are known to undergo a series of conformational changes as the cargo is passed from the cytosol through a membrane domain and then released to the distal side of the membrane. Thus, the zinc ion may interact in different ways in various steps in the metal transfer process as adjacent domains of the transporter, such as the N-terminal 45 amino acids or the Cys-motif in the C-terminal membrane segment, manipulate the coordination and position of the ion.

The metal binding loop: A Role of the Conserved Met? If the function of the protein is to release the Zn(II) ion to partner domains of the transporter in a facile manner, the conformation of the highly conserved GMDCXXC metal-binding loop will need to undergo displacements. The methionine in loop 1 (Met 57) is highly conserved between other N-terminal, membrane-tethered domains of heavy metal ATPases and small metallochaperones(9). Met 57 does not show large chemical shift differences upon zinc binding (Figure 3-1B) and it is not directly involved in metal ion coordination, as it points towards the hydrophobic core of the protein (Figure 3-6B). The conformation of its side-chain is well defined by several NOEs and its contacts with the residues surrounding it change little between the apo and Zn(II) bound forms. Met 57 makes key hydrophobic interactions with two aromatic residues, Phe 83 and Tyr 109, which are conserved in the sequences of putative zinc and cadmium transporting ATPases. Solvent accessibility calculations of the latter three residues demonstrate a low level of solvent exposure (from the lowest value of 1% for Met 57 to a maximum of 20% for Phe 83), confirming

that the region is highly hydrophobic. These results suggest that Met 57 functions in ZntA(46-118) as it does in Atx1 and Ccc2: as a hydrophobic tether that anchors the metal-binding loop via hydrophobic interactions that can modulate the conformational mobility of this region. (45,56).

Loop 3 shows higher RMSD values in the apo form (Figure 3-3). In particular Phe 83 is more ordered in the zinc-bound form with respect to the apo- form and adopts a different conformation in the two structures (Figure 3-6B). This residue, together with the conserved hydrophobic residue Val 81, also exhibits sizable chemical shift variations between the apo- and the metal bound form. All these data suggests that the zinc binding affects the structural rearrangement of this region, which, together with Tyr 109, may force the metal binding loop to assume a specific orientation for the metal binding.

Metal ion specificity. Biochemical and physiological data suggest that there is some overlap in the specificity of these Atx1-like domains (11,57). Furthermore, metal binding to the domain need not correlate with activity. For example, ZntA is biochemically activated by and confers resistance to Zn(II), Cd(II) and Pb(II). The N-terminal domain of ZntA can also bind Hg(II) and this metal can stimulate the ATPase activity of the full length protein(58); however ZntA does not confer any resistance against mercury toxicity. Likewise, ZntA does not appear to transport Ag(I), but this metal can stimulate ATPase activity competing with the ability of Zn(II) to stimulate the formation of key intermediate phosphorylation state of the enzyme. Thus metal specificity in these domains is not a simple function of the coordination site. This being said,

there are several structural, mechanistic and physiological features that can be gleaned by comparing this ZntA domain with other ATPases.

The structures of apo- and Zn(II)-ZntA(46-118) share the identical βαββαβ protein fold of copper(I) chaperones (53) (59,60) and of the N-terminal soluble domains of ATPases involved in the copper(I) transfer (48,61). These proteins also share the same metal binding motif MXCXXC which raises the question of how they discriminate between different metal ions. Clearly, discrimination between Cu(I) and Zn(II) is a significant physiological issue in bacterial, fungal and mammalian cells. Comparison of the coordination site in ZntA(46-118) with those in the copper chaperone-like proteins provides some of the structural underpinnings for understanding metal specificity.

In Figure 3-7A the structure of Zn(II)-ZntA(46-118) is shown superimposed with those of the first soluble domain of an eukaryotic ATPase, Ccc2a from *Saccharomyces cerevisiae*, and of the second domain of a bacterial ATPase, CopAb from *Bacillus subtilis*, both in the Cu(I) loaded states. The overall folding of the proteins is essentially identical, the global backbone RMSD value between the Zn(II)-ZntA(46-118) and the two copper proteins being 1.46 Å (Ccc2a) and 1.67 Å (CopAb). The secondary structure elements are well superimposed, and loop 5, which contains the conserved Tyr/Phe residue (109 in the present protein), does not exhibit conformational differences. Only a few key-residues belonging to loop 1 shows significant differences in the local RMSD. The most relevant conformational change involves the Asp/Thr residue (Asp 58 in the present structure) and the first cysteine, whose side-chains have a different arrangements in the zinc bound form with respect to the copper-bound forms, while the second cysteine, located in helix α1, does not change position (Figure 3-7B).

Sequence analysis lead to an earlier suggestion that Asp 58, which is found in the first variable position of the GMXCXXC consensus motif for all predicted ZntA-like sequences, may modulate metal-binding affinity/specificity(9). Moreover, in this position there is almost always a Thr residue in the copper chaperone-like sequences. In other copper-protein structures a short Cu(I)-Oγ(Thr) distance is found, which might suggest a second shell interaction (49,61,62). Furthermore, in a recent metal bridged homodimeric structure of human Atx1 this Thr is involved in hydrogen bond formation with a coordinated Cys(60); this interaction may modulate the Cu(I)-S-Cys bond strength and can thus assist in the metal transfer event.

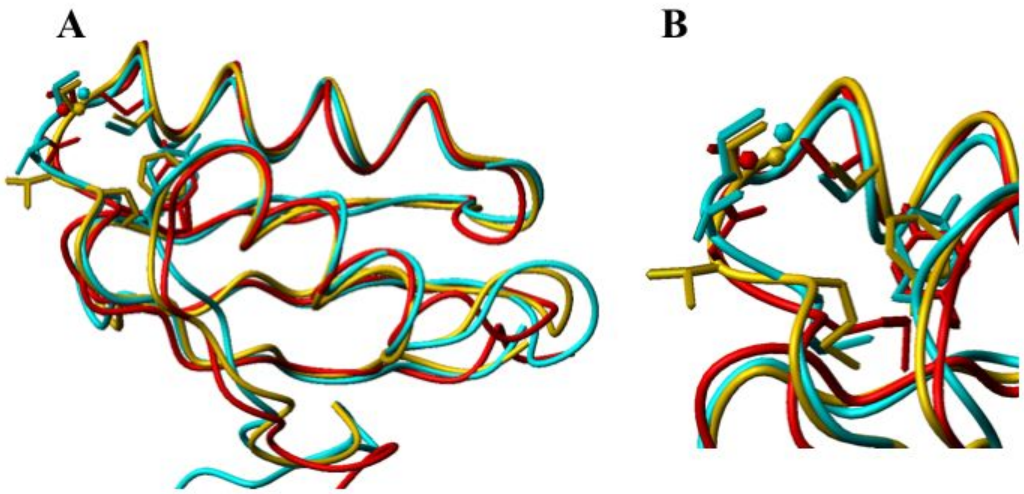

Figure 3-7. (a) Comparison of the backbone of Zn(II)-ZntA(46–118) (red) with Cu(I)-Ccc2a from S. cerevisiae (yellow) and Cu(I)-CopAb from B. subtilis (cyano). (b) Comparison of the metal binding region. The ligands involved in the metal binding, the metal ions and other relevant residues are shown.

All these data suggest that the amino acid at the position immediately preceding the N-terminal Cys in the metal binding loop (Asp 58 in ZntA(46-118)) plays a role in metal ion specificity. As described above we conclude that the aspartate belonging to loop 1 forms a coordinate-covalent bonding interaction with the Zn(II), thus discriminating against binding of Cu(I) in favor of Zn(II) on the basis of two facts. Firstly, the presence of three negative charges (one aspartate and two cysteines) will provide a more favorable electrostatic contribution to the bond energies for a 2+ zinc ion over the 1+ copper ion. Secondly, in terms of hard/soft acid base theory, the Asp oxygen will stabilize binding of the harder or less polarizable Zn(II) ion with respect to highly polarizable ion Cu(I).

These domain structure differences do not come down to a simple division between +2 transition metal ion binding to ZntA-like sites and +1 cations to Atx1-like sites. For instance MerP, a protein involved in bacterial mercury detoxification, uses the MXCXXC motif to bind Hg(II), another +2 ion; however, unlike ZntA(46-118), there is a Thr at the first variable position corresponding to Asp 58 (63). The structure is similar to that of ZntA(46-118) with the Hg(II) bound by two cysteines (Figure 3-8A). The most important differences are observed in the shallow binding pocket, in particular for the side chain of the first cysteine (Figure 3-8B), which is differently oriented in the two structures, and for residue Thr 13, which is far from the metal flipping away towards the solution. The conformation of the other cysteine is very similar between the two structures. This environment allows the Hg(II) to adopt a linear two coordinate

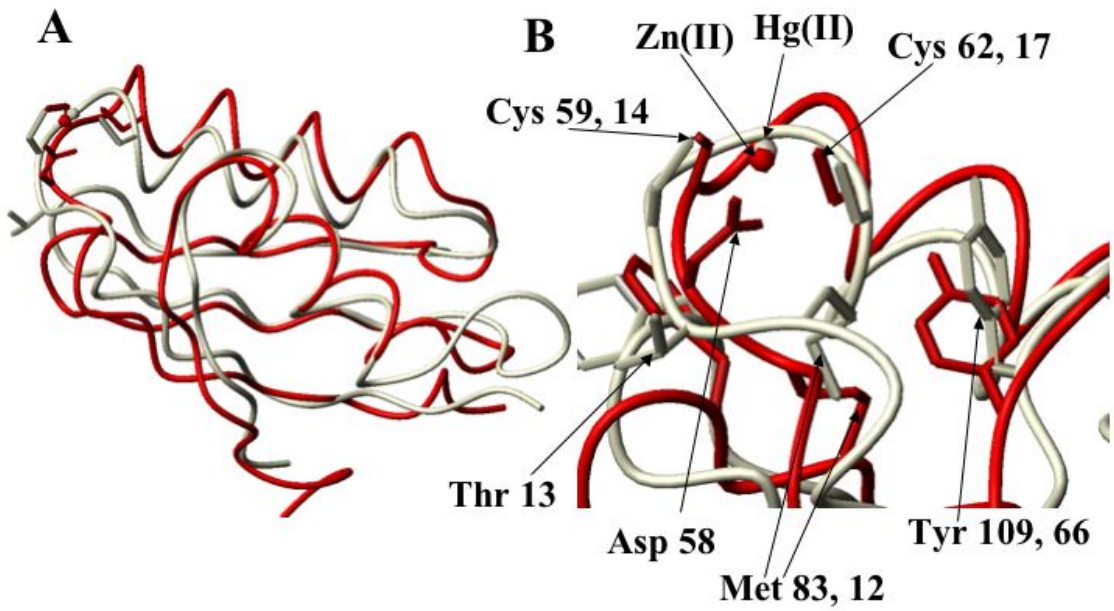

Figure 3-8. (a) Comparison between the backbone of Zn(II)-ZntA(46–118) (red) with Hg(II)-MerP from *Shigella flexineri* (light yellow). (b) Comparison of the metal binding region. The ligands involved in the metal binding, the metal ions and other relevant residues are shown. The structures were superimposed according to the sequence alignment and the global backbone RMSD.

S-Hg-S geometry that is quite stable for Hg(II) (64,65). The energetic contribution to stabilization from a third ligand can be minimal in the case of Hg(II) (66).

Therefore, we propose that the absence of the Asp residue in the MerP protein is one factor that favors MerP binding of Hg(II) over Zn(II). Given that Hg(II) can accommodate three and even four coordinate geometries, the converse is not likely to be true, namely the Asp in ZntA is not likely to provide significant discrimination against Hg(II) binding, as indeed ZntA binds Hg(II).

Finally, ZntA(46-118) and MerP share a common structural feature involving the Phe located in loop 3, Phe 83 and 38 respectively. This aromatic residue undergoes a similar structural rearrangement upon metal binding. This might be another factor determining the metal-binding affinity and specificity or it might be important for protein-protein interaction with its protein partner (63).

CHAPTER 4

Chapter 4. Coordination Chemistry of the N-terminal Domain of ZntA, ZntA(46-118).

Abstract

The NMR structure of ZntA(46-118) suggested a biologically novel –cys-cys-asp- coordination of the zinc ion. Here we report changes in the coordination chemistry of the Zn(II) ion that involve its function as a trafficking protein. The results for Zn(II) and other cations, such as Cd(II) and Co(II), provide insights into whether, in the physiological context of the cytoplasm, where zinc concentrations are differentially small, this coordination will be observed. In addressing these questions, the coordination of zinc in the Atx1-like domain of ZntA, ZntA(46-118), was examined by EXAFS at various levels of metal loading and found that the coordination changed from S_4 at low Zn(II) levels to S_2O_2 at higher levels of Zn(II). Additionally, we investigated the ^{113}Cd-NMR and behavior of the protein by gel filtration

chromatography under these conditions and found that the coordination of the cations at high concentrations may be more specifically described as S_2O_2. The results lead to a zinc transfer mechanism for this metal traffick problem in which the metal-loaded domain interacts with a metal-free domain to form a metal-bridged homodimer. We propose that this type of reversible dimer formation is part of the physiological function as a metal trafficking protein.

Introduction

Many transition metals, including zinc, are both physiologically necessary and yet toxic when accumulated at high levels(1). To provide the necessary levels under such strict control, the metal ions inside the cell are controlled by a variety of import, trafficking, and export proteins(2). E. coli, for example has several zinc transporting proteins, including the export pump ZntA, which is a P-type ATPase, and uses energy to actively pump zinc out of the cell(3-5). It is predicted to consist of two cytoplasmic and eight transmembrane domains(6). The structure of one of these cytoplasmic domains, which is homologous to the yeast copper chaperone Atx1, was determined by NMR as described in the previous chapter(7). It bears remarkable homology to Atx1, even within its conserved –(M,L)XCXXC- metal binding motif, which raises the question of how this domain is able to selectively bind zinc whereas its counterpart binds copper. Additionally, the NMR structure suggested a biologically novel –cys-cys-asp- coordination of the zinc ion in the case where the protein is fully loaded with one zinc per monomer.

Yet the NMR study did not directly interrogate the coordination of the Zn(II) ion. Nor did it address whether this coordination was physiologically relevant; in the physiological context of the cytoplasm, where zinc concentrations are differentially small, will this coordination be observed? To address these questions, the coordination of zinc in the Atx1-like

domain of ZntA, ZntA(46-118), was examined by EXAFS at various levels of metal loading. Additionally, the coordination of this site by Cd(II), another metal ion known to bind this protein *in vivo* was also examined.

While the EXAFS data provides information about the number and kind of ligand, it cannot distinguish a nitrogen ligand from an oxygen ligand. The ^{113}Cd nuclei is known to be sensitive to the difference between these two ligands. To further probe these subtle differences in coordination sphere, the ^{113}Cd-NMR of the site was determined.

Furthermore, the characterization of the coordination sphere is greatly simplified if it can be determined whether the ligands coordinating the metal ion are provided by one or multiple proteins. Therefore, we investigated the behavior of the protein by gel filtration chromatography under the same conditions as that of the Zn(II) EXAFS.

Experimental Procedures

ZntA(46-118) Cloning and Purification. ZntA(46-118) was cloned and purified as described in the previous chapter.

Analytical Gel Filtration. Analytical gel filtration was performed on a Superdex 75 HR 10/30 column at 4°ΔC using a BIO-RAD Biologic HR chromatography system. After equilibration in 100 mM Tris/Cl, 150 mM NaCl, pH 8.0, 250 μL of 100 μM apo- or Zn(II) ZntA were injected onto the column. The samples were then eluted in 100 mM Tris/Cl, 150 mM NaCl, pH 8.0 at a flow rate of 0.5 mL/minute. The retention volume (Ve) of each peak was recorded. These retention volumes were then compared to a calibration curve of vitamin B12, aprotinin, and Rnase A where (Ve-Vo) /(Vt-Vo) was plotted against the log of the molecular weight to give a straight line, Vo being the void volume of the column and Vt the bed volume of the column.

Preparation of Zn-EXAFS Samples. All sample preparation was performed an a Vac Atmospheres glovebox under nitrogen to prevent oxidation of the cysteines. Samples of ZntA (46-118) were prepared in an Amicon ultrafiltration device with a YM3 membrane in 100 mM Tris/Cl, pH 8.0. Apo-ZntA was pre-reduced by the addition of DTT to a final concentration of 5 mM. Excess reductant was then removed by three rounds of successive dilution and concentration with the Tris buffer. Following this, $ZnSO_4$ was added in the stoichiometric ratio

desired of the final sample. Unbound metal was removed by three rounds of successive dilution and concentration with the Tris buffer. The protein and metal ion concentrations of the final samples were measured by calibrated Bradford assay and ICP-AES, respectively. Samples were prepared to have approximate Zn:ZntA ratios of 0.5 :1 and 1:1. At final dilution, the samples were prepared to have a 1.0 (2) mM final concentration in ZntA and 30% concentration of glycerol. The samples were then loaded into EXAFS cells in the glovebox, and frozen at -37° C.

Preparation of Cd-EXAFS Sample. Sample preparation was performed by Dr. Caryn Outten. Briefly, the sample preparation followed the same preparation as that for the Zn-EXAFS samples described above with the exception that Cd was added in place of the Zn (?).

Preparation of ^{113}Cd-NMR Sample. Sample preparation was performed by Dr. Caryn Outten. The sample preparation generally followed that described above for the Cd-EXAFS sample, except that the ^{113}CdO (U.S. Services, 89% enrichment) was used as the Cd source. Additionally, the sample was placed into a final buffer of deuterated 50 mM PO_4/Na^+, pH^* 7.4. The final concentration of this sample was 7.7 mM ZntA with a Cd:ZntA ratio of 0.9 as determined by calibrated Bradford assay and ICP-AES respectively.

Co(II)-ZntA(1-118) UV-Vis. These experiments were carried out in a Vac Atmosphere anaerobic chamber to prevent oxidation of the cysteines or the cobalt. An equivalent of ultrapure cobalt nitrate was presented to ~200 μM protein in 100 mM Bis-Tris, pH 7.4. The concentration

of cobalt was determined by ICP-AES using a Thermo Harrell Ash AtomScan 25 ICP-AE spectrometer. The concentration of protein was determined by using the Bradford assay (Bio-Rad), which had been independently calibrated to overestimate protein concentrations by a factor of 2.15. A UV-Vis spectrum of the sample was also run.

Results

EXAFS spectroscopy of Zn(II)-ZntA(46-118). In the case where 0.5 Zn(II) per ZntA monomer is bound, the EXAFS data is a single peak at R+α = 2.35 Å. In the case where 1 Zn(II) per monomer is bound, a second peak corresponding to R+α = 2.02 Å also appears. An intermediate case, where 0.8 Zn/ZntA are loaded, has data which is also intermediate, and best fit by S_3(N/O) coordination (Figure 4-1, 4-2). The fully loaded case is most consistent with $S_2(N/O)_2$ coordination (Table 4-1). This is in agreement with the NMR structure which shows Zn(II) coordination of fully loaded Zn(II)-ZntA(46-118) by two cysteines and an aspartate. The half zinc loaded case is best described as a shell of four cysteine ligands.

Analytical Gel Filtration of apo-and Zn-ZntA(46-118). By gel filtration chromatography, the apo protein appears to run on a size exclusion column as a single gaussian peak (Figure 4-3), corresponding to about 9700 Da, which may indicate some anisotropy in its shape. At low levels of metal loading, such as for 0.5 Zn/ZntA, the protein runs as two overlapping peaks, with one of the peaks aligning with the apo protein and a second appearing at a higher molecular weight,

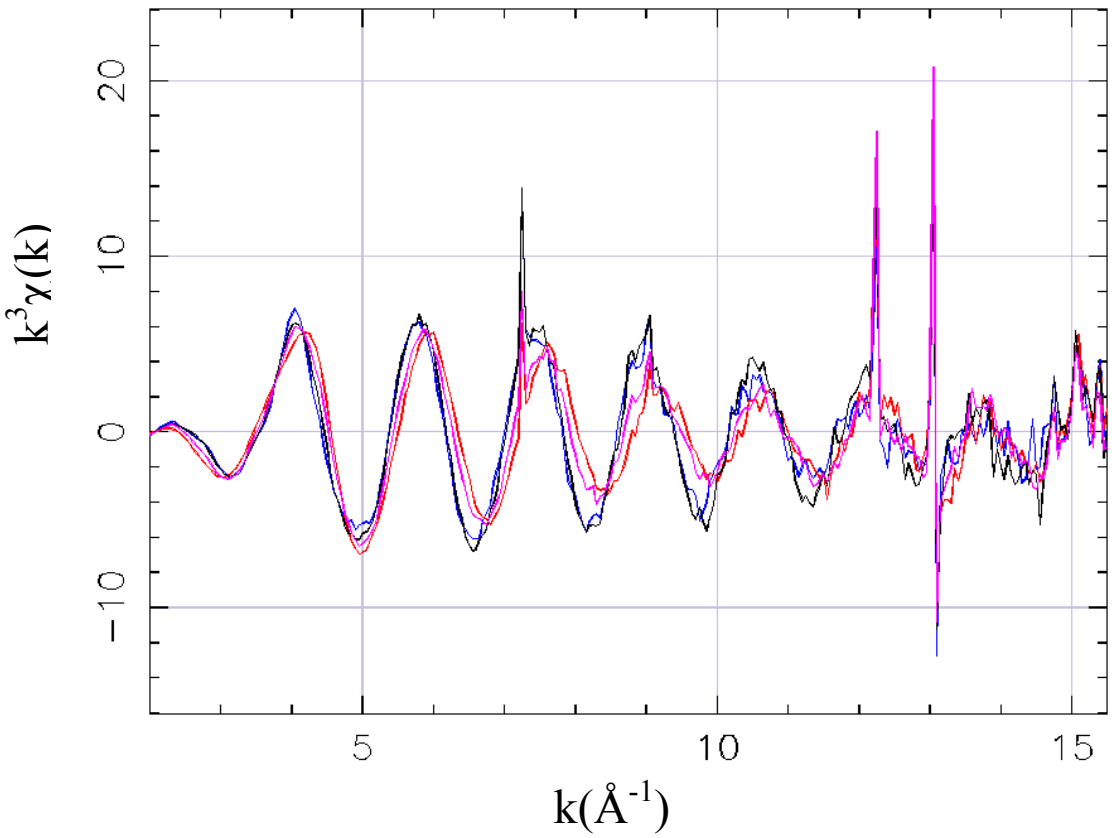

Figure 4-1. The k^3 weighted Zn K-edge EXAFS data on Zn-ZntA(46-118). Samples with approximately 0.5 Zn/ZntA (black and blue), 0.8 Zn/ZntA (pink), and 1.1 Zn/ZntA (red) are shown.

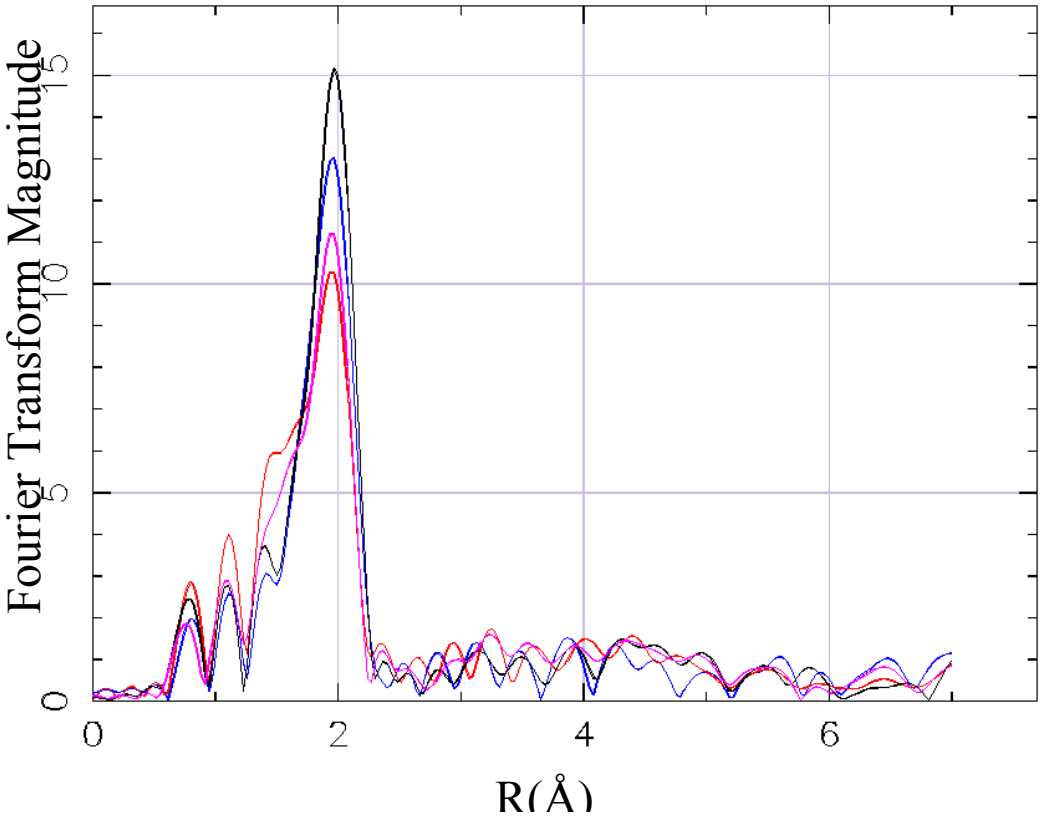

Figure 4-2. Fourier Transform of EXAFS data on Zn-ZntA(46-118). Samples with approximately 0.5 Zn/ZntA (black and blue), 0.8 Zn/ZntA (pink), and 1.1 Zn/ZntA (red) are shown. The increase in the intensity at lower radii as a function of increasing levels of Zn(II) is indicative of the greater number of (N/O) ligands bound to Zn in these samples.

Sample	Pi	Coordination Number	Bond Length	DW	F'
ZntA1	94.8 %S	4S	2.346	5.5	1.34
0.47:1					
ZntA2	51.3 %S	2N	2.039	4.5	3.33
1.09:1		2S	2.311	2.6	
ZntA3	91.4 %S	4S	2.342	4.3	1.58
0.49:1					
ZntA4	68.8 %S	1N	2.024	3.6	1.04
0.79:1		3S	2.324	4.5	

Table 4-1. Zn(II)-ZntA(46-118) EXAFS Fit Results. Integer coordination numbers giving the best fit are shown. The Bond length is given in angstroms. Also given is the Debye-Waller factor x 10^3 in $Å^2$. In the case where 0.5 Zn(II) per ZntA monomer is bound, the EXAFS data is a single peak at $R+\alpha = 2.35$ Å. In the case where 1 Zn(II) per monomer is bound, a second peak corresponding to $R+\alpha = 2.02$ Å also appears. An intermediate case, where 0.8 Zn/ZntA are loaded, has data which is also intermediate, and best fit by $S_3(N/O)$ coordination (Figure 4-1, 4-2). The fully loaded case is most consistent with $S_2(N/O)_2$ coordination.

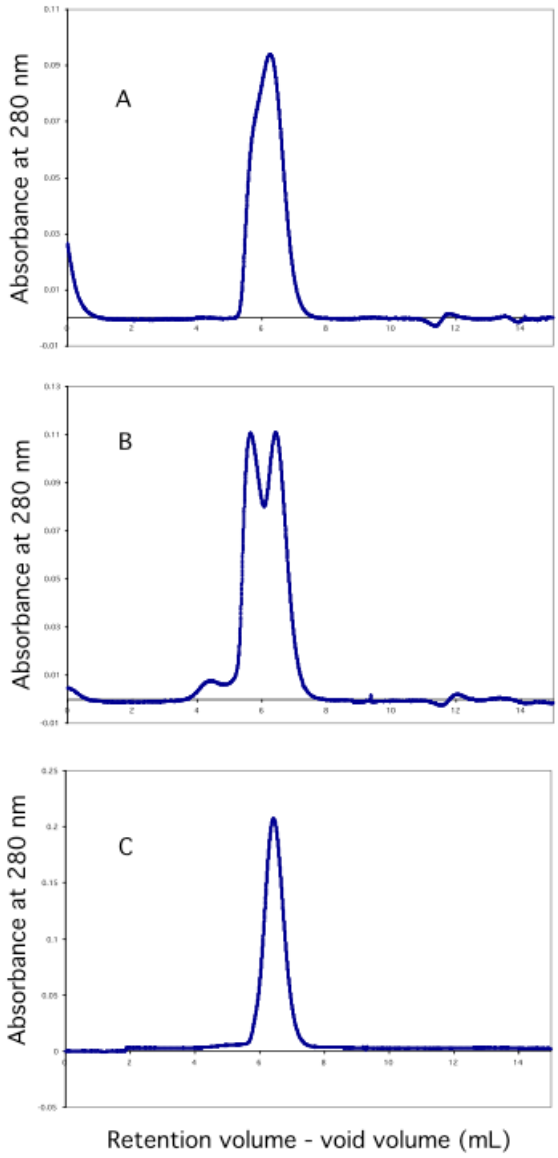

Figure 4-3. Gel Filtration Chromatograms of ZntA(46-118). Panel A is a sample of 1.1 Zn:ZntA(46-118), panel B is 0.47 Zn:ZntA(46-118), and panel C is apo-ZntA(46-118). All of the samples are injected as 250 uL of 100uM ZntA(46-118) and run in 100 mM Tris/Cl, 150 mM NaCl, pH 8 buffer on a Superdex HR 10/30 column.

around 12,200 and 9700 Da,. At levels of metal loading equivalent to one metal per monomer the second, higher molecular weight peak diminishes greatly. This data is thus consistent with an explanation of the EXAFS data that includes the presence of a dimer under low metal conditions.

Cd-EXAFS and ^{113}Cd-NMR(8). The Cd-EXAFS for the 0.9 Cd:ZntA sample was best fit by a $S_2(N/O)_2$ coordination shell as shown (Table 4-2). Furthermore, the ^{113}Cd shift in the ^{113}Cd-NMR (Figure 4-4) is indicative of S_2O_2 coordination specifically.

Co-ZntA(46-118) UV-Vis. The UV-Vis of Co-ZntA(46-118) was consistent with the S_2O_2 coordination described above (Figure 4-5). Strong MLCT bands are observed around 350 nm. Additionally, absorption is observed in the 600-750 nm region that are attributed to d-d transitions.

N	R(Å)[d]	σ (Å^{2}x10^3)[c]	N	R(Å)[d]	σ (Å^{2}x10^3)[c]	F'[a]	BVS[e]
4S	2.530	9.7				3.54	2.2
3S	2.524	8.8	1(O/N)	2.336	3.4	2.42	2.0
2S	2.524	5.6	2(O/N)	2.308	8.0	1.90	1.8
2S	2.516	5.5	3(O/N)	2.326	13.2	1.82	2.1
1S	2.532	1.4	3(O/N)	2.286	7.5	1.77	1.6
			4(O/N)	2.310	5.5	5.35	1.3

[a] Goodness of Fit. F_=[k^6(data-fit)^2]/ (N_{ind}-No. vars)

$$N_{ind} = \frac{2(\Delta k)(\Delta R)}{\Pi}$$

[b] Description of the sample concentration and metal content is provided in the Experimental section.

[c] The Debye Waller factor.

[d] Average bond length for the particular shell being fit (N).

[e] Bond valence shell

Table 4-2. Cd-EXAFS Fit Results of Cd(II)-ZntA(46-118).

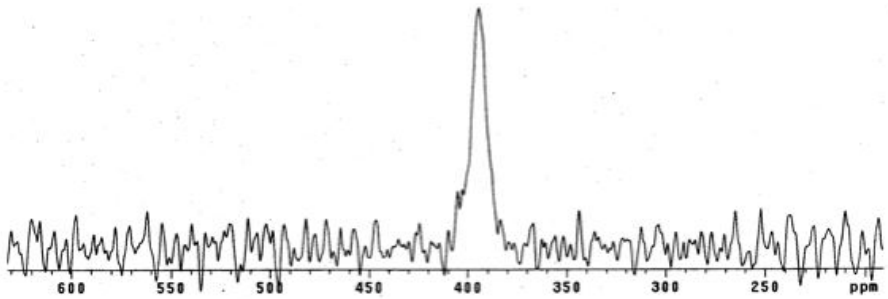

Figure 4-4 ^{113}Cd-NMR of ^{113}Cd(II)-ZntA(46-118). The resonance of the ^{113}Cd is best described by an S_2O_2 coordination environment.

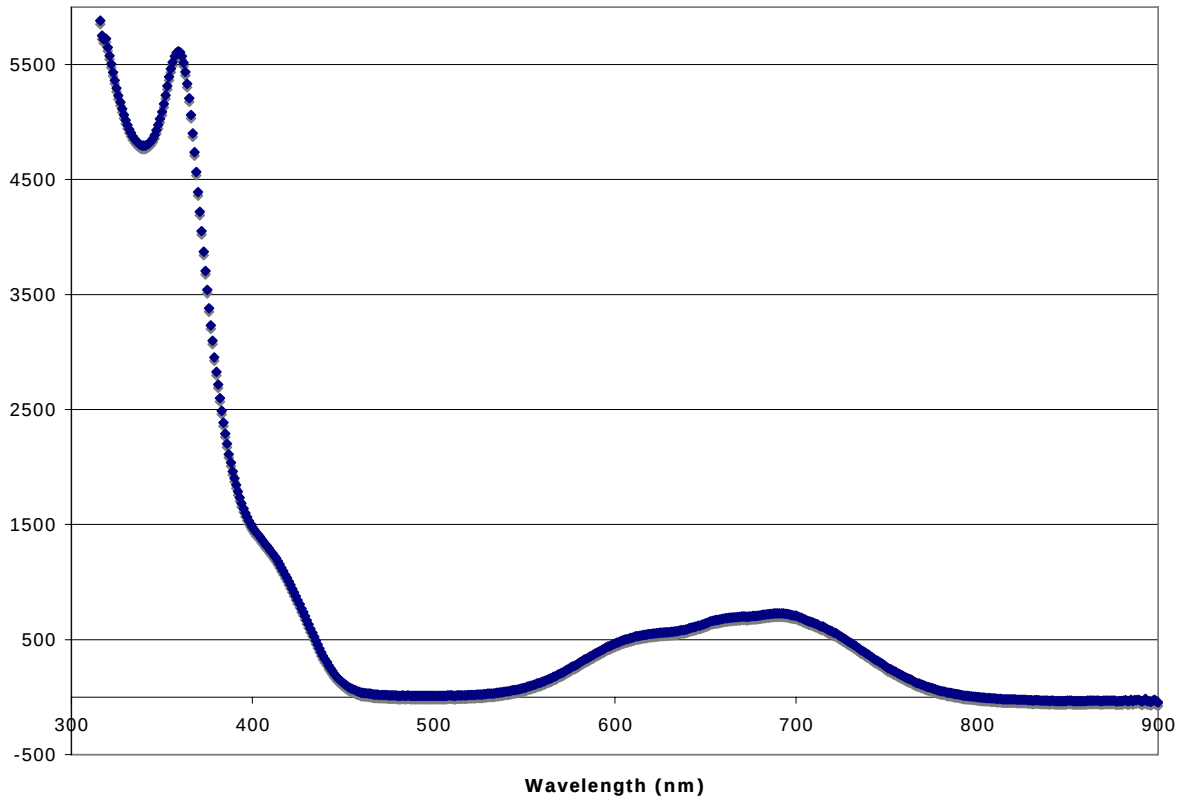

Figure 4-5. UV-Vis of Co-ZntA(46-118). The UV-Vis of 1:1 Co-ZntA(46-118) in 100 mM Bis-Tris, pH 7.4 is consistent with the S_2O_2 coordination described above. Strong MLCT bands are observed around 350 nm. Additionally, absorbtion is observed in the 600-750 nm region that is attributed to d-d transitions.

Discussion

Changing coordination chemistry with increasing Zn(II) availability in ZntA(46-118). Previous EXAFS analysis of the Zn-ZntA(46-118) protein had indicated $S_3(N/O)$ coordination. In these studies, the Zn:ZntA ratio was about 0.8:1, most likely due to air oxidation of the cysteines, since the samples were prepared aerobically. To sort this out, an experiment was designed such that samples were studied under various levels of Zn loading. Such studies had been useful to our collaborators in the past to better determine the number of cysteines bound to a zinc ion. Unexpectedly, the number of cysteines changed with the amount of Zn present in the sample (Figure 4-2). In the case where the Zn:ZntA ratio is 1:1, the coordination is best fit as $S_2(N/O)_2$. This is in agreement with the NMR structure which shows Zn(II) coordination of fully loaded Zn(II)-ZntA(46-118) by two cysteines and an aspartate. The half-zinc-loaded case is best described as a shell of four cysteine ligands (Table 4-1). Most surprisingly, the sample, which contained only 0.5 Zn/ZntA was best fit by S_4 coordination. Since the protein fragment has only two cysteines, it is not possible to explain this with a one zinc per protein model. Because exogenous thiols are not present in the sample, the data implies the interaction of two ZntA(46-118) monomers to bind the zinc, forming a metal-bridged dimer. It is not hard to believe that this might happen, since this domain is homologous to the human Atx1, Hah1, which has been shown to be a dimer in its crystal structure. To explore this further, gel filtration chromatography was used to examine the dimerization state of the protein in solution.

Changing oligomerization state with increasing Zn(II) concentration. By gel filtration chromatography, the apo protein appears to run on a size exclusion column as a single gaussian peak (Figure 4-3), corresponding to about 9700 Da, which may indicate some anisotropy in its shape. At low levels of metal loading, such as for 0.5 Zn/ZntA, the protein runs as two overlapping peaks, with one of the peaks aligning with the apo protein and a second appearing at a higher molecular weight, around 12,200 and 9700 Da. At levels of metal loading equivalent to one metal per monomer the second, higher molecular weight peak diminishes greatly. This data is thus consistent with an explanation of the EXAFS data that includes the presence of a dimer under low metal conditions.

Insights from the coordination of biologically relevant Cd(II). Just as in the case of the fully loaded Zn-ZntA(46-118) samples, the fully loaded Cd-ZntA(46-118) protein coordinates the protein with what is best described by EXAFS to be $S_2(N/O)_2$ coordination (Table 4-2). Thus, it is likely that the coordination of both Cd and Zn are accomplished using the same residues in this site. Additionally, from the ^{113}Cd-NMR it can be further ascertained that the coordination of Cd in this domain is most consistent with S_2O_2 coordination (Figure 4-4). In analyzing the ^{113}Cd-NMR, it should be noted that its shift falls closest to that of the 'blue copper' sites. However, since ZntA(46-118) has none of the histidine residues present in those coordination sites, this eliminates that possibility. Additionally, work by Bobsein et al. with horse LADH characterized an S_2NO site with a chemical shift of 440 ppm (9). If one considers that replacing the nitrogen in

LADH with a more shielding O would shift the resonance of the Cd close to 400, the resonance of the Cd at 390 ppm is best described as that of an S_2O_2 coordination site. This is in complete agreement with what was suggested by the NMR structural studies of this protein, namely that Zn(II) is coordinated by two cysteines, an aspartate oxygen, and another, possibly exogenous, oxygen source.

Additional confirmation of coordination chemistry is provided by the Zn(II) substitute, Co(II). While Zn(II), a natural cofactor of ZntA, is spectroscopically silent, Co(II) has many detectable d-d transitions and has historically been used as a mimic for Zn(II) to study it's coordination sites(10). Although a recent study has suggested that the coordination of Co(II) is unlike that of Zn(II) in ZntA, it also reports substoichiometric binding of Co(II), suggesting that oxidation of ZntA may have occurred during the course of their work(11). Co(II) has also been shown to be a functional substitute for Zn(II) in ZntA, albeit at lower levels(12). The UV-Vis of 1:1 Co-ZntA(46-118) in 100 mM Bis-Tris, pH 7.4 is consistent with the S_2O_2 coordination described above. Strong MLCT bands are observed around 350 nm. Additionally, absorbtion is observed in the 600-750 nm region that is attributed to d-d transitions. This absorption is consistent with the S_2O_2 coordination described above in that the two oxygen ligands have shifted its absorption hypsochromically relative to known S_4 peptide models such as Co^{2+}-DF which have absorbance maxima at 740, 707, and 618 nm (Table 4-3) with an extinction coefficient of about 2500$M^{-1}cm^{-1}$ (13,14). The absorption bands are shifted to lower wavelengths, since oxygen has a higher ligand

Peptide	Site	λ_a(nm)	ε_a($M^{-1}cm^{-1}$)	λ_b(nm)	ε_b($M^{-1}cm^{-1}$)	λ_c(nm)	ε_c($M^{-1}cm^{-1}$)	Reference
Co^{2+}-DF	2 sites, S_4	618	900	707	1800	740	2400	1
Co^{2+}-CF	1 site, S_4	622	500	707	700	742	950	1
Co^{2+}CP1	S_3N	590	375	650	550	725	450	2
Co^{2+}-CP	S_2N_2	568	300	637	880	637	880	3
Co-ZntA (46-118)	S_2O_2	610	450	675	550	722	350	This work

1. Ghering, et. al. Biochemistry, 2004, 43, 8346-8355.
2. Krizek, et. al. Inorg. Chem. 1993, 32, 937-940.
3. Harper, L.V. Ph. D. Thesis, Johns Hopkins University, 1993.

Table 4-3. Comparison of Co-ZntA(46-118) UV-Vis to other peptide models.

field splitting energy than sulfur, and this bond thus absorbs higher energy frequencies and thus shorter wavelengths of light. With absorption maxima at 722, 675, and 610 nm, it is more similar to Co^{+2}-CP, a Cys_2His_2 peptide model with an absorption maxima at 637 and 568 nm but it is bathochromically shifted relative to that model because the ligand field splitting energy of oxygen is less than that of nitrogen(15). It is quite similar to the Cys_3His site in Co^{2+}-CP-1, which also has a ligand field splitting energy mid-way between the S_2N_2 and S_4 cases. Since the d-d transitions of cobalt are sensitive not only to whether the ligand is oxygen or nitrogen but also the nature of the functional group, different ligands have different ligand fields and thus varying effects on the spectrum. Additionally, the symmetry greatly affects the spectrum as well; distortions from T_d or O_h symmetry will lead to shifts and splittings(16). However, based on current knowledge, the spectrum is consistent with the coordination geometry we have assigned.

This picture of the coordination chemistry of Zn(II)-ZntA(46-118) is thus consistent with its NMR structure, which also showed the apo protein and the fully Zn(II) loaded protein to be monomeric. However, it indicates that the physiology of the protein may be much different in the cellular milieu than it is when studied in vitro with stoichiometric levels of metal. Since there is an extraordinary overcapacity of chelators for Zn(II) in the cell, it is unlikely that conditions occur where the cell's entire copy number of this domain of ZntA would be fully loaded with Zn(II). Thus, the behavior of the protein that we observe here, with four cysteines bound by two proteins, may be more biologically relevant.

This data also compares well with the first proposed function of the Atx1-like domains, namely, the direct metal-transfer from one metal-binding site to another (17). Also, it nicely parallels the observation that the structural homolog of this domain, Hah1, which also forms a metal bridged dimer (18). The discovery of that structure was cited as an example of how yeast copper chaperones may interact with their receptor proteins, and the structure was used as template to model their interaction (19). Thus, while it may not be surprising that this domain would form a homodimer, the formation of such a homodimer *in vitro* raises the question of whether similar interaction could be happening *in vivo*. The trafficking of zinc in *E. Coli* is still not very well understood. Import and export pumps and metal transcription factors are known and well characterized(20-22) (23-25), but it is still unclear how the pumps are acquiring metal from the cytoplasm. Perhaps there could there be another protein, homologous to this domain, in E. Coli that might interact with this domain of the ZntA pump *in vivo*.

The Atx1-like domain of ZntA described here thus shares many characteristics with the other metal-trafficking proteins described earlier. Like Atx1 and PcoC, it has been shown to utilize biologically unprecedented coordination chemistry. Its metal ion coordination site is highly solvent exposed and its oligomerization state is metal-dependant. All of these traits are emerging as commonalities, uniquely suited to the purpose of metal-ion delivery, that separate the chemistry of metal-trafficking proteins as distinct from that of other metalloproteins.

CHAPTER 5

Chapter 5. ZntA (1-118): An additional N-terminal moiety with an unusual cysteine rich motif has a significant impact on metal ion coordination.

Abstract

Many transition metals, including zinc, are both physiologically necessary and yet toxic when accumulated at high levels. To provide the necessary levels under such strict control, the metal ions inside the cell are controlled by a variety of import, trafficking, and export proteins. E. coli, for example has several zinc transporting proteins, including the export pump ZntA, which is a P-type ATPase, and uses energy to actively pump zinc out of the cell. Measurements of the copy number of full length ZntA and its 10-fold increase with the addition of zinc to cell culture underscore the importance of this metal binding domain in cytosolic chemistry. It is predicted to consist of two cytoplasmic and eight transmembrane domains. The structure of one of these cytoplasmic domains, ZntA(46-118), which is homologous to the yeast copper chaperone Atx1, was described in the previous chapters. But, the N-terminal region of this protein contains an additional 45 residues that are cysteine rich. Metal interaction with this

protein is increased by the presence of these residues; however, a variety of lines of evidence described here reveal that this moiety appears to be largely unstructured and the addition of zinc does not appear to increase structural order in this region. While it is unclear that they represent another binding site for zinc, this moiety may alter the binding of zinc in the site previously characterized. Interestingly, a similar situation is found for a small terminal domain of a copper trafficking protein. This unstructured region places ZntA in an emerging class of proteins that contain unstructured domains that often have important physiological roles.

Introduction

Numerous systems keep the concentrations of the essential, but toxic metal ions necessary for life processes in check. ZntA, a zinc export protein found in *E. Coli* and also discussed in the previous chapter, is an example of such a metal trafficking protein. It is a member of the P-type ATP-ase superfamily of proteins that includes heavy metal ion transporters both in eukaryotic and prokaryotic organisms (2,3). ZntA itself is a Zn(II)/Pb(II)/Cd(II) transporter and has been predicted to have eight transmembrane domains and an N-terminal, metal-binding, cytoplasmic domain (Figure 5-1) (4,5). Previous work has characterized the structure and function of the Atx1-like region of the N-terminal domain of this protein as a fragment (6). While these studies revealed important information about this domain, questions remain.

The specific role of this domain has been controversial. Based on inference from other P-type ATPases, such as Ccc2 described previously, this metal binding domain might intuitively be thought to confer specificity (3), others have asserted that it plays no part in that role(7). Thus, while studies of the Atx1-like domain have given us insight into the structure and function of this protein, in addressing these questions about its role *in vivo* it is much more important to look at the cytoplasmic domain as a whole, including the N-terminal 45 residues. Additionally, the importance of examining this domain in its entirety is underscored by the dramatic increase in ZntA's copy number seen under conditions of zinc stress.

As shown in Figure 5-1, the 45 N-terminal residues are also very cysteine rich. This has led us to postulate that this region contains a second metal-binding site. While this is possible, given the flexibility of this region, the participation of these cysteines in binding at the site in the Atx1-like domain as has been proposed by others cannot be ruled out(8). A protein database search on this 45-residue sequence using the program BLASTP 2.2.4 produces very few hits (9), including: ZntA in *E. coli* K12, identical homologs in *E. coli* 0157:H7 and *E. coli* W3110, and heavy metal transporting ATPases in *Salmonella enterica* and *Salmonella typhimurium* LT2 with 44% and 45% identity, respectively.

This chapter describes the dramatic response of the copy number of ZntA to environmental zinc, the stabilization of this cytosolic domain of ZntA against adventitious hydrolysis *in vitro*, characterization of the protein's ability to bind Zn(II) and Co(II), and preliminary NMR analysis of the protein's structure. While the structural details of this domain have yet to be fully revealed, little structure in this N-terminal moiety is seen. Yet, these analyses have shown that the 45 N-terminal residues have a significant impact on the biophysics and coordination chemistry of this protein. While a complete structural picture of the cytosolic domain of this protein remains elusive, the impact of the 45 N-terminal residues upon its chemistry *in vitro* is significant. This significance is further underscored by the remarkable increase in the copy number of ZntA in response to zinc stress. The impressive number of copies of the cytosolic domain of this protein present in the cytosol under conditions of zinc stress demonstrates the importance of the role of its chemistry in zinc detoxification.

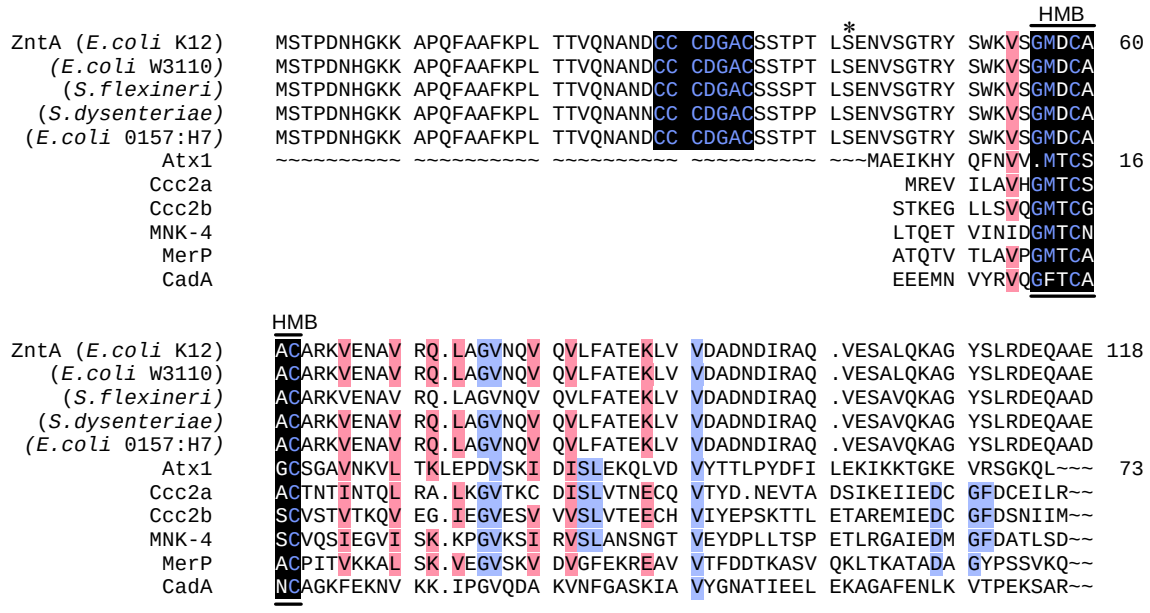

Figure 5-1. Sequence of ZntA(1-118) and Homology with other Atx1-like proteins and domains. The conserved heavy metal binding domain (HMB) is marked, along with the cysteine rich region, in black. Identical residues are highlighted in blue, while similar residues are highlighted in pink. It is interesting to note that while the Atx1-like domain is utilized by many metal trafficking proteins, regions similar to the unusual N-terminal moiety of ZntA are only found in a small number of homologs, including an *E. coli* 0157:H7, an *E. coli* W3110, and two *Salmonella* homologs, and show very high levels of conservation.

Experimental Procedures

Determination of the copy number of ZntA. The copy number of ZntA was determined in collaboration with Mr. Ben Staehlin. Cultures of *E. coli* were grown in LB media to which varying levels of $ZnSO_4$ had been added. Samples of all the cultures were taken at the same time-point. These samples were then run on an SDS-PAGE gel, along with calibration standards of known concentrations of ZntA(1-118). The gel was then analyzed by western blot using primary antibodies for the ZntA(1-118) domain (BioDesign) and secondary antibodies and developing reagents in the ECL+ kit (Amersham). The western blot was scanned using the Storm 860 phosphorimager (Molecular Dynamics), and a calibration curve was plotted from the protein standards using the software ImageQuant (Molecular Dynamics). The copy number of each sample was then determined using the calibration curve.

ZntA(1-118) Overexpression and Purification. Cloning of this gene was previously described(5). The resulting plasmid (pET11c/ZntA(1-118)) was transformed into strain BL21(DE3) for overexpression. The cells were grown in LB media, to an A_{600} of 0.6. At this point, overexpression was induced by the addition of 500 μM IPTG. The culture was then incubated for 2.5 more hours, and then harvested by centrifugation at 9000 rpm (Sorvall GS-3), 4

degrees, 15 minutes. The cell pellets thus obtained were then extracted through three freeze-thaw cycles into 20 mM MES, 1 mM EDTA, 5 mM DTT, pH 6.0. The protein in the lysis extract was then precipitated by the slow addition of solid $(NH_4)_2SO_4$to a final concentration of 60%, which was let stir at 4 degrees for about 1 hour. The solid ammonium sulfate precipitate was removed by centrifugation at 9000 rpm, 4 degrees, 15 minutes. The pellet thus obtained was dissolved into 20 mL of 50 mM Tris, 2 mM EDTA, 5 mM DTT, pH 8.0. This was then loaded, in 2, 10 mL runs, onto a desalting column that had been equilibrated in the same buffer. The fractions containing the protein were pooled and combined with 450 uL each of 1 mg/mL leupeptin and aprotinin, 63.4 uL of 50 mM PMSF, and 76.5 uL of 0.5 mg/mL pepstatin A (Protease Inhibitor Cocktail -PIC). These pooled protein fractions were then purified by anion exchange chromatography on a DEAE Sepharose column (Amersham Biosciences) using 20 mM Bis-Tris, 5 mM DTT, pH 7.0 against a gradient of 20 mM Bis-Tris, 1 M NaCl, 5 mM DTT, pH 7.0. The protein containing fractions were then combined, protease inhibitor cocktail (PIC) added, and they were directly loaded onto a phenyl sepharose hydrophobic exchange column (Amersham Biosciences). The hydrophobic column had previously been equilibrated with 50 mM Na_2HPO_4, 1M $(NH_4)_2SO_4$, 5 mM DTT, pH 7.0 and a gradient of 50 mM Na_2HPO_4, 5 mM DTT, pH 7.0 was applied during the run. Following this, the protein containing fractions were pooled, PIC was added, the fractions were conentration, and they were purified by gel filtration chromatography on a Superdex 75 FF (Amersham Biosciences) in 50 mM Bis-Tris, 200 mM NaCl, 5 mM DTT, pH 7.0. The ZntA(1-118) containing fractions were pooled and then stored in

50 mM Bis-Tris, 200 mM NaCl, 5 mM DTT, pH 7.0 at -80 degrees. Typical yields were around 40 mg.

Overexpression and Purification of ^{15}N-ZntA(1-118). ^{15}N labeled samples were prepared by inoculating a transformed colony of BL21(DE3)/pET11c/ZntA(46-118) into 2 L of minimal media (10.5 g/L K_2HPO_4, 4.5 g/L KH_2PO4_4, 1 g/L $(NH_4)_2SO_4$, 0.5 g/L sodium citrate, supplemented with 10 mL 20% glucose, 5 mL 20% casamino acids, 1 mL 1 M $MgSO_4$, 2 mL 0.2% thiamine, and 1 mL 500 mg/mL carbenicillin). This culture was grown for 7 hours, then pelleted, and the pellets resuspended into minimal *labeling* media (11.3 g Na_2HPO_4 $7H_2O$, 3 g KH_2PO_4, 0.5 g NaCl, 2 g $^{15}NH_4Cl$ per 1L) supplemented with 15 mL of 20% glucose, 2 mL of 1M $MgSO_4$, 2 mL of 0.2% thiamine, and 1 mL of 100 mg/mL carbenicillin. This culture was then incubated at 37°C until the glucose was used up as determined by glucose test strip. At this point protein expression was induced with the addition of 500 µM IPTG, the culture was further supplemented with 1 g/L $^{15}NH_4Cl$ and 4 g/L glucose, and 2.5 hours later the cells were harvested by centrifugation and stored at -80 °C. The protein was then extracted and purified as described above. The purified protein was stored at -80°C in 20 mM Mes, pH 6.0, 200 mM NaCl, 5 mM DTT. Typical yield of ^{15}N-labeled protein was 40 mg per liter of cell culture.

Protein concentration was determined by the Bradford assay. This assay is run relative to a bovine IgG standard, which induced less dye color development than ZntA(1-118). Therefore, the concentration of a sample of ZntA(1-118) was independently calibrated by amino acid

hydrolysis and it was determined that the Bradford assay overestimates the concentration of ZntA(1-118) by a factor of 1.28 relative to the bovine IgG standard.

Analysis of the hydrolysis of ZntA(1-118). Proteolysis of the protein was identified in 15% SDS-Page gels. This proteolysis of ZntA(1-118) was characterized by MALDI-TOF mass spectrum (Voyager-DE Pro). The proteolysis of the protein was followed while varying conditions, such as a variety of protease inhibitors, varied levels of Zn(II) or Cd(II), varied protein concentrations, and varied temperatures.

Apo-ZntA(1-118) NMR sample preparation. As a precaution against disulfide formation in proteins that contain a CXXC motif, this sample was prepared in a Vac atmospheres nitrogen chamber at 12º C. The NMR sample was in 100 mM sodium phosphate buffer, pH 7.0, 90% H_2O/10% D_2O. The final protein concentration range was between 0.9 and 1.0 mM. The sample was determined by ICP-AES to contain no zinc. Approximately 0.5 ml of sample was loaded into a high quality NMR tube (Wilmad 535-PP 5 mm) which were capped with latex serum caps in the Vac Atmospheres chamber.

Preparation of a Zn-ZntA(1-118) NMR sample. An NMR sample was prepared from ^{15}N-ZntA(1-118). The NMR sample was in 100 mM sodium phosphate buffer, pH 7.0, 90% H_2O/10% D_2O. The final protein concentration was 0.8 (1) mM. The zinc concentration was

determined by ICP-AES to be 1.12 mM, giving a Zn:ZntA ratio of 1.4. Approximately 0.5 ml of sample was loaded into a high quality NMR tube (Wilmad 535-PP 5 mm).

NMR measurements.

The NMR spectra were acquired at 278 K for the Zn sample or 298 for the apo sample on Avance 700 Bruker spectrometer operating at a proton nominal frequency of 700.13 MHz. A TXI 5-mm probe was used on the 700 spectrometers. The probe was equipped with Pulsed Field Gradients along the z-axis.

For the apo sample, 2D ^{15}N–^{1}H HSQC (1)maps and 3D NOESY–^{15}N HSQC experiments (100 ms mixing time) were obtained at 700 MHz with an INEPT delay of 5.3 ms, a recycle time of 1 s and spectral windows of 15 ppm and 40 ppm for the 1H and 15N dimensions, respectively (^{15}N labeled sample). For the Zn(II) sample, a 2D 15N-1H HSQC (1)map was obtained at 700 MHz with an INEPT delay of 5.3 ms, a recycle time of 1s and spectral windows of 15 ppm and 40 ppm for the 1H and 15N dimensions, respectively (^{15}N labeled sample).

Results

The copy number of ZntA increases dramatically with exogenous zinc. The copy number of ZntA was determined to be approximately 180 proteins per cell in cells grown in LB media where the zinc concentration of media has been determined to be $1.2x10^{-5}$M (5,10). This increases dramatically with the addition of zinc, up to nearly 12 fold in the presence of 800 uM $ZnSO_4$ (Figure 5-2) to over 2000 copies per cell. While other bands are observed in the cell extract lanes, they are also observed in a control sample of a ZntA knockout obtained as a gift from B. P. Rosen of Wayne State University and thus may be classified as non-specific interactions. Since this knockout is a kanamycin insert, a slightly truncated portion of the protein is produced and is seen on the Western blot.

Analysis of ZntA(1-118) Proteolysis. The proteolysis of ZntA(1-118) was observed by SDS-Page. The gels showed that approximately half of this sample ran at a much lower mass than the anticipated 12 kDa, running at approximately 10 kDa (Figure 5-3).

This was confirmed by the MALDI-TOF spectrum of the ZntA(1-118). The calculated mass (after N-terminal methionine processing) of 12, 483 (+/- 4) Da, was observed, but also a significant peak at about 10440 Da and a large number of peaks at a mass less than 1 kDa. (Figure 5-4). It was furthermore seen that MALDI-TOF spectra of the proteolyzed protein consistently showed this peak at 10440 Da. The peak at 10440 was further analyzed relative to the sequence of the protein using the FindPept program maintained by

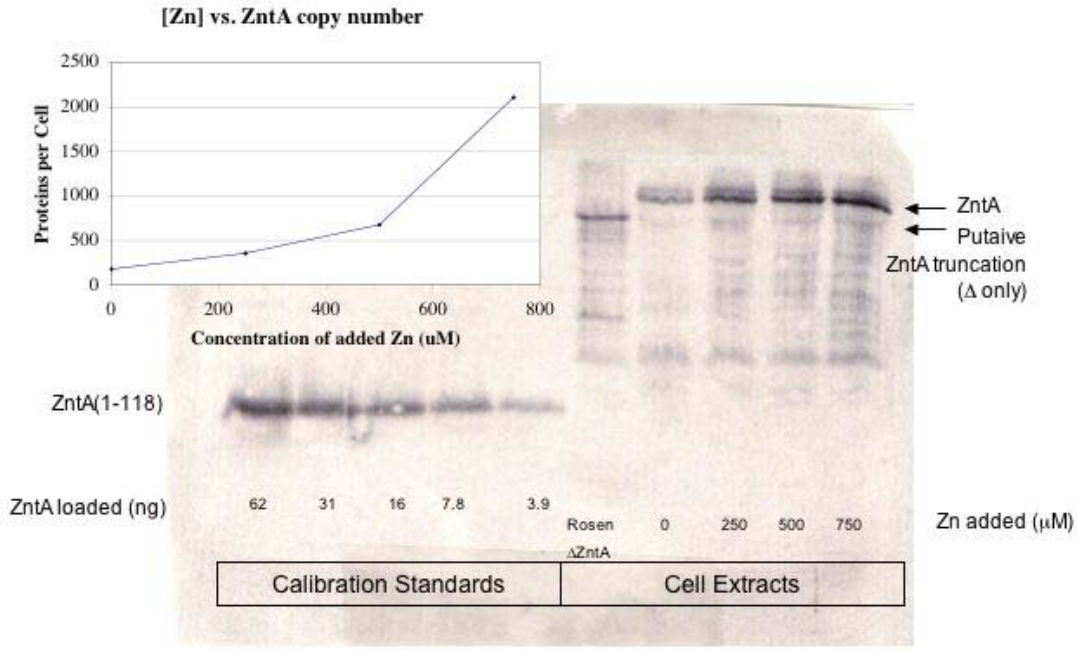

Figure 5-2. Copy number of ZntA as a function of added Zn(II). Western blot analysis was used to create a calibration curve based on measured amounts of purified ZntA(1-118) (left). The amount of ZntA in the cell lysate samples as a function of added Zn(II) was then determined from this calibration curve (right). A sample of a ZntA knockout obtained from B. P. Rosen is also shown as a control for non-specific interactions of the ZntA(1-118) antibody. The inset graph shows the response of the ZntA copy number as Zn(II) is added to the cell media.

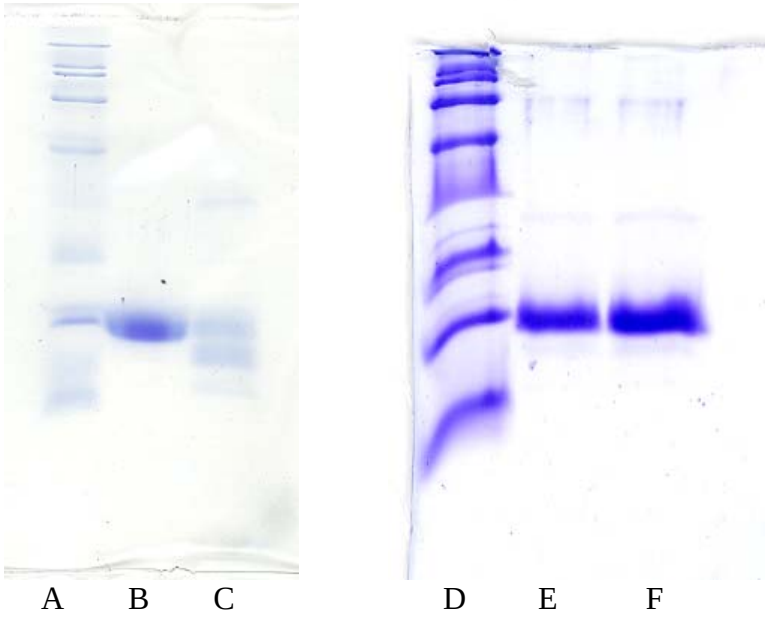

Figure 5-3. SDS-PAGE Gel of Zn-ZntA(1-118). Unproteolyzed ZntA (B) is shown beside a sample of ZntA(1-118) which has gone through proteolysis (C) both of which were run with a molecular weight marker (A). Approximately 50% of the protein appears to run at a lower molecular weight than monomeric protein. A small amount of a higher molecular weight band is also seen which likely represents some oligomerization of the protein. In a second gel, the protein has been kept at 4°C to prevent proteolysis. Lane (D) is the molecular weight marker, lane (E) is intact apo-ZntA(1-118) and lane (F) is intact Zn-ZntA(1-118).

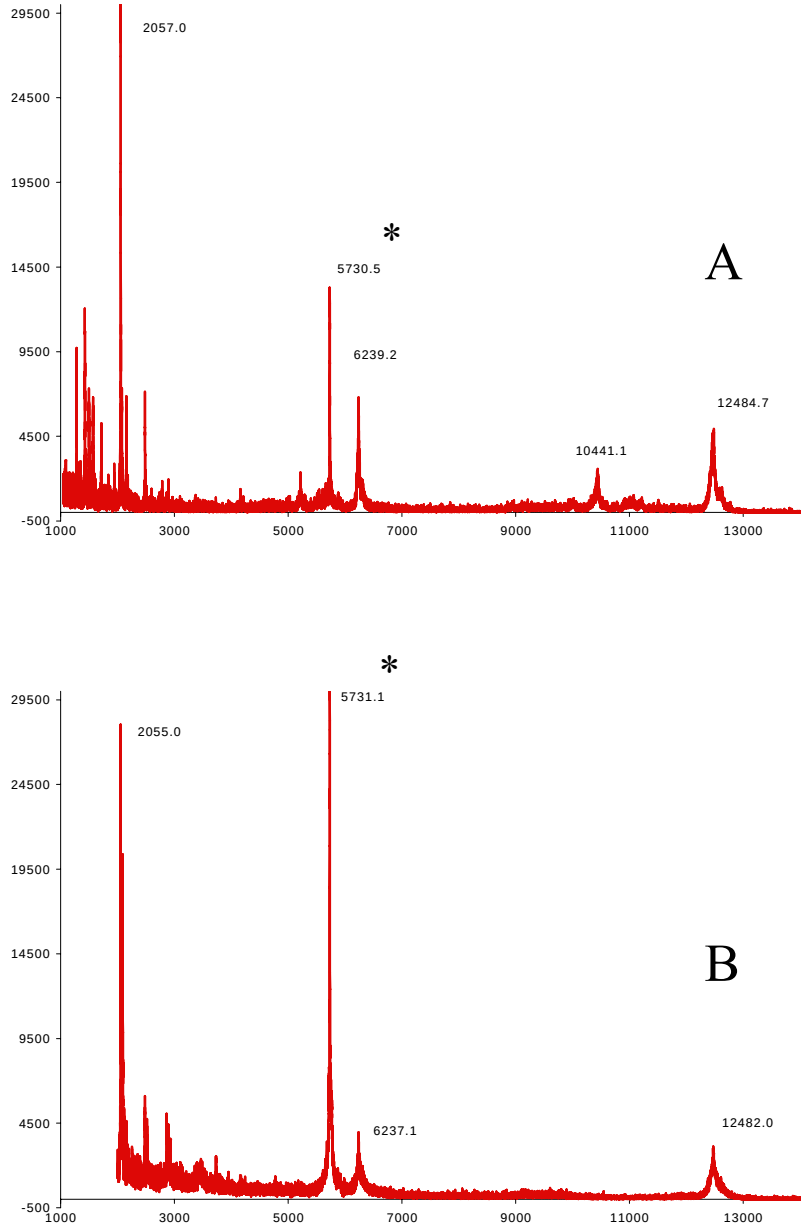

Figure 5-4. MALDI-TOF Mass Spectrum of Zn-ZntA(1-118). A) Proteolyzed Zn-ZntA(1-118) Bands for the protein are evident at 12485 and 6239 Da. Bands for a proteolysis product of the protein are also present at 10441 and 5719 Da. B) Intact ZntA(1-118) Bands for the protein are evident at 12482 and 6237 Da. The spectra were acquired using a Voyger DE-Pro Spectrometer from dried spots of 75% CHCA matrix (10 mg/mL α-CHCA, 0.1%TFA in 50:50 acetonitrile:water); 17% 1 mg/mL ZntA in 100 mM sodium phosphate buffer, pH7.0; 8% 1 mg/mL bovine insulin internal standard. The internal standard was used to calibrate the mass spectrum, and it is marked.

ExPASY(11). This analysis revealed that the proteolysis was most likely taking place between residues 21 and 22, which would correspond to the 10441 mass with an error of 1 unit, although it could be proteolyzed in other places with a greater deviation from the measured mass.

ZntA(1-118) is Stabilized against proteolysis by Lower Temperatures. Following this discovery, the effect of many factors on this proteolysis was investigated. The proteolysis was observed even in the presence of general protease inhibitors as well as metalloprotease inhibitors, and did not appear to be sensitive to changes in the concentration of ZntA. It was observed in the presence of zinc as well as cadmium, but was more prominent with zinc. The temperature, however, was found to have an effect. Carefully keeping the temperature at or below 4°C stabilized the protein. This proved to effectively slow the progress of proteolysis such that no proteolysis was apparent for at least nine days, thus providing us with samples that were amenable to our studies. (Figure 5-3). These observations are consistent with studies on the trypsin digestion of ZntA(1-118) as measured by others (12).

ZntA(1-118) NMR studies. ^{1}H-^{15}N NMR studies of apo-ZntA(1-118) reveal structured peptide only for the 46-118 residue region that had been previously characterized (6). In this region, the structure appeared similar to that determined for the shorter truncation, although the signals were somewhat broader. Signals from residues 1-45 could not be assigned, but were observed as a number of undifferentiated chemical shifts. Analysis of the Zn-ZntA(1-118)

sample also indicated that the residues in the 1-45 region were highly conformationally flexible. The NOEs of these residues showed patterns most consistent with that of unfolded protein (Figure 5-5). Mobility studies on the proteins produced HSQCs that confirmed that the 1-45 region of the protein was confirmationally flexible in both the apo- and Zn(II) forms, and perhaps slightly more so in the Zn(II) form.

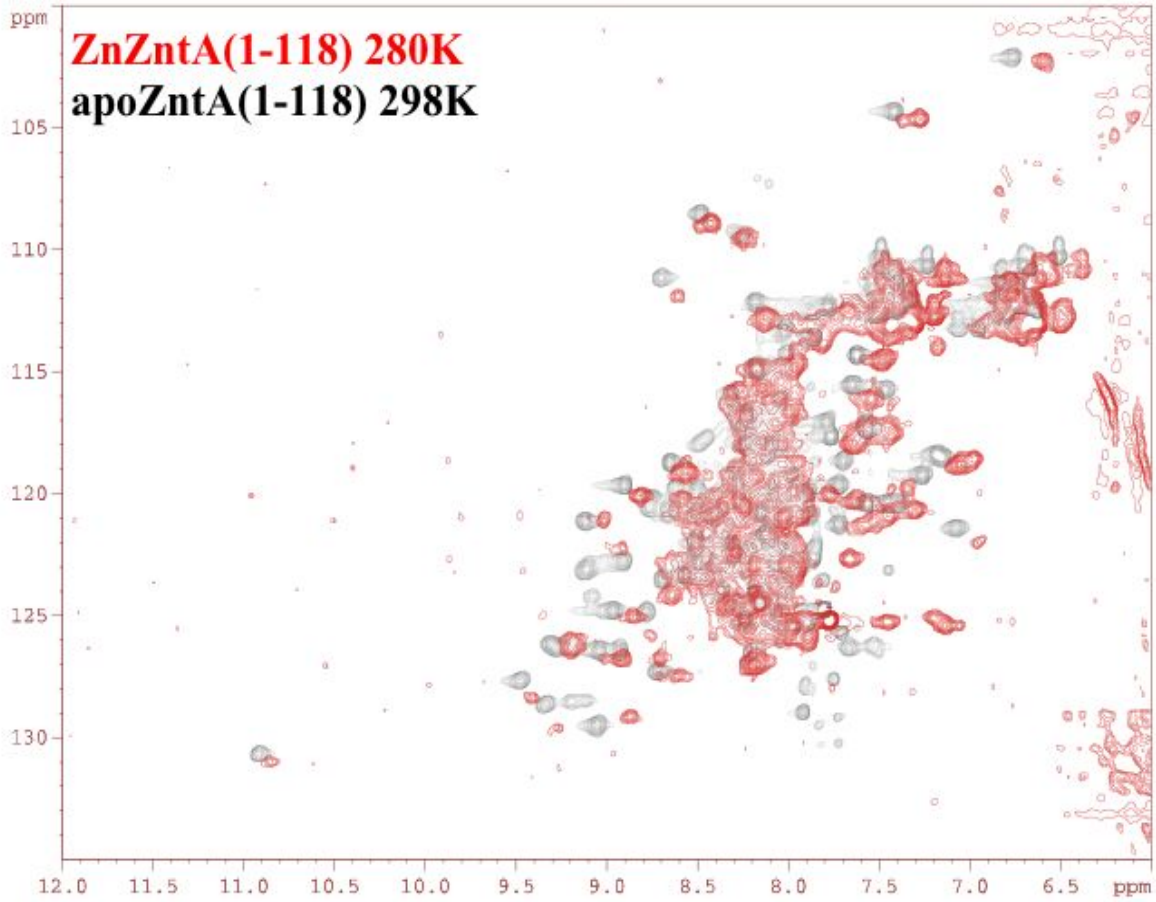

Figure 5-5. HSQC Plots of apo ZntA(1-118) (black) and Zn(II)-ZntA(1-118) (red). The lack of differentiation of the chemical shifts is characteristic of the presence of unfolded protein. The apo ZntA NMR sample was 1.0 (1) mM in 100 mM sodium phosphate buffer, pH 7.0, 90% H_2O/10% D_2O. The Zn ZntA NMR sample was 0.8 (1) mM in 100 mM sodium phosphate buffer, pH 7.0, 90% H_2O/10% D_2O. The 2D 15N-1H HSQC (1)map was obtained at 700 MHz with an INEPT delay of 5.3 ms, a recycle time of 1s and spectral windows of 15 ppm and 40 ppm for the 1H and 15N dimensions, respectively (^{15}N labeled sample).

Discussion

The addition of zinc dramatically increases the copy number of ZntA in vivo. While the copy number of ZntA under normal conditions is only around 178 per cell, this level increases a dramatic 12-fold in the presence of additional zinc. This is not entirely surprising, since ZntA is known to be part of the cellular zinc detoxification machinery, yet it is interesting to note that the copy number of the protein itself increases as part of this response. While the structure of the 1-45 tail remains elusive, it is clearly quite conformationally flexible *in vitro*, and significantly alters the coordination chemistry of the cytosolic domain. The importance of understanding the structure and role of this cytosolic domain is underscored by the great increase in the amount of this protein present in the cell under conditions of zinc stress. Clearly, the presence of this domain in such numbers during zinc stress makes it a key player in cytosolic zinc chemistry.

Adventitious proteolysis of ZntA(1-118) is stabilized by lower temperatures. While this protein had been purified by others, and its metal binding stoichiometry, kinetics and EXAFS have been examined in both published and unpublished studies(5,8,13), none of the final samples thus generated had been examined either by MALDI-TOF spectrometry or SDS-PAGE following preparation. In the course of further structural studies on Zn-ZntA(1-118), characterization by these methods found the sample to be non-homogeneous. Rather than appearing as a single protein with a mass of 12482 Da, as it does immediately following

purification, it appeared to also contain a 10 kDa, and a large number of peaks at a mass less than 1 kDa. This proteolysis may in part explain some observations of substoichiometric metal ion binding(8,13).

It was hypothesized that the Zn(II) might be playing a role in the proteolysis since it was in the preparation of a Zn(II) sample that this was first noticed, and a precedent for such a mechanism exists in cysteine-switch proteases(14). However, in a control study where the apo protein was kept at the same temperature for the same length of time as a second sample that is loaded with Zn(II) in the anaerobic chamber, similar levels of proteolysis occurred. While none of the protease inhibitors or chelators used seemed to have a significant effect, temperature was found to be very important. At the temperature of 12°C maintained in the anaerobic chamber, the sample was not stable for the 1 day required to prepare the Zn(II)-ZntA(1-118). However, when the sample was chilled to 4 degrees, either on ice in the anaerobic chamber, or aerobically in a refrigerator, the sample was found to be stable for at least nine days. This provides more than sufficient time for the analyses of interest. The exact cause of the proteolysis is still not well understood. While the protein appears to be purified to a high degree of purity, it is possible that traces of co-purified protease may be able to catalyze a large amount of proteolysis. Based on the appearance of a peak at 10440 Da associated with the proteolysis, and analysis of this relative to the sequence using ProtFind (ExPASY)(11), it appears likely that the proteolysis is occurring between residues 21 and 22. Using this information, one might predict what proteases could be cutting the ZntA protein. However, only for a few proteases has enough information been accumulated that allow a statistical treatment (15,16). Using the tool Peptide Cutter

(ExPASY) (16), enzymes that are predicted to cut this sequence at this site include protinase K and Thermolysin. While it is unlikely that these specific proteases are responsible for the cleavage, since they come from *Thitirachium album limber* mold and *Bacillus thermoproteolyticus*, respectively, it is possible cleavage could occur via *E. coli* proteases with similar mechanisms.

An alternative explanation for this observed proteolysis of apparently pure protein is autoproteolysis. Given the relative rarity of auto-proteolysis (17) as compared to other proteolytic mechanisms, it is unlikely to be the cause in this case, although it has not been ruled out.

Flexibility of the 1-45 region of ZntA(1-118). Initial NMR studies on apo-ZntA(1-118) indicated that the 1-45 region was very flexible in solution and could accommodate a wide variety of conformations. Given the function of this protein as a transporter, it is possible that this allows the metal binding residues in this region to be very accessible to the Zn(II) ion. While it was anticipated that the presence of Zn might stabilize the structure, this region also appears to be largely unfolded in the Zn-ZntA(1-118) complex as well. The high degree of conformational flexibility of this moiety is also consistent with its susceptibility to proteolysis. Subsequent DTNB analysis of similarly treated protein has indicated at least some degree of oxidation of the cysteine residues, and a contribution from oxidized protein to the apparent flexibility of the structure cannot be ruled out.

While the function of a protein has long been related to its well-defined native structure, recent structural and genomic data have indicated that not all proteins have unique folded structures under physiological conditions. Genomic analyses estimate that between 6 and 33% of all bacterial proteins have naturally disordered regions of ≥ 40 residues (18). New functions of this intrinsic disorder are continually emerging and have recently been reviewed(19). The advantages of this disorder include increased binding specificity at the expense of thermodynamic stability, regulation by proteolysis and the ability to recognize a range of proteins. At times, the natively unfolded protein performs specific biological functions, but in other cases the unfolded region of protein becomes compact and structured upon binding a ligand or cofactor. Functions that such unfolded regions have been seen to perform include the regulation of transcription and translation, cellular signal transduction, protein phosphorylation, the storage of small molecules, and the regulation of large multiprotein complexes such as the bacterial flagellum and the ribosome(19).

Recently, a precedent for disordered domains in metal trafficking proteins has been observed, namely in the structure of yCCS (20). Previous structural characterization had revealed the structure of the second domain of this protein, and that it forms heterodimers with its target protein, SOD1 (21,22). In these structural studies, it was suggested that the C-terminal domain III of the protein was missing due to proteolysis during crystal growth. This proteolysis has been attributed to the flexibility of this domain in the absence of any bound copper ion. The C-terminal domain is, in contrast, present in the heterodimer. Thus it is possible that

unstructured domains that physiologically acquire structure may be a common characteristic of metal trafficking proteins.

While the binding of zinc does not appear to induce conformational stability in the 1-45 residue region or within the 46-118 region, other functional explanations are possible. It is possible that the function of the ZntA transporter is gated by a posttranslational modification that removes this moiety. Another postulate is that lack of structure in the 1-45 region could allow it to increase the rate of zinc binding by ZntA (Figure 5-7). In this postulate, the unstructured N-terminal moiety rapidly picks up Zn(II) from a cytosolic source and releases it to the binding site in the 46-118 region. Once Zn(II) is bound in the (46-118) domain, ATPase and Zn(II) transport occur. This mechanism would help to explain results seen by others (7) that indicate that the presence of the 1-118 domain increases the rate of zinc transport.

The existence of a disordered region comes at a physiological cost. Such regions are the sites of many chromosomal translocations that are associated with disease, and disordered regions can also have a biological cost in terms of the promotion and proliferation of protein folding diseases (19). Given this, it is unlikely that this moiety would be conserved unless it has a crucial physiological role, contrary to what others have asserted (7). As study of this transporter continues, the role of these residues will reveal insights into the homeostasis of zinc and the mechanistic details of zinc trafficking in *E. coli.*

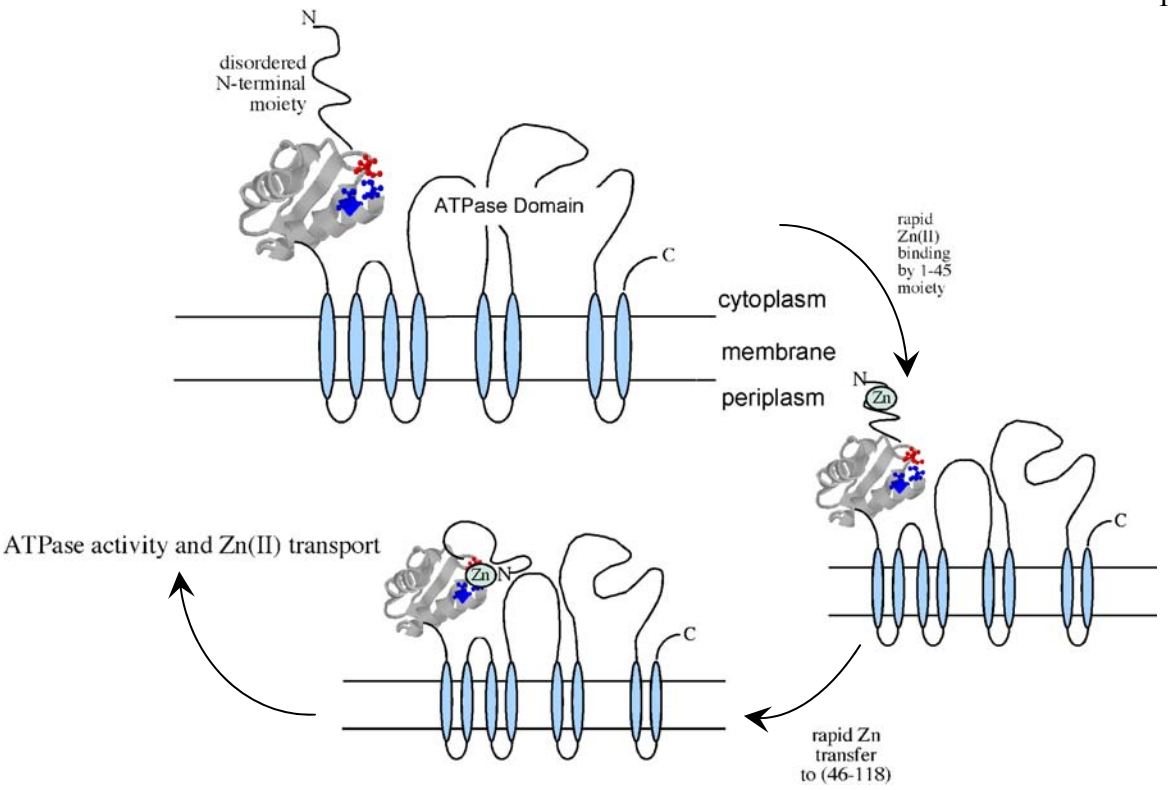

Figure 5-7. Hypothetical functional role for the unstructured N-terminal moiety. In this postulate, the unstructured N-terminal moiety rapidly picks up Zn(II) from a cytosolic source and releases it to the binding site in the 46-118 region. Once Zn(II) is bound in the (46-118) domain, ATPase and Zn(II) transport occur.

References

Chapter 1

1. Outten, C. E., and O'Halloran, T. V. (2001) *Science* **292**, 2488-2492
2. Loehr, T. M. (ed) (1989) *Iron Carriers and Iron Proteins* Vol. 5. Physical Bioinorganic Chemistry Series. Edited by Lever, H. B. G. a. A. B. P. 5 vols., VCH Publishers, Inc., New York
3. O'Halloran, T. V., and Culotta, V. C. (2000) *J Biol Chem* **275**, 25057-25060
4. Huffman, D. L., and O'Halloran, T. V. (2001) *Annu Rev Biochem* **70**, 677-701
5. Lin, S. J., and Culotta, V. C. (1995) *Proc Natl Acad Sci U S A* **92**, 3784-3788
6. Culotta, V. C., Klomp, L. W., Strain, J., Casareno, R. L., Krems, B., and Gitlin, J. D. (1997) *J Biol Chem* **272**, 23469-23472
7. Lin, S. J., Pufahl, R. A., Dancis, A., O'Halloran, T. V., and Culotta, V. C. (1997) *J Biol Chem* **272**, 9215-9220
8. Pufahl, R. A., Singer, C. P., Peariso, K. L., Lin, S. J., Schmidt, P. J., Fahrni, C. J., Culotta, V. C., Penner-Hahn, J. E., and O'Halloran, T. V. (1997) *Science* **278**, 853-856
9. Rosenzweig, A. C., Huffman, D. L., Hou, M. Y., Wernimont, A. K., Pufahl, R. A., and O'Halloran, T. V. (1999) *Structure Fold Des* **7**, 605-617
10. Arnesano, F., Banci, L., Bertini, I., Huffman, D. L., and O'Halloran, T. V. (2001) *Biochemistry* **40**, 1528-1539

11. Gitschier, J., Moffat, B., Reilly, D., Wood, W. I., and Fairbrother, W. J. (1998) *Nat Struct Biol* **5**, 47-54

12. Wernimont, A. K., Huffman, D. L., Lamb, A. L., O'Halloran, T. V., and Rosenzweig, A. C. (2000) *Nat Struct Biol* **7**, 766-771

13. Banci, L., Bertini, I., Ciofi-Baffoni, S., Huffman, D. L., and O'Halloran, T. V. (2001) *J Biol Chem* **276**, 8415-8426

14. Arnesano, F., Banci, L., Bertini, I., Cantini, F., Ciofi-Baffoni, S., Huffman, D. L., and O'Halloran, T. V. (2001) *J Biol Chem* **276**, 41365-41376

15. Xiao, Z., and Wedd, A. G. (2002) *Chem Commun (Camb)*, 588-589

16. Rosenzweig, A. C. (2001) *Acc Chem Res* **34**, 119-128

17. Hamza, I., Prohaska, J., and Gitlin, J. D. (2003) *Proc Natl Acad Sci U S A* **100**, 1215-1220

18. Tottey, S., Rondet, S. A., Borrelly, G. P., Robinson, P. J., Rich, P. R., and Robinson, N. J. (2002) *J Biol Chem* **277**, 5490-5497

19. Puig, S., and Thiele, D. J. (2002) *Curr Opin Chem Biol* **6**, 171-180

20. Martina Ralle, M. J. C., Svetlana Lutsenko, and Ninian J. Blackburn. (1998) *J. Am. Chem. Soc.* **120**, 13525-13526

21. Rosenzweig, A. C., and O'Halloran, T. V. (2000) *Curr Opin Chem Biol* **4**, 140-147

22. Arnesano, F., Banci, L., Bertini, I., Ciofi-Baffoni, S., Molteni, E., Huffman, D. L., and O'Halloran, T. V. (2002) *Genome Res* **12**, 255-271

23. Cobine, P. A., George, G. N., Jones, C. E., Wickramasinghe, W. A., Solioz, M., and Dameron, C. T. (2002) *Biochemistry* **41**, 5822-5829

24. Banci, L., Bertini, I., Ciofi-Baffoni, S., Del Conte, R., and Gonnelli, L. (2003) *Biochemistry* **42**, 1939-1949

25. Winge, D. R. (2003) *In press*

26. Beers, J., Glerum, D. M., and Tzagoloff, A. (1997) *J Biol Chem* **272**, 33191-33196

27. Heaton, D. N., George, G. N., Garrison, G., and Winge, D. R. (2001) *Biochemistry* **40**, 743-751

28. Puig, S., Rees, E., and Thiele, D. (2002) *Structure (Camb)* **10**, 1292

29. Stoyanov, J. V., Hobman, J. L., and Brown, N. L. (2001) *Mol Microbiol* **39**, 502-511

30. Outten, F. W., Huffman, D. L., Hale, J. A., and O'Halloran, T. V. (2001) *J Biol Chem* **276**, 30670-30677

31. Rensing, C., Fan, B., Sharma, R., Mitra, B., and Rosen, B. P. (2000) *Proc Natl Acad Sci U S A* **97**, 652-656

32. Outten, F. W., Outten, C. E., Hale, J., and O'Halloran, T. V. (2000) *J Biol Chem* **275**, 31024-31029

33. Roberts, S. A., Weichsel, A., Grass, G., Thakali, K., Hazzard, J. T., Tollin, G., Rensing, C., and Montfort, W. R. (2002) *Proc Natl Acad Sci U S A* **99**, 2766-2771

34. Huffman, D. L., Huyett, J., Outten, F. W., Doan, P. E., Finney, L. A., Hoffman, B. M., and O'Halloran, T. V. (2002) *Biochemistry* **41**, 10046-10055

35. Peariso, K., Huffman, D. L., Penner-Hahn, J. E., and O'Halloran, T. V. (2003) *J Am Chem Soc* **125**, 342-343

36. Lee, S. M., Grass, G., Rensing, C., Barrett, S. R., Yates, C. J., Stoyanov, J. V., and Brown, N. L. (2002) *Biochem Biophys Res Commun* **295**, 616-620

37. Wernimont, A. K., Huffman, D. L., Finney, L. A., Demeler, B., O'Halloran, T. V., and Rosenzweig, A. C. (2003) *J Biol Inorg Chem* **8**, 185-194

38. Arnesano, F., Banci, L., Bertini, I., and Thompsett, A. (2002) *Structure (Camb)* **10**, 1337

39. Arnesano, F., Banci, L., Bertini, I., Mangani, S., and Thompsett, A. R. (2003) *Proc Natl Acad Sci U S A* **100**, 3814-3819

40. Banci, L., Bertini, I., Ciofi-Baffoni, S., Finney, L. A., Outten, C. E., and O'Halloran, T. V. (2002) *J Mol Biol* **323**, 883-897

41. Auld, D. S. (2001) *Biometals* **14**, 271-313

42. Mitra, B., and Sharma, R. (2001) *Biochemistry* **40**, 7694-7699

43. Hou, Z. J., Narindrasorasak, S., Bhushan, B., Sarkar, B., and Mitra, B. (2001) *J Biol Chem* **276**, 40858-40863

44. Rensing, C., Mitra, B., and Rosen, B. P. (1997) *Proc Natl Acad Sci U S A* **94**, 14326-14331

45. Sharma, R., Rensing, C., Rosen, B. P., and Mitra, B. (2000) *J Biol Chem* **275**, 3873-3878

46. Cavet, J. S., Borrelly, G. P. M., Robinson, N. J. (in press) *FEMS Microbiology Reviews* **27**

47. Gaither, L. A., and Eide, D. J. (2001) *Biometals* **14**, 251-270

48. Andrews, G. K. (2001) *Biometals* **14**, 223-237

49. McMahon, R. J., and Cousins, R. J. (1998) *J Nutr* **128**, 667-670

50. Schulz, H., and Thony-Meyer, L. (2000) *J Bacteriol* **182**, 6831-6833

51. Thony-Meyer, L. (2002) *Biochem Soc Trans* **30**, 633-638

52. Arnesano, F., Banci, L., Barker, P. D., Bertini, I., Rosato, A., Su, X. C., and Viezzoli, M. S. (2002) *Biochemistry* **41**, 13587-13594

53. Helmann, J. D. (2002) *Chem Biol* **9**, 1055-1057

54. Chivers, P. T., and Sauer, R. T. (2002) *Chem Biol* **9**, 1141-1148

55. Ciurli, S., Safarov, N., Miletti, S., Dikiy, A., Christensen, S. K., Kornetzky, K., Bryant, D. A., Vandenberghe, I., Devreese, B., Samyn, B., Remaut, H., and Van Beeumen, J. (2002) *J Biol Inorg Chem* **7**, 623-631

56. Remaut, H., Safarov, N., Ciurli, S., and Van Beeumen, J. (2001) *J Biol Chem* **276**, 49365-49370

57. Song, H. K., Mulrooney, S. B., Huber, R., and Hausinger, R. P. (2001) *J Biol Chem* **276**, 49359-49364

58. Keyer, K., and Imlay, J. A. (1996) *Proc Natl Acad Sci U S A* **93**, 13635-13640

59. Andrews, N. C. (2002) *Curr Opin Chem Biol* **6**, 181-186

60. Li, L., Chen, O. S., McVey Ward, D., and Kaplan, J. (2001) *J Biol Chem* **276**, 29515-29519

61. Chen, O. S., and Kaplan, J. (2000) *J Biol Chem* **275**, 7626-7632

62. Luk, E. E., and Culotta, V. C. (2001) *J Biol Chem* **276**, 47556-47562

Chapter 2

1. Millardet, P. M. A. (1885) *J. Agr. Prat.* **2**, 801-805
2. Munson, G. P., Lam, D. L., Outten, F. W., and O'Halloran, T. V. (2000) *J Bacteriol* **182**, 5864-5871
3. Outten, F. W., Outten, C. E., Hale, J., and O'Halloran, T. V. (2000) *J Biol Chem* **275**, 31024-31029
4. Stoyanov, J. V., Hobman, J. L., and Brown, N. L. (2001) *Mol Microbiol* **39**, 502-511
5. Petersen, C. a. M., L. B. (2000) *Gene* **261**, 289-298
6. Rensing, C., Fan, B., Sharma, R., Mitra, B., and Rosen, B. P. (2000) *Proc Natl Acad Sci U S A* **97**, 652-656
7. Bryson, J. W., O'Halloran, T. V., Rouch, D. A., Brown, N. L.,, and Camakaris, J., and Lee, B. T. O. (1993) in *Bioinorganic Chemistry of Copper* (Karlin, K., and Tyeklar, Z., ed), pp. 101-105, Chapman & Hall, New York
8. Tetaz, T. J., and Luke, R. K. (1983) *J Bacteriol* **154**, 1263-1268
9. Williams, J. R., Morgan, A. G., Rouch, D. A., Brown, N. L., and Lee, B. T. (1993) *Appl Environ Microbiol* **59**, 2531-2537
10. Mellano, M. A., and Cooksey, D. A. (1988) *J Bacteriol* **170**, 2879-2883

11. Bender, C. L., and Cooksey, D. A. (1987) *J Bacteriol* **169**, 470-474

12. Voloudakis, A. E., Bender, C. L., and Cooksey, D. A. (1993) *Appl Environ Microbiol* **59**, 1627-1634

13. Lee, Y. A., Hendson, M., Panopoulos, N. J., and Schroth, M. N. (1994) *J Bacteriol* **176**, 173-188

14. Brown, N. L., Barrett, S. R., Camakaris, J., Lee, B. T., and Rouch, D. A. (1995) *Mol Microbiol* **17**, 1153-1166

15. Rouch, D. A., and Brown, N. L. (1997) *Microbiology* **143 (Pt 4)**, 1191-1202

16. Solomon, E. I., Sundaram, U. M., and Machonkin, T. E. (1996) *Chem Rev* **96**, 2563-2606

17. Askwith, C., Eide, D., Van Ho, A., Bernard, P. S., Li, L., Davis-Kaplan, S., Sipe, D. M., and Kaplan, J. (1994) *Cell* **76**, 403-410

18. Yuan, D. S., Stearman, R., Dancis, A., Dunn, T., Beeler, T., and Klausner, R. D. (1995) *Proc Natl Acad Sci U S A* **92**, 2632-2636

19. Kaplan, J., and O'Halloran, T. V. (1996) *Science* **271**, 1510-1512

20. Brouwers, G. J., de Vrind, J. P., Corstjens, P. L., Cornelis, P., Baysse, C., and de Vrind-de Jong, E. W. (1999) *Appl Environ Microbiol* **65**, 1762-1768

21. Outten, F. W., Huffman, D. L., Hale, J. A., and O'Halloran, T. V. (2001) *J Biol Chem* **276**, 30670-30677

22. Grass, G., and Rensing, C. (2001) *Biochem Biophys Res Commun* **286**, 902-908

23. Cha, J. S., and Cooksey, D. A. (1991) *Proc Natl Acad Sci U S A* **88**, 8915-8919

24. Bryson, J. W., O'Halloran, T. V., Rouch, D. A., Brown, N. L., Camakaris, J., and Lee, B. T. O. (1993) in *Bioinorgainc chemistry of copper* (Karlin, K. D., and Tyeklar, Z., ed), pp. 101-109, Chapman & Hall, New York

25. Cooksey, D. A. (1994) *FEMS Microbiol Rev* **14**, 381-386

26. Dancis, A., Yuan, D. S., Haile, D., Askwith, C., Eide, D., Moehle, C., Kaplan, J., and Klausner, R. D. (1994) *Cell* **76**, 393-402

27. Lee, S. M., Grass, G., Rensing, C., Barrett, S. R., Yates, C. J., Stoyanov, J. V., and Brown, N. L. (2002) *Biochem Biophys Res Commun* **295**, 616-620

28. Huffman, D. L., and O'Halloran, T. V. (2000) *J Biol Chem* **275**, 18611-18614

29. Rae, T. D., Schmidt, P. J., Pufahl, R. A., Culotta, V. C., and O'Halloran, T. V. (1999) *Science* **284**, 805-808

30. Huffman, D. L., Huyett, J., Outten, F. W., Doan, P. E., Hoffman, B. M., and O'Halloran, T. V. (2002) *Biochemistry*

31. Katrina Peariso, D. L. H., James E. Penner-Hahn, and Thomas V. O'Halloran. (in press)

32. Peariso, K., Huffman, D. L., Penner-Hahn, J. E., and O'Halloran, T. V. (2003) *J Am Chem Soc* **125**, 342-343

33. Wernimont, A. K., Huffman, D. L., Finney, L. A., Demeler, B., O'Halloran, T. V., and Rosenzweig, A. C. (2003) *J Biol Inorg Chem* **8**, 185-194

34. Demeler, B. (2002), 6.0 Ed., University of Texas Health Science Center at San Antonio, San Antonio

35. Laue, T. M., Shah, B. D., Ridgeway, T. M., and Pelletier, S. L. (1992) in *Analytical Ultracentrifugation in Biochemistry and Polymer Science* (Harding, S. E., Rowe, A. J. and Horton, J. C., ed), pp. 90-125, Royal Society of Chemistry, Cambridge

36. Cohn, E. J. a. E., J. T. (1943) *Proteins, Amino Acids and Peptides as Ions and Dipolar Ions*, Reinhold, New York

37. Johnson, M. L., Correia, J. J., Yphantis, D. D. and Halvorson, H. R. (1981) *Biophysical Journal* **36**, 575-588

38. Gill, S. C., and von Hippel, P. H. (1989) *Anal Biochem* **182**, 319-326

39. Huffman, D. L., and O'Halloran, T. V. (2001) *Annu Rev Biochem* **70**, 677-701

Chapter 3

1. Outten, C. E., and O'Halloran, T. V. (2001) *Science* **292**, 2488-2492

2. Finney, L. A., and O'Halloran, T. V. (2003) *Science* **300**, 931-936

3. Rensing, C., Mitra, B., and Rosen, B. P. (1997) *Proc Natl Acad Sci U S A* **94**, 14326-14331

4. Mitra, B., and Sharma, R. (2001) *Biochemistry* **40**, 7694-7699

5. Sharma, R., Rensing, C., Rosen, B. P., and Mitra, B. (2000) *J Biol Chem* **275**, 3873-3878

6. Okkeri, J., and Haltia, T. (1999) *Biochemistry* **38**, 14109-14116

7. Banci, L., Bertini, I., Ciofi-Baffoni, S., Finney, L. A., Outten, C. E., and O'Halloran, T. V. (2002) *J Mol Biol* **323**, 883-897

8. Brocklehurst, K. R., Hobman, J. L., Lawley, B., Blank, L., Marshall, S. J., Brown, N. L., and Morby, A. P. (1999) *Mol Microbiol* **31**, 893-902

9. Hantke, K. (2001) *Biometals* **14**, 239-249

10. Hantke, K. (2002) *J Mol Microbiol Biotechnol* **4**, 217-222

11. Outten, C. E., Tobin, D. A., Penner-Hahn, J. E., and O'Halloran, T. V. (2001) *Biochemistry* **40**, 10417-10423

12. Rensing, C., Mitra, B., and Rosen, B. P. (1998) *Biochem Cell Biol* **76**, 787-790

13. Hitomi, Y., Outten, C. E., and O'Halloran, T. V. (2001) *J Am Chem Soc* **123**, 8614-8615

14. Arnesano, F., Banci, L., Bertini, I., Ciofi-Baffoni, S., Molteni, E., Huffman, D. L., and O'Halloran, T. V. (2002) *Genome Res* **12**, 255-271

15. Rensing, C., Sun, Y., Mitra, B., and Rosen, B. P. (1998) *J Biol Chem* **273**, 32614-32617

16. Outten, C. E. (2001) in *Chemistry*, pp. 263, Northwestern University, Evanston, IL

17. Bax, A. a. D., D. C. (1985) *J. Magn. Reson.* **63**, 207-213

18. Griesinger, C., Otting, G., Wu¨ thrich, K. & Ernst, R. R. (1988) *J. Am. Chem. Soc.* **110**, 7870–7872

19. Macura, S., Wu¨ thrich, K. & Ernst, R. R. (1982) *J. Magn. Reson.* **47**

20. Marion, D., and Wuthrich, K. (1983) *Biochem Biophys Res Commun* **113**, 967-974

21. Kay, L. E., Marion, D. & Bax, A. (1989) *J. Magn. Reson.* **84**, 72-84

22. Kay, L. E., Keifer, P. & Saarinen, T. (1992) *J. Am. Chem. Soc.* **114**, 10663-10665

23. Schleucher, J., Schwendinger, M., Sattler, M., Schmidt, P., Schedletzky, O., Glaser, S. J., Sorensen, O. W., and Griesinger, C. (1994) *J Biomol NMR* **4**, 301-306

24. Vuister, G. W. B., A. (1993) *J Am Chem Soc* **115**, 7772-7777

25. Piotto, M., Saudek, V., and Sklenar, V. (1992) *J Biomol NMR* **2**, 661-665

26. Guntert, P., Braun, W., and Wuthrich, K. (1991) *J Mol Biol* **217**, 517-530

27. Bax, A. W., A. C. (1995) *J Am Chem Soc* **117**, 1810-1813

28. Weisemann, R., Lohr, F., and Ruterjans, H. (1994) *J Biomol NMR* **4**, 587-593

29. Gagne, S. M., Tsuda, S., Li, M. X., Chandra, M., Smillie, L. B., and Sykes, B. D. (1994) *Protein Sci* **3**, 1961-1974

30. Guntert, P., Mumenthaler, C., and Wuthrich, K. (1997) *J Mol Biol* **273**, 283-298

31. Pearlman, D. A., Case, D. A., Caldwell, J. W., Ross,, and W. S., C., T. E., Ferguson, D. M. et al. (1997), University of California,, San Francisco

32. Banci, L., Bertini, I., Bruni, B., Carloni, P., Luchinat, C., Mangani, S., Orioli, P. L., Piccioli, M., Ripniewski, W., and Wilson, K. S. (1994) *Biochem Biophys Res Commun* **202**, 1088-1095

33. Stote, R. H., and Karplus, M. (1995) *Proteins* **23**, 12-31

34. Suarez, D., and Merz, K. M., Jr. (2001) *J Am Chem Soc* **123**, 3759-3770

35. Ryde, U. (1995) *Proteins* **21**, 40-56

36. Borgias, B., Thomas, P. D. & James, T. L. (1989), University of California, San Francisco

37. Laskowski, R. A., MacArthur, M. W., Moss, D. S. &, and Thornton, J. M. (1993) *J. Appl. Crystallog.* **26**, 283-291

38. Kay, L. E., Torchia, D. A., and Bax, A. (1989) *Biochemistry* **28**, 8972-8979

39. Palmer, A. G., III, Skelton, N. J., Chazin, W. J.,Wright,, and P. E. & Rance, M. (1992) *Mol. Phys.* **75**, 699-711

40. Kay, L. E., Nicholson, L. K., Delaglio, F., Bax, A. &, and Torchia, D. A. (1992) *J. Magn. Reson.* **97**, 359–375.

41. Barbato, G., Ikura, M., Kay, L. E., Pastor, R. W., and Bax, A. (1992) *Biochemistry* **31**, 5269-5278

42. Marquardt, D. W. (1963) *J. Soc. Ind. Appl. Math.* **11**, 431–441

43. Press, W. H., Flannery, B. P., Teukolsky, S. A. &, and Vetterling, W. T. (1988) *Numerical Recipes in C—The Art of Scientific Computing,*, Cambridge University Press, New York

44. Palmer, A. G., III, Rance, M. & Wright, P. E. (1991) *J Am Chem Soc* **113**, 4371–4380

45. Peng, J. W., and Wagner, G. (1992) *Biochemistry* **31**, 8571-8586

46. Zinn-Justin, S., Berthault, P., Guenneugues, M. &, and Desvaux, H. (1997) *J. Biomol. NMR*, **10**, 363–372

47. Tjandra, N., Feller, S. E., Pastor, R. W. & Bax, A. (1995) *J Am Chem Soc* **117**, 12562–12566

48. Garrett, D. S., Seok, Y. J., Liao, D. I., Peterkofsky, A., Gronenborn, A. M., and Clore, G. M. (1997) *Biochemistry* **36**, 2517-2530

49. Arnesano, F., Banci, L., Bertini, I., Cantini, F., Ciofi-Baffoni, S., Huffman, D. L., and O'Halloran, T. V. (2001) *J Biol Chem* **276**, 41365-41376

50. Foster, T. J. (1987) *CRC Crit. Rev. Microbiol.* **15**, 117-140

51. Laskowski, R. A., Rullmannn, J. A., MacArthur, M. W., Kaptein, R., and Thornton, J. M. (1996) *J Biomol NMR* **8**, 477-486

52. Bentrop, D., Bertini, I., Iacoviello, R., Luchinat, C., Niikura, Y., Piccioli, M., Presenti, C., and Rosato, A. (1999) *Biochemistry* **38**, 4669-4680

53. Cantor, R. C. S., P. R. (1980) *Biophysical Chemistry*, W. H. Freeman, San Francisco

54. Banci, L., Bertini, I., Ciofi-Baffoni, S., Huffman, D. L., and O'Halloran, T. V. (2001) *J Biol Chem* **276**, 8415-8426

55. Arnesano, F., Banci, L., Bertini, I., Huffman, D. L., and O'Halloran, T. V. (2001) *Biochemistry* **40**, 1528-1539

56. Auld, D. S. (2001) *Biometals* **14**, 271-313

57. Castagnetto, J. M., Hennessy, S. W., Roberts, V. A., Getzoff, E. D., Tainer, J. A., and Pique, M. E. (2002) *Nucleic Acids Res* **30**, 379-382

58. Huffman, D. L., and O'Halloran, T. V. (2001) *Annu Rev Biochem* **70**, 677-701

59. Hou, Z. J., Narindrasorasak, S., Bhushan, B., Sarkar, B., and Mitra, B. (2001) *J Biol Chem* **276**, 40858-40863

60. Banci, L., Bertini, I., Del Conte, R., Markey, J., and Ruiz-Duenas, F. J. (2001) *Biochemistry* **40**, 15660-15668

61. Wernimont, A. K., Huffman, D. L., Lamb, A. L., O'Halloran, T. V., and Rosenzweig, A. C. (2000) *Nat Struct Biol* **7**, 766-771

62. Banci, L., Bertini, I., Ciofi-Baffoni, S., D'Onofrio, M., Gonnelli, L., Marhuenda-Egea, F. C., and Ruiz-Duenas, F. J. (2002) *J Mol Biol* **317**, 415-429

63. Gitschier, J., Moffat, B., Reilly, D., Wood, W. I., and Fairbrother, W. J. (1998) *Nat Struct Biol* **5**, 47-54

64. McRee, D. E. (1998) *Nat Struct Biol* **5**, 8-10

65. Steele, R. A., and Opella, S. J. (1997) *Biochemistry* **36**, 6885-6895

66. Corazza, A., Harvey, I., and Sadler, P. J. (1996) *Eur J Biochem* **236**, 697-705

67. Cheesman, B. V., Arnold, A. P. & Rubenstein, D. L. (1998) *J Am Chem Soc* **110**, 6359–6364

68. Wright, J. W., Natan, M. J., MacDonnell, F. M.,, and Ralston, D. M. O. H., T. V. (1990) in *Progress in Inorganic Chemistry* (Lippard, S. J., ed), pp. 323–412, Wiley, New York

Chapter 4

1. Outten, C. E., and O'Halloran, T. V. (2001) *Science* **292**, 2488-2492

2. Finney, L. A., and O'Halloran, T. V. (2003) *Science* **300**, 931-936

3. Rensing, C., Mitra, B., and Rosen, B. P. (1997) *Proc Natl Acad Sci U S A* **94**, 14326-14331

4. Mitra, B., and Sharma, R. (2001) *Biochemistry* **40**, 7694-7699

5. Sharma, R., Rensing, C., Rosen, B. P., and Mitra, B. (2000) *J Biol Chem* **275**, 3873-3878

6. Okkeri, J., and Haltia, T. (1999) *Biochemistry* **38**, 14109-14116

7. Banci, L., Bertini, I., Ciofi-Baffoni, S., Finney, L. A., Outten, C. E., and O'Halloran, T. V. (2002) *J Mol Biol* **323**, 883-897

8. Singer, C. P. (2005) in *Chemistry*, pp. 175, Northwestern University, Evanston, IL

9. Bobsein, B. R., and Myers, R. J. (1980) *J. Biol. Chem.* **256**, 5313-5316

10. Bertini, I., and Luchinat, C. (1984) *Advances in Inorganic Biochemistry* **6**, 71-111

11. Liu, J., Stemmler, A., Fatima, J., and Miletti, S. (2005) *Biochemistry* **44**, 5159-5167

12. Hou, Z. J., and Mitra, B. (2003) *Journal of Biological Chemistry* **278**, 28455-28461

13. Ghering, A. B., Shokes, J. E., Scott, R. A., Omichinski, J. G., and Godwin, H. A. (2004) *Biochemistry* **43**, 8346-8355

14. Krizek, B. A., Merkle, D. L., and Berg, J. M. (1993) *Inorganic Chemistry* **32**, 937-940

15. Harper, L. V. (1995) Determination and Utilization of the Magnetic Susceptibility Tensor for a Consensus Zinc Finger Peptide, PhD Thesis, pp. 110, Johns Hopkins University, Baltimore

16. Magyar, J. S. (2002) Study of Coordination Chemistry, Thermodynamics, and Kinetics of Metal Binding to Zinc-Binding Peptides, PhD Thesis, pp. 171, Northwestern University, Evanston, IL

17. Pufahl, R. A., Singer, C. P., Peariso, K. L., Lin, S. J., Schmidt, P. J., Fahrni, C. J., Culotta, V. C., Penner-Hahn, J. E., and O'Halloran, T. V. (1997) *Science* **278**, 853-856

18. Wernimont, A. K., Huffman, D. L., Lamb, A. L., O'Halloran, T. V., and Rosenzweig, A. C. (2000) *Nat Struct Biol* **7**, 766-771

19. Arnesano, F., Banci, L., Bertini, I., Cantini, F., Ciofi-Baffoni, S., Huffman, D. L., and O'Halloran, T. V. (2001) *J Biol Chem* **276**, 41365-41376

20. Hitomi, Y., Outten, C. E., and O'Halloran, T. V. (2001) *J Am Chem Soc* **123**, 8614-8615

21. Brocklehurst, K. R., Hobman, J. L., Lawley, B., Blank, L., Marshall, S. J., Brown, N. L., and Morby, A. P. (1999) *Mol Microbiol* **31**, 893-902

22. Outten, C. E., Tobin, D. A., Penner-Hahn, J. E., and O'Halloran, T. V. (2001) *Biochemistry* **40**, 10417-10423

23. Patzer, S. I., and Hantke, K. (1998) *Mol Microbiol* **28**, 1199-1210

24. Grass, G., Wong, M. D., Rosen, B. P., Smith, R. L., and Rensing, C. (2002) *J Bacteriol* **184**, 864-866

25. Patzer, S. I., and Hantke, K. (2000) *J Biol Chem* **275**, 24321-24332

Chapter 5

1. Palmer, A. G., III, Cavanagh, J., Wright, P. E. & Rance,, and M. (1991) *J. Magn. Reson.* **93**

2. Rensing, C., Mitra, B., and Rosen, B. P. (1997) *Proc Natl Acad Sci U S A* **94**, 14326-14331

3. Arnesano, F., Banci, L., Bertini, I., Ciofi-Baffoni, S., Molteni, E., Huffman, D. L., and O'Halloran, T. V. (2002) *Genome Res* **12**, 255-271

4. Okkeri, J., and Haltia, T. (1999) *Biochemistry* **38**, 14109-14116

5. Outten, C. E. (2001) in Mechanistic Studies of Metalloregulatory Proteins Controlling Metal Ion Homeostasis in Escherichia coli, PhD Thesis, pp. 263, Northwestern University, Evanston, IL

6. Banci, L., Bertini, I., Ciofi-Baffoni, S., Finney, L. A., Outten, C. E., and O'Halloran, T. V. (2002) *J Mol Biol* **323**, 883-897

7. Mitra, B., and Sharma, R. (2001) Biochemistry **40**, 7694-7699

8. Liu, J., Stemmler, A., Fatima, J., and Miletti, S. (2005) *Biochemistry* **44**, 5159-5167

9. Altschul, S. F., Madden, T. L., Schaffer, A. A., Zhang, J., Zhang, Z. (1997) *Nucleic Acids Res* **25**, 3389-3402

10. Outten, C. E., and O'Halloran, T. V. (2001) *Science* **292**, 2488-2492

11. Gattiker, A., Bienvenut, W. V., Bairoch, A.,Gasteiger, E. (2002) *Proteomics* **2**, 1435-1444

12. Singer, C. P. (2005) in Mercury-199 and Cadmium-113 Heteronuclear NMR Spectroscopy Useful in Probing Metal Ion Coordination Sites in Copper and Zinc Metalloproteins, PhD Thesis, pp. 175, Northwestern University, Evanston, IL

13. Dutta, S., Liu, J., and Mitra, B. (2005) *Biochemistry* **44**, 14268-14274

14. Loechel, F., Overgaard, M., Oxvig, C., Albrechtsen, A., and Wewer, U. (1999) *Journal of Biological Chemistry* **274**, 13427-13433
15. Keil, B. (1992) *Specificity of Proteolysis*, Springer-Verlag, New York.

16. Gasteiger E., H. C., Gattiker A., Duvaud S., Wilkins M.R., Appel R.D., Bairoch A. (2005) in *The Proteomics Protcols Handbook* (Walker, J. M., ed), Humana Press.

17. Perler, F. B., Zu, M.-Q., Paulus, H. (1997) *Current Opinion in Chemical Biology* **1**, 292-299

18. Chatterjee, A., Kumar, A., Chugh, J., Srivastava, S., Bhavesh, N., Hosur, R. (2005) *Journal of Chemical Science* **117**, 3-21

19. Dyson, H. J., and Wright, P. E. (2005) *Nature Reviews Molecular Cell Biology* **6**, 197-208

20. Arnesano, F., Banci, L., Bertini, I., Martinelli, M., Furukawa, Y., and O'Halloran, T. V. (2004) *Journal of Biological Chemistry* **279**, 47998-48003

21. Lamb, A. L., Wernimont, A. K., Pufahl, R. A., O'Halloran, T. V., and Rosenzweig, A. C. (2000) *Biochemistry* **39**, 1589-1595

22. Torres, A. S., Petri, V., Rae, T. D., O'Halloran, T. V. (2001) *Journal of Biological Inorganic Chemistry* **276**, 38410-38416

Appendix A

1. Banci, L., Bertini, I., Ciofi-Baffoni, S., Finney, L. A., Outten, C. E., and O'Halloran, T. V. (2002) *J Mol Biol* **323**, 883-897

2. Rosenzweig, A. C., Huffman, D. L., Hou, M. Y., Wernimont, A. K., Pufahl, R. A., and O'Halloran, T. V. (1999) *Structure Fold Des* **7**, 605-617

3. Pufahl, R. A., Singer, C. P., Peariso, K. L., Lin, S. J., Schmidt, P. J., Fahrni, C. J., Culotta, V. C., Penner-Hahn, J. E., and O'Halloran, T. V. (1997) *Science* **278**, 853-856

4. Rensing, C., Mitra, B., and Rosen, B. P. (1997) *Proc Natl Acad Sci U S A* **94**, 14326-14331

5. Arnesano, F., Banci, L., Bertini, I., Ciofi-Baffoni, S., Molteni, E., Huffman, D. L., and O'Halloran, T. V. (2002) *Genome Res* **12**, 255-271

6. Huffman, D. L., and O'Halloran, T. V. (2000) *J Biol Chem* **275**, 18611-18614

APPENDIX A

Preparation of ZntA Mutants to Explore the Role of D58 in Metal Ion Selectivity

ZntA(46-118) and Atx1 share remarkably similar folds (1,2). Yet they preferentially bind different metal ions(3,4). In fact, genomic studies looking at proteins that share this same fold found that while many of them bind Cu(I), many others bind Zn(II)/Pb(II)/Cd(II) instead(5). A key difference found in these studies was the equivalent position of D58 in ZntA(46-118). In Cu(I) proteins this residue was conserved as a tyrosine, whereas in the Zn(II)-binding proteins this position held a conserved aspartate. (Figure A-1) This proposed explanation gained further support from the NMR structure and EXAFS of ZntA(46-118), which indicated that this aspartate binds the Zn(II) ion(1). To expand our understanding of the mechanism of metal ion selectivity in proteins with this fold we mutated this residue in both ZntA(46-118) and ZntA(1-118).

Since this residue is conserved as a tyrosine in the Cu(I) binding proteins, one of the mutants we chose to make was the D58T mutant of ZntA(46-118) and ZntA(1-118). Furthermore, since it was also postulated that the negative charge of the aspartate ion helped to balance the positive charge of the Zn(II) ion, we chose to make mutants that varied this factor as well. To do this, the D58N and D58R mutants were chosen. Arginine was chosen for its

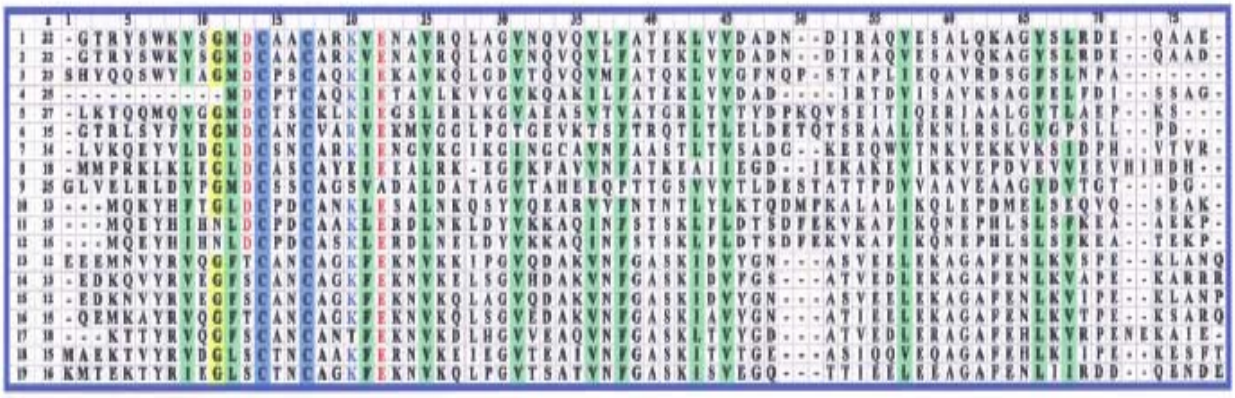

Figure A-1. Sequence alignment of zinc- and cadmium-transporting ATPases(5). At the top, amino acid numbering is reported including gaps. The two metal-binding cysteines are shaded in blue.

Some conserved negative (Glu and Asp) and positive (Arg and Lys) residues are indicated in red and blue, respectively. Positions where hydrophobic residues are conserved are highlighted in green. In column *a* we report sequence identity to Ccc2a from *S. cerevisiae.* **1** gi|586655 *E. coli*, strain K-12 (ZntA); **2** gi|15803981 *E. coli*, strain EDL-933; **3** gi|15641046 *Vibrio cholerae*; **4** gi|2624376 *P. mirabilis*; **5** gi|3123078 *Synechocystis*; **6** gi|15807741 *D. radiodurans*; **7** gi|7436386 *B. subtilis*; **8** gi|14521140 *Pyrococcus abyssi*; **9** gi|15789464 *Halobacterium sp*., strain NRC-1; **10** gi|10720043 *H. felis*; **11** gi|15611794 *H. pylori*, strain J99; **12** gi|2493007 *H. pylori*, strain 26695; **13** gi|79893 *Staphylococcus aureus* (CadA); **14** gi|14020985 *S. aureus II*, 1st domain; **15** *S. aureus II*, 2nd domain; **16** gi|231677 *Bacillus firmus*; **17** gi|15616598 *Bacillus halodurans*; **18** gi|3121832 *Listeria monocytogenes*; **19** gi|9789448 *L. lactis*

positive charge, but since it also is much larger, we chose to make a more conservative mutation to asparagine as well. (Figure A-2)

Mutation of D58R, D58T, and D58N ZntA. The mutation of D58 to Tyr, Arg, and Asn was created in expression vectors for ZntA (PET11c/ZntA(46-118) and PET11c/ZntA(1-118) by site directed mutagenesis using the QuikChange mutagenesis kit (Stratagene) according to the manufacturer's protocol. The mutagenic primers 5'-GGAAAGTCAGCGGCATGAGGTGCGCCGCCTGTGCGCGC – 3' and its reverse compliment were used to create the D58R mutation. The primers 5' – GGAAAGTCAGCGGCATGACCTGCGCCGCCTGTGCGCGC- 3' and its reverse compliment were used to create the D58T mutation. The primers 5' – GGAAAGTCAGCGGCATGAACTGCGCCGCCTGTGCGCGC- 3' and its reverse compliment were used to create the D58N mutation. Mutagenesis was confirmed by sequencing the genes (ABI Prism) at the Biotechnology Facility (Evanston campus).

Overexpression of D58N, D58T, and D58R ZntA (46-118) and ZntA(1-118). The overexpression of each of these mutants was then verified. For each mutant plasmid, four 5 mL tubes of LB were inoculated with one colony from a transformation and 5 microliters of 1 mg/mL ampicillin was added to each tube. These tubes were then incubated with shaking for 1.5 hours, until their optical density was 0.5-.7. Non-induced samples were then taken (0.5 mL) and saved for a gel. The cultures were then induced with 5 microliters of 500 mM IPTG and

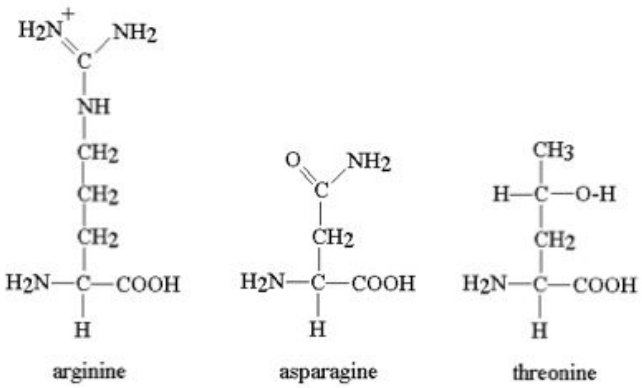

Figure A-2. Amino acids used in mutating aspartate 58. The mutation to arginine reverses the charge of the residue, but also changes the size. The mutation to asparagine alters the charge, with little change in size. The threonine mutation changes this residue to the conserved residue at this position in copper trafficking proteins with the same fold.

incubated a further 3 hours until 0.5 mL samples were taken and pelleted for a SDS-PAGE gel. (Figure A-3).

Since this position is a conserved tyrosine in the copper-binding homologs, it is anticipated that mutation of D58 to Tyr would reverse its selevtivity for Zn(II) over copper. This hypothesis could be tested by measuring its affinity for Zn(II) and Cu(I) relative to Atx1. Simply, apo and metallated samples could be mixed, separated by ion exchange chromatography, and then analyzed for their metal and protein content in a manner similar to the experiments carried out by D. Huffman(6).

Since it is postulated that the negative charge of D58 helps to stabilize the positive charge of the Zn(II) ion, it is expected that the mutation of this residue to Asn and Arg would decrease the affinity of this protein for Zn(II). In this case, the hypothesis could also be tested by a similar method. The relative affinity for Zn of the wild-type ZntA truncation could be established relative to Atx1, from which it can be chromatographically separated. Following this, the same procedure could be used to establish the relative affinities of the other mutants. While it is likely that the zinc affinity of both of these mutants will be lower than the wild-type truncation, the Arg mutation is both a greater change in size and a greater change in charge. If the Arg mutant binds Zn(II) significantly less well than the Asn mutation, it will be difficult to determine which of these factors is the root cause of the difference.

It is also possible that the strength of effect of mutating this residue will be different in the ZntA(46-118) mutant than in the (1-118) mutant. Since several more binding residues are

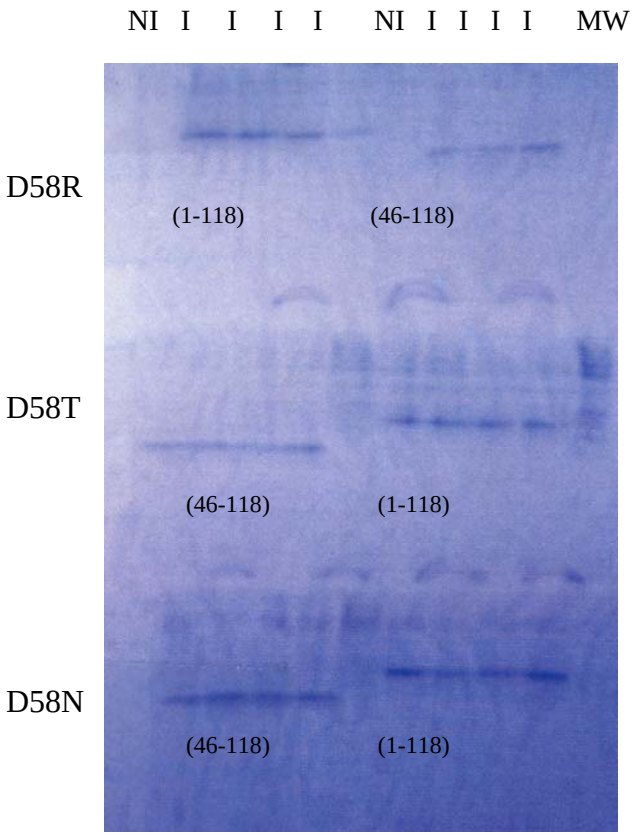

Figure A-3. Overexpression gels of D58R, D58T, and D58N mutants of ZntA(46-118) and ZntA(1-118).

present in the (1-118) truncation, it is possible that the D58 residue plays a less important role in this truncation. Since the entire 1-118 cytosolic portion of the protein is present in the cell, knowing how important this residue is in the truncation could provide us with insights into the biological relevance of the novel coordination seen in the (46-118) structure.

Curriculum Vitae

Lydia A. Finney

EXPERIENCE

1999-present **NORTHWESTERN UNIVERSITY** *Evanston, Illinois*
Graduate Assistant Studying the mechanisms by which protein-protein interactions control metal ion homeostasis in eukaryotes with Dr. Thomas V. O'Halloran. Experienced in protein expression and purification, site-directed mutagenesis, electrophoresis, FPLC, HPLC, MALDI-TOF MS, ICP-AES, UV-Vis and fluorescence spectroscopy, and air sensitive techniques.

1998-1999 **MICHIGAN STATE UNIVERSITY** *East Lansing, Michigan*
Research Assistant Investigated properties of non-heme-iron small molecule model complexes under Dr. J. B. Broderick.

STATE UNIVERSITY OF NEW YORK AT ALBANY *Albany, New York*
Engaged in independent research in bioinorganic chemistry under Dr. W. E. Broderick.

EDUCATION

1999-present **NORTHWESTERN UNIVERSITY** *Evanston, Illinois*
Ph.D. Candidate in Inorganic Chemistry under Dr. Thomas. V. O'Halloran.

STATE UNIVERSITY OF NEW YORK AT ALBANY *Albany, New York*
B.S. in Chemistry with Mathematics minor (3.99/4.00 GPA).

G. RAY BODLEY HIGH SCHOOL *Fulton, New York*
Valedictorian.

HONORS

2002 **Elected as an Associate Member to Sigma Xi.**

1999 **John and Fannie Hertz Graduate Fellowship**
National Science Foundation Graduate Fellowship Honorable Mention.
American Institute of Chemists Foundation Student award.

1998 **National Science Foundation Research Experience for Undergraduates Scholarship**

1997 **Barry M. Goldwater Scholar**
State University of New York Chancellor's Award for Academic Excellence

CRC Press Freshman Chemistry Award

1995 **Robert C. Byrd Scholar** State of New York.
University Honors Scholarship State University of New York at Albany.

PROFESSIONAL DEVELOPMENT AND AFFILIATION

Test Method Validation: Analysis, Bioanalysis and Regulation August 26-27, 2003. Short course on the expectations set by the Quality System Regulations for the development and validation of test methods for FDA-regulated industry. Taught by Neal Siegel, Ph.D. of Abbott Labs..
American Chemical Society Student affiliate.
Phi Beta Kappa Member.
Golden Key National Honor Society Member.
Search Committee for Dean of College of Arts and Sciences *SUNY Albany, 1998* Member.

PUBLICATIONS

2003 Finney, L.A., O'Halloran, T.V. **Transition Metal Speciation in the Cell: Insights from the Chemistry of Metal Ion Receptors** Science 2003, *300,* 931-936.

Wernimont, A.K., Huffman, D.L., Finney, L.A., Demeler, B., O'Halloran, T.V., Rosenzweig, A.C. **Crystal structure and dimerization equilibria of PcoC, a methionine rich copper resistance protein from *Escherichia coli*.** J. Biol. Inorg. Chem. 2003, *8*, 185-194.

2002 Banci, L. Bertini, I., Ciofi-Baffoni, S., Finney, L. A., Outten, C. E., and O'Halloran, T. V. **A new zinc protein coordination site in an intracellular metal-trafficking protein: Solution structure of the apo and Zn(II) forms of ZntA(46-118)**. J. Mol. Biol., 2002, *323*, 883-897.

Huffmann, D. L., Huyett, J., Outten, F. W., Doan, P. E., Finney, L. A., Hoffman, B. W., and O'Halloran, T. V**. Spectroscopy of Cu(II)-PcoC and the multicopper oxidase function of PcoA, Two Essential components of *Escherichia coli pco* copper resistance operon.** Biochemistry, *41*, (31), pp 10046 – 10055.

POSTERS AND PRESENTATIONS

2004 **Gordon Research Conference: Graduate Research Seminar: Bioinorganic Chemistry.** January 22-25, 2004. Ventura, CA. "The Chemical Secrets of Metal Trafficking Proteins". **Presentation.**

2003 **17th Symposium of the Protein Society: *Pathways to Human Health*.** July 26-30, 2003. Boston, MA. **"**Transition Metal Selectivity: An Emerging Role for Protein-Protein Interactions". Finney, L.A. and O'Halloran, T.V. **Poster.**

2nd Annual Midwest Metals Meeting. May 16-18, 2003. Washington University, St. Louis, MO. "Novel Biological Coordination Chemistry: The Chemical Secrets of Metal Trafficking Proteins". Finney, L.A. and O'Halloran T.V. **Poster.**

2001 **10th International Conference on Bioinorganic Chemistry.** August 26-31, 2001. University of Florence, Florence, Italy. "Unraveling the Mechanism of the Copper Chaperones: What Rules Govern Copper Trafficking in the Cell?". Finney, L.A. and O'Halloran, T.V. **Poster.**